DOT/FAA/TC-16/33

Federal Aviation Administration
William J. Hughes Technical Center
Aviation Research Division
Atlantic City International Airport
New Jersey 08405

Probabilistic Damage Tolerance-Based Maintenance Planning for Small Airplanes

October 2017

Final Report

This document is available to the U.S. public through the National Technical Information Service (NTIS), Springfield, Virginia 22161.

This document is also available from the Federal Aviation Administration William J. Hughes Technical Center at actlibrary.tc.faa.gov.

U.S. Department of Transportation
Federal Aviation Administration

NOTICE

This document is disseminated under the sponsorship of the U.S. Department of Transportation in the interest of information exchange. The U.S. Government assumes no liability for the contents or use thereof. The U.S. Government does not endorse products or manufacturers. Trade or manufacturers' names appear herein solely because they are considered essential to the objective of this report. The findings and conclusions in this report are those of the author(s) and do not necessarily represent the views of the funding agency. This document does not constitute FAA policy. Consult the FAA sponsoring organization listed on the Technical Documentation page as to its use.

This report is available at the Federal Aviation Administration William J. Hughes Technical Center's Full-Text Technical Reports page: actlibrary.tc.faa.gov in Adobe Acrobat portable document format (PDF).

Technical Report Documentation Page

1. Report No.	2. Government Accession No.	3. Recipient's Catalog No.
DOT/FAA/TC-16/33		

4. Title and Subtitle	5. Report Date
Probabilistic Damage Tolerance-Based Maintenance Planning for Small Airplanes	October 2017
	6. Performing Organization Code

7. Author(s)	8. Performing Organization Report No.
Harry Millwater and Juan Ocampo	

9. Performing Organization Name and Address	10. Work Unit No. (TRAIS)
University of Texas at San Antonio One UTSA Circle San Antonio, TX 78249	
	11. Contract or Grant No. Grant No. 12-G-012

12. Sponsoring Agency Name and Address	13. Type of Report and Period Covered
U.S. Department of Transportation Federal Aviation Administration FAA Central Regional Office 901 Locust St Kansas City, MO 64106	Final Report August 2009–December 2013
	14. Sponsoring Agency Code ACE-113

15. Supplementary Notes

The FAA William J. Hughes Technical Center Aviation Research Division COR was Dr. Sohrob Mottaghi.

16. Abstract

Most general aviation (GA) aircraft are designed for safe-life based on a crack-initiation-type failure mechanism (e.g., Miner's rule). However, newer GA aircraft have fatigue crack growth as a design option. In addition, it may be necessary to evaluate a field event, such as a cracked structure, to ascertain the remaining life.

A comprehensive probabilistic damage-tolerance (DT) method requires the combination of a deterministic crack growth model, inspection methods, probabilistic methods, and random variable modeling to provide a single probability-of-failure (POF), cumulative POF, and hazard rate with and without inspection.

In this work, a general methodology to conduct a probabilistic crack growth-based DT methodology for small airplanes was developed and incorporated in computer software. The methodology overcomes the limitations from previous DT programs, such as the number of random variables, extreme value distribution (EVD) loading generation, inspections/repair programs, and reduction in the computational time. Additional random variables were included in the model using Monte Carlo sampling, efficient numerical integration algorithms, and a surrogate model for crack growth modeling. Algorithms to determine the EVD from real aircraft loading, generated in this research as well, were developed and incorporated into the code. New efficient inspection and repair programs were studied, improved if necessary, and implemented into the code.

17. Key Words	18. Distribution Statement
Damage tolerance, Inspection and repairs, Extreme value distribution, Loading generation, Surrogate models, Monte Carlo sampling, Numerical integration, Random variables	This document is available to the U.S. public through the National Technical Information Service (NTIS), Springfield, Virginia 22161.

19. Security Classif. (of this report)	20. Security Classif. (of this page)	21. No. of Pages	22. Price
Unclassified	Unclassified	142	

ACKNOWLEDGEMENTS

The authors would like to acknowledge the contributions of Anthony Castaldo, research faculty at the University of Texas at San Antonio, and Andrew Bodling, undergraduate research assistant at the University of Texas at San Antonio.

TABLE OF CONTENTS

APPENDICES

LIST OF FIGURES

LIST OF TABLES

LIST OF ACRONYMS

AFGROW	Air Force Growth (software)
CDF	Cumulative density function
CTPOF	Cumulative total probability-of-failure
DT	Damage tolerance
DTA	Damage tolerance analysis
EIFS	Equivalent initial flaw size
EVD	Extreme value distribution
FCG	Fatigue crack growth
GA	General aviation
GAG	Ground-air-ground
GUI	Graphical user interface
PDF	Probability density function
PDTA	Probabilistic damage tolerance analysis
POD	Probability-of-detection
POF	Probability-of-failure
RS	Residual strength
SFPOF	Single flight probability-of-failure

EXECUTIVE SUMMARY

Structural integrity of aircraft structures is of continual interest to the aviation community. Although air travel is remarkably safe, there is unwavering interest in reducing the probability of structural failure, particularly as the number of flights continues to increase annually. In 1991, Congress mandated that the FAA establish an Aging Aircraft Program. The focus of this program was age-related structural problems with airplanes used in public transportation. At the time, Congress excluded the general aviation (GA) fleet from the mandate. However, the FAA determined that as the GA fleet continues to age, there is a concern about ensuring the continued airworthiness of the diverse GA fleet.

To guide future efforts in addressing the effects of aging on GA airplanes, the FAA's Small Airplane Directorate developed an FAA Aging GA Roadmap that serves as a guide to proactively manage the overall airworthiness of aging GA airplanes. One of the four major focus areas of the Roadmap is data-driven risk assessment and management. As a result, a research and development program was undertaken to develop the required methodology, computer software, and supporting data to conduct structural risk assessments.

Although the U.S. Air Force has been employing damage tolerance analysis methods since the early 70s to design new aircraft and determine inspection intervals for aging aircraft, until now, little work has been done on probabilistic damage tolerance (DT) for GA. A probabilistic DT evaluation of the GA fleet can provide important insights into the criticality/severity of a potentially serious structural issue and provide mechanisms whereby inspection and maintenance operations can be included into the simulation, giving operators the opportunity to assess the benefits of maintenance actions.

In this research, a methodology and a computer code, SMART|DT, were developed to address probabilistic DT of GA structural issues. The methodology and computer code considers the random variables: loading (gust and maneuver loads, sink rate, flight velocity duration, flight weight duration), material behavior (fracture toughness, crack growth rate constants, yield stress, ultimate stress), geometric variables (initial crack size, hole diameter, hole edge distance, aircraft ratio), and inspections (repair crack size, probability-of-detection, probability-of-inspection). These random variables are used within a Monte Carlo simulation or numerical integration algorithm to calculate the probability-of-failure as a function of hours/flights and to assess the benefits of maintenance actions. This methodology can be used for any section of the aircraft—such as the wing, fuselage, and vertical stabilizer—if the loading, geometry, and material properties are available for the desired location.

1. INTRODUCTION

In 1991, Congress mandated that the FAA establish an Aging Aircraft Program. The focus of this program was age-related structural problems with airplanes used in public transportation. At the time, Congress excluded the general aviation (GA) fleet from the mandate. However, the FAA determined that as the GA fleet continues to age, there is a concern about ensuring the continued airworthiness of the diverse GA fleet. To guide future efforts in addressing the effects of aging on GA airplanes, the FAA's Small Airplane Directorate developed an FAA Aging GA Roadmap that serves as a guide to proactively managing the overall airworthiness of aging GA airplanes. One of the four major focus areas of the Roadmap is data-driven risk assessment and management. As a result, a research and development program was undertaken to develop the required methodology, computer software, and supporting data to conduct structural risk assessments.

The GA fleet includes approximately 150,000 airplanes that were certificated with no fatigue evaluation requirements. The average age of these airplanes is approximately 40 years and many are high-time. There is little information regarding airworthiness limitations for this aging GA fleet. In recent years, the industry and the FAA have reacted to several fatigue-related accidents and incidents on these fleets. To mitigate the aging effects on the GA fleet, an efficient probabilistic damage tolerance analysis (PDTA) approach is needed [1–3]. A probabilistic damage tolerance (DT) method requires a combination of deterministic crack growth, inspection methods, probabilistic methods, and random variable modeling to provide a single probability-of-failure (POF), cumulative POF, and hazard rate. A PDTA approach also provides a mechanism whereby inspection and maintenance operations can be included in the simulation, therefore providing engineers with the opportunity to assess the benefits of maintenance actions.

2. METHODOLOGY OVERVIEW

The methodology in this work encompasses the required elements necessary to conduct DT analysis: aircraft loading generation, extreme value of the maximum load per flight distribution, crack growth analysis, inspection and repairs, and POF calculations. Figure 1 shows, schematically, the probabilistic DT process developed in this research.

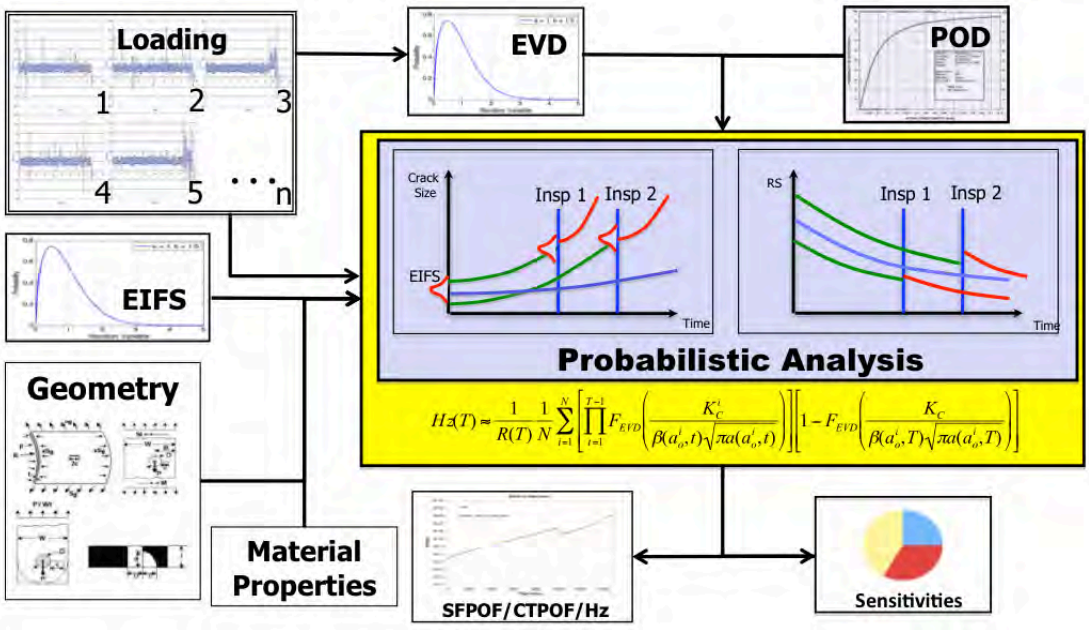

Figure 1. Schematic representation of probabilistic DT analysis

2.1 LOAD AND STRESS SPECTRUM GENERATION

Load generation is one of the most important components in DT analysis. No commercial software is available to generate realistic load spectra; each aircraft manufacturer usually has its own computer code to generate aircraft loading. This section reviews how this research generates realistic load spectra accounting for five different flight regimes: maneuver, gust, taxi, landing and rebound, and ground-air-ground (GAG).

The input parameters used to generate a load spectrum are given in Table 1. Table 1. Variables used to generate load spectra

Variable	Description
Number of Flights	Number of flights to be generated in the flight spectra
Exceedance Curves	Usage exceedance curves
Maneuver Load Limit Factor	Maximum load limit factors for maneuver load
Gust Load Limit Factor	Maximum load limit factors for gust load
Maximum Ground Stress	Airplane ground stress in psi
Maximum One g Stress	One g stress of an airplane in psi
Maximum Aircraft Velocity	Average speed during flight, maximum aircraft safe cruise speed (VNO) or VMO. In nautical miles.
Flight Length-Velocity Matrix	Probabilistic flight length and airspeed data
Flight Length-Weight Matrix	Probabilistic flight length and weight data

VMO = maximum operating limit speed; VNO = maximum aircraft safe cruise speed

The steps to generate the spectrum are:

1. Provide input parameters (a summary of the input parameters is presented in Table 1).
2. Generate random realizations of the parameters: maneuver and gust exceedance curves; flight-length and aircraft velocity, as per flight length-velocity and maximum aircraft velocity; and one-g-stress, as per flight length-weight and maximum one-g-stress.
3. Calculate the number of occurrences for each of the flight stages using the methodology in 4 (also shown in appendix A).
4. Add incomplete cycles from previous flights to the current flight stresses after each of the stresses and occurrences are calculated for the current flight. Next, extract the complete stresses and save the incomplete stresses from the current flight for the next flight.
5. Randomize the load pairs within a flight generated in the previous steps.
6. Save the maximum load per flight to later estimate the extreme value distribution (EVD).
7. Repeat steps 1–6 for the given number of flights.
8. Randomize the flights using a uniform density function after they have all been generated so that there is an equal probability that the high severity loads will appear at any flight during the crack growth analysis.

Figure 2 shows, schematically, the process to generate a flight spectrum. Figure 3 shows a spectrum example, including all the flight stages for a single flight.

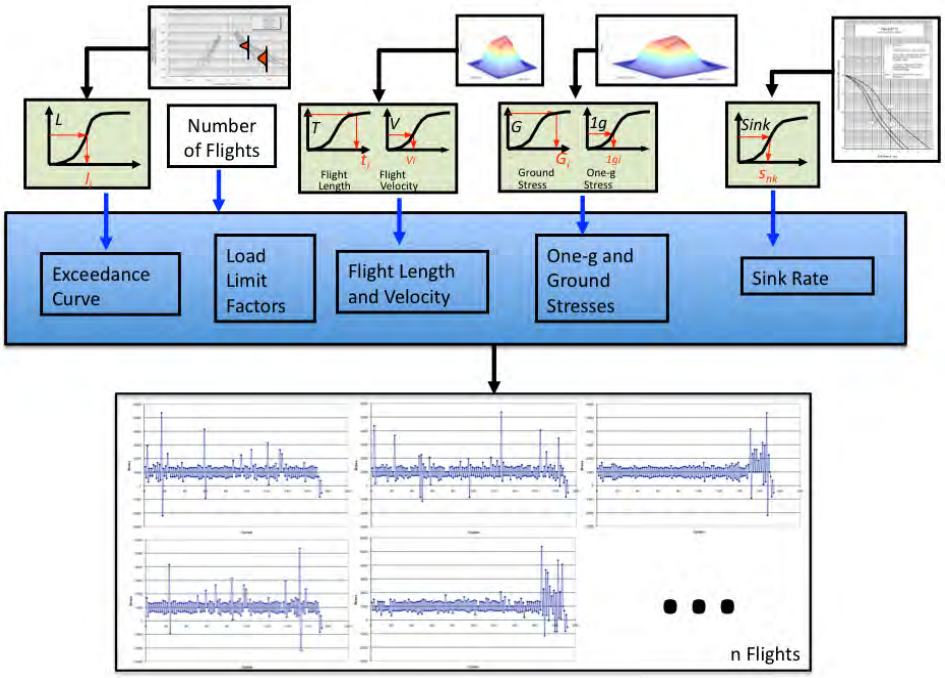

Figure 2. Schematic representation of spectrum generation and input variables

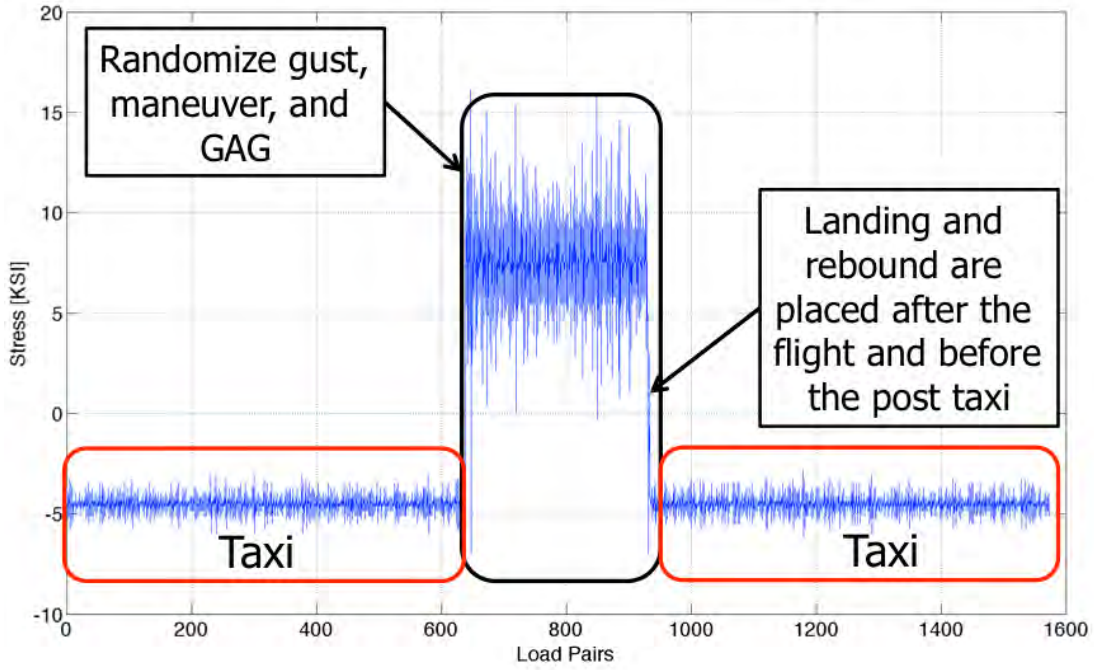

Figure 3. A representative spectrum

2.1.1 User-defined Spectrum

A user-defined spectrum is also allowed when the SMART exceedance libraries do not include the user application. The user spectrum uses the same format as the one used by the AFGROW (Air Force Growth) software. AFGROW is a damage tolerance analysis (DTA) framework that allows users to analyze crack initiation, fatigue crack growth (FCG), and fracture to predict the life of metallic structures. The Air Force Research Laboratory originally developed AFGROW. It is now being developed and maintained by LexTech, Inc. [5].

This option bypasses the internal generation of a spectrum using the exceedance curves, and the user spectrum is used instead. Figures 4 and 5 present a simple example of the AFGROW spectrum files (.sp3 and .sub).

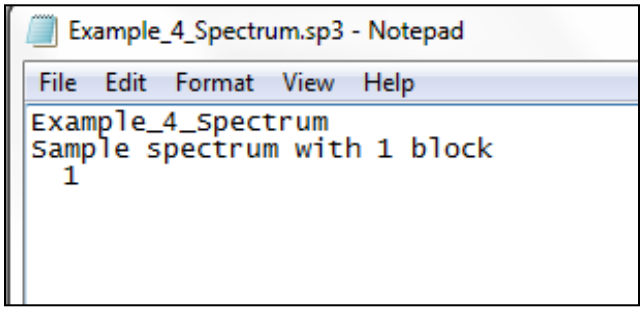

Figure 4. AFGROW user spectrum input data file

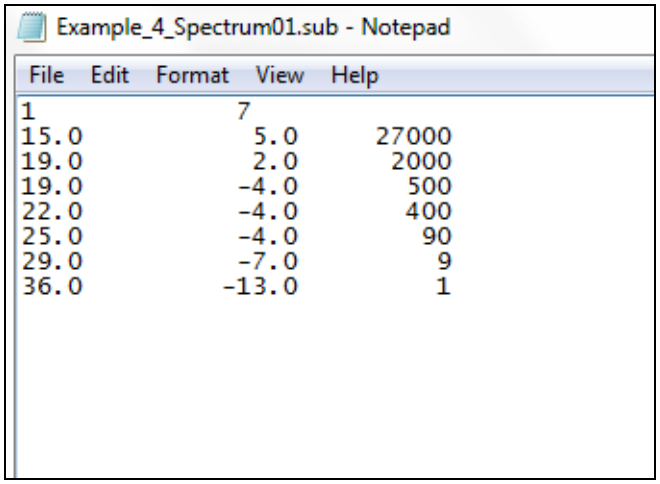

Figure 5. AFGROW user spectrum companion data file

2.2 EXTREME VALUE MAXIMUM LOAD PER FLIGHT DISTRIBUTION GENERATION

An EVD of the maximum load per flight of the loading spectrum is critical for a PDTA of a GA aircraft. The EVD parameters are important because the structural integrity of the aircraft depends on the maximum load seen by the structure during a specified number of flights.

In PDTA, the EVD must be generated from the same loading used for crack growth analysis. In this program, the maximum load per flight is extracted and the software continues generating sets of flights until the parameters converge, as shown schematically in Figure 6. The convergence is computed by comparing the empirical cumulative density function (CDF) against the CDF determined by the fitting parameters and ensuring that the difference is less than the threshold (1E-6).

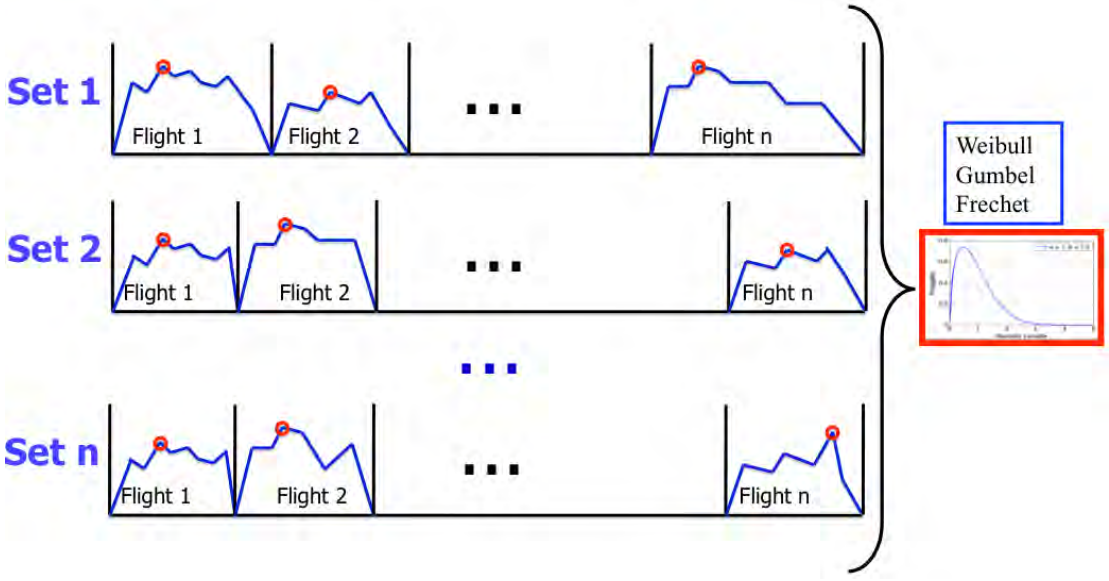

Figure 6. EVD generation

Using this set of maximum load per flight, the EVD is calculated using the generalized extreme value theory. The generalized extreme value theory can be explained as follows: Suppose $X_1, X_2, ..., X_p$ is a sequence of independent random variables having a common distribution function, $F(x)$. If Mp represents the maximum of the process over *n* observations, then, as per the extreme value theory, the distribution of M_p can be derived exactly for all the values of *p* using:

$$P\{M_p \le z\} = P\{X_1 \le z\} \times P\{X_2 \le z\} \times ... \times P\{X_p \le z\} = F(z)^n \tag{1}$$

where $P\{M_p \le z\}$ is the probability that random variable M_p is less than or equal to the number *z,* and *n* is the number of flights [6, 7]. Therefore, if the CDF of a random variable is given, then an EVD of the variable over *p* samples (realizations) can be estimated using equation 1. This may not be immediately helpful in practice because the probability density function (PDF) of aircraft loading is typically available in a closed-form equation. The generalized extreme value theory provides the exact solution for a standard distribution, such as uniform, normal, or Weibull distribution. When the PDF of the parent distribution is not available and the above approach cannot be used, the following approach can be employed.

From the extreme value theory, it is known that the asymptotic form of the extreme value of maximum data, as $p \to \infty$, can take one of three forms: Gumbel, Frechet, or Weibull, Types I, II, and III, respectively. The three possible models for the maximum can be encapsulated in the generalized extreme value model as:

$$F(x;\mu,\sigma,\xi) = P = \exp\left\{-\left[1+\xi\left(\frac{x-\mu}{\sigma}\right)\right]^{-1/\xi}\right\} \tag{2}$$

The distribution in equation 2 is known as the generalized EVD [6, 7. Here, μ is the location, σ is the scale, and ξ is the shape parameter of the generalized EVD. The value of the shape parameter determines the type of distribution. The EVD converges to Weibull, Gumbel, or Frechet if the shape parameter value is less than zero, equal to zero, or greater than zero, respectively. Figure 7 shows an example PDF and CDF for each of the three generalized EVD distributions.

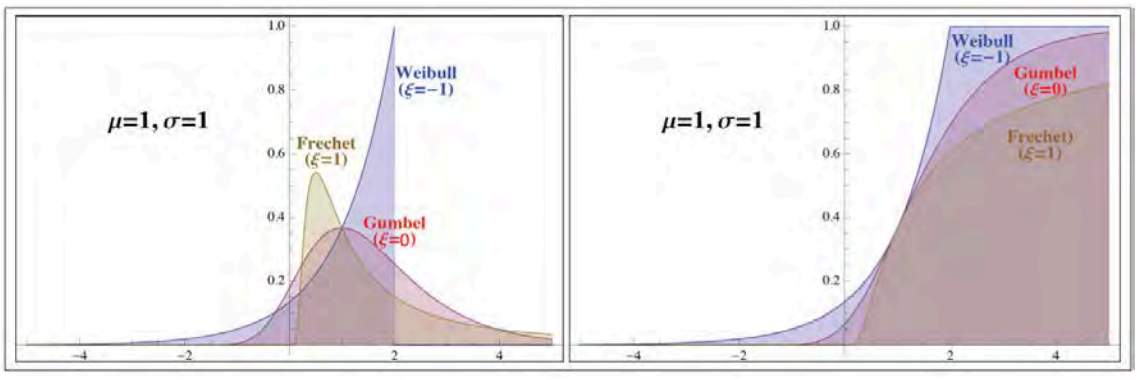

Figure 7. EVD: PDF and CDF examples

The inverse of the generalized EVD, also known as the quantile function, for $P \in (0,1)$ is [6, 7]:

$$F^{-1}(P;\mu,\sigma,\xi) = x = \mu - \left(\frac{\sigma}{\xi}\right) + \left(\frac{\sigma}{\xi}\right) \cdot [\ln(P)]^{-\xi} \tag{3}$$

For a given value of x and its probability, the inverse function is an equation with three unknowns: location, scale, and shape. Therefore, three equations are required to obtain unique values for μ, σ, and ξ. In the absence of known equations, their estimated values can be obtained as follows.

Sorting all of the maximum-load-per-flight elements will produce an empirical CDF. The position of a given x value within the sort is its probability. For example, the median value in the sorted array has a probability of 0.50. Thus, it is possible to choose three such values and solve for the parameters of the EVD. For example, the method can choose the values associated with p=(0.50, 0.25, 0.125). This methodology chooses at least seven distinct sets of three values, solves the three equations for μ,σ,ξ, and averages the results to obtain good initial estimates of μ,σ,ξ.

The method described above is called the method of quantiles. The average of the seven distinct points in the method of quantiles is the starting point for a minimization method. The minimization method used is the Nelder-Mead algorithm. This algorithm finds a set of parameters that minimizes the total absolute error while maintaining a conservative probability-of-survival. The EVD fits using this method tend to have correlations above 99.5% when the fits are compared with the empirical CDFs [8, 9].

Figure 8 and Figure 9 show PDFs and CDFs for different GA aircraft usages.

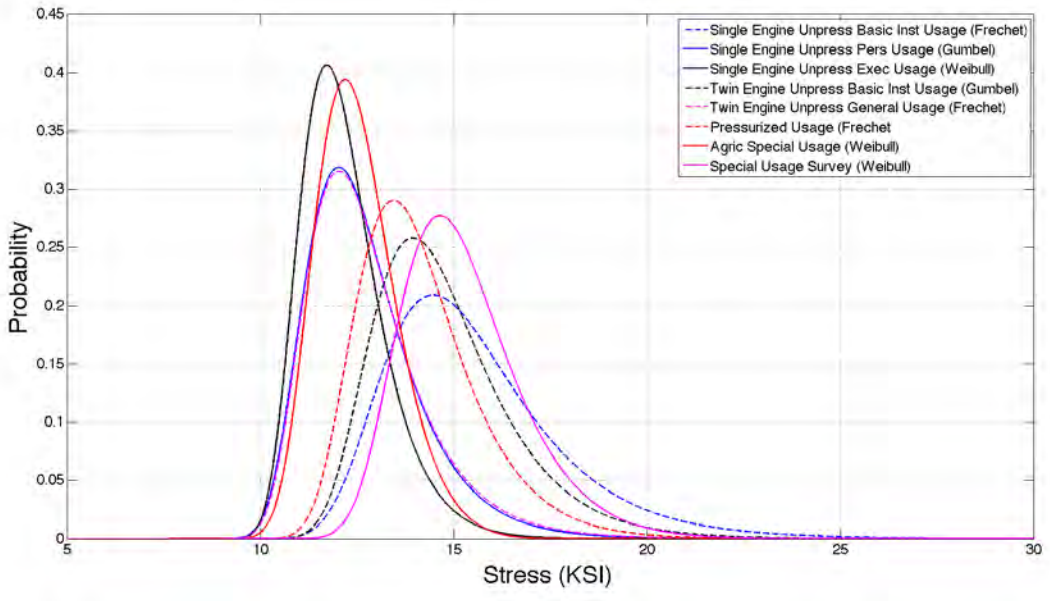

Figure 8. EVD PDF distributions

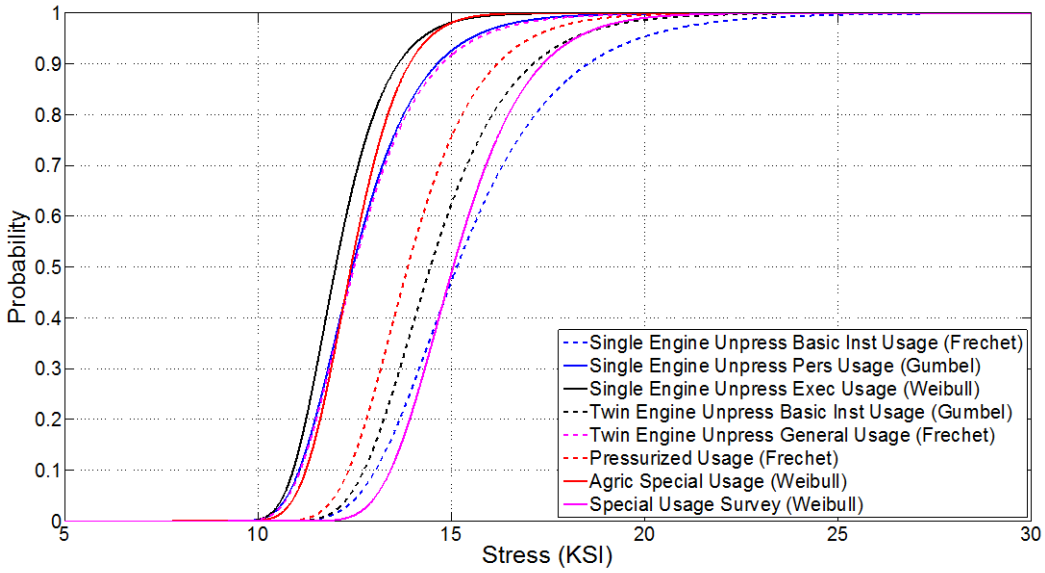

Figure 9. EVD CDF distributions

2.3 POF CALCULATIONS

The single flight probability-of-failure (SFPOF) is defined as the POF[1] on the next flight assuming survival until the current flight (*t*). Failure is defined as the occurrence of unstable fracture, $K_I \geq K_C$, where K_I denotes the stress intensity factor and K_C is the fracture toughness. An equivalent statement is that failure occurs when the residual strength (RS), σ_{RS}, is less than or equal to the max stress per flight, σ_{EVD}. The RS is defined as:

$$\sigma_{RS} = \frac{K_C}{\beta(a(a_i,t))\sqrt{\pi a(a_i,t)}} \tag{4}$$

where a denotes the crack size, which is a function of the initial crack size (a_i)and the time (*t*); β is the geometry correction factor; and t is the time in flights. The definition of the RS can also encompass net section yield. The RS used in the calculation is the minimum of the RS due to fracture and net section yield.

Defining the limit state as:

$$g(a_i, K_C, C, m, D, t) = \sigma_{RS}(a(a_i,t), K_C, C, m, D) - \sigma_{EVD} \tag{5}$$

[1] The probability-of-failure is defined as the probability that the maximum stress per flight will exceed the residual strength of the part.

failure occurs then $g \le 0$. C and m represent the crack growth random variables (i.e., Paris constants and D represents the hole diameter). The POF is then given in terms of the maximum stress per flight, σ_{EVD}, and the RS, σ_{RS}

$$P_f = P[\sigma_{RS}(a(a_i,t),K_C,C,m,D) \le \sigma_{EVD}] \tag{6}$$

or

$$P_f = P[g \le 0] \tag{7}$$

Assuming only three of the parameters in equation 6 are random variables (a_i, K_C, and σ_{EVD}), the SFPOF is determined by integrating the joint PDFs over the failure domain:

$$P_f = \int\int\int_{g\le 0} f_{K_C} f_{a_i} f_{\sigma_{EVD}} da_i dK_C d\sigma_{EVD} \tag{8}$$

where f_{K_C}, f_{a_i}, and $f_{\sigma_{EVD}}$ are the PDFs for fracture toughness, initial crack size, and loading. This equation is cumbersome to use because the integration limits of the random variables depend on the inequality equation $g \le 0$. A better computational formulation is to rewrite equation (8) in terms of the indicator function as:

$$P_f = \int_{-\infty}^{\infty}\int_{-\infty}^{\infty}\int_{0}^{\infty} \left(I(\sigma_{EVD}, \sigma_{RS}(a(a_i,t),K_C)\right) f_{K_C} f_{a_i} f_{\sigma_{EVD}} da_i dK_C d\sigma_{EVD} \tag{9}$$

where the indicator function, I, is nonzero only in the failure domain. That is:

$$\begin{aligned} I(\sigma_{EVD}, \sigma_{RS}(a(a_i,t),K_C) &= 1 \quad g \le 0 \\ I &= 0 \qquad\quad \text{Otherwise.} \end{aligned} \tag{10}$$

Therefore, the range of each random variable in equation 9 spans the range of the corresponding probability distribution. The SFPOF formulation used here is monotonically increasing with t.

2.3.1 Conditional Expectation Formulation

Equation 9 can be simplified by using a conditional expectation (CE) approach. For CE, one random variable is integrated analytically. For SFPOF calculations, a_i and K_C are considered to be deterministic (e.g., $a_i = a_i^*, K_C = K_C^*$ where a_i^* and K_C^* are known values of the initial fracture crack size and fracture toughness, respectively). Then, the RS is deterministic and the SFPOF is the probability of having a stress greater than the RS. This probability equals $1 - F_{EVD}(\sigma_{RS}^*(a_i = a_i^*, K_c = K_C^*))$, where F_{EVD} is the CDF of the extreme value loading. The actual randomness in a_i and K_c is then incorporated within the multidimensional integral as:

$$P_f = \int_0^{\infty} \int_{-\infty}^{\infty} (1 - F_{EVD}(\sigma_{RS}(a(a_i,t),K_C)))f_{K_C} f_{a_i} da_i dK_C = E[1 - F_{EVD}] \quad (11)$$

In other words, the SFPOF becomes the expected value of the complementary CDF of the max stress per flight.

Additional random variables can be added to equation 11 in a straightforward manner, as shown for multiple random variables $\boldsymbol{x}$ in equation 12. Computer codes such as PROF [10–12] and SMART|DT solve the conditional expectation equation (i.e., equation 11). This SFPOF formulation is monotonically increasing with t.

2.3.2 Design Limit Load

It may be desirable to use a fixed value for the max stress per flight (e.g., the design limit load). In this case, the problem formulation is unchanged, except F_{EVD} becomes a step function at the limit load value. Equation 11 is still used to compute the SFPOF. The step function in equation 11 works as follows: if $\sigma_{RS} > \sigma_{EVD-LIMIT\ LOAD}$, the POF is equal to zero; otherwise the POF is equal to one.

2.3.3 Lincoln and Freudenthal Formulations

The SFPOF that assumes all samples will survive until time t is often called the Lincoln formulation and is expressed as follows:

$$POF(t) = \int_{-\infty}^{\infty} \left[1 - F_{EVD}(\sigma_{RS}(a(a_i,t),K_C))\right] f_{\mathbf{x}}(\mathbf{x}) d\mathbf{x} \quad (12)$$

where $f_x(\mathbf{x})$ is the PDF for a set of random variables, $\mathbf{x}$.

The Freudenthal formulation considers survival until time t as:

$$POF(t) = \int_{-\infty}^{\infty} \int_0^{\infty} \left[\prod_{t=1}^{T-1} F_{EVD}(\sigma_{RS}(a(a_i,t),K_C))\right] \left[1 - F_{EVD}(\sigma_{RS}(a(a_i,t),K_C))\right] f_{a_0}(a_0) f_{K_C}(K_C) da_0\, dK \quad (13)$$

where the term $\prod_{t=1}^{T-1} F_{EVD}(\sigma_{RS}(a(a_i,t),K_C))$ is the probability of surviving until time t [10].

2.3.4 Cumulative POF

The cumulative POF for SFPOF is calculated assuming independence as [10–12]:

$$CTPOF(t) = 1 - \prod_{t=1}^{T} (1 - SFPOF(t)) \quad (14)$$

The cumulative total probability-of-failure (CTPOF) is always monotonically increasing and approaches 1 as $t \to \infty$.

2.3.5 Hazard Rate

The hazard function is defined as the probability that, if an airplane survives until time *t*, it will fail at the next flight normalized by the reliability term ($R(t) = 1 - CTPOF(t)$). The hazard function can be expressed as [10–12]:

$$Hz(T) = \frac{1}{R(T)} \int_{-\infty}^{\infty} \left[\prod_{t=1}^{T-1} F_{EVD}\left(\frac{K_C}{\beta(a_o,t)\sqrt{\pi a(a_o,t)}} \right) \right] \left[1 - F_{EVD}\left(\frac{K_C}{\beta(a_o,T)\sqrt{\pi a(a_o,T)}} \right) \right] f_{\mathbf{X}}(\mathbf{x}) d\mathbf{x} \qquad (15)$$

2.4 INSPECTIONS AND REPAIRS

The PDTA provides a mechanism whereby inspection and maintenance operations can be included into the simulation, therefore providing engineers with the opportunity to assess the benefits of maintenance actions. Those benefits include optimizing inspections in which the user inputs a risk level and an optimization algorithm can find the optimum inspections times; additionally, cost optimization can be analyzed. This section reviews two different methods that can be employed.

2.4.1 Probability of Inspection

The fundamental concept regarding the consideration of inspection is based on branching over the probable events after each inspection. The probability of occurrence of each branched event is then determined based on the probability of crack detection.

The inspection method constructs a weighted tree of POF curves that reflect the probability of detecting a crack (and conducting a repair). To better understand the methodology, consider Figure 10. The inspection points are denoted as $I_1, I_2, ..., I_K$, where k is the total number of inspections. The inspection points are indicated with *i*; so a generic inspection point is I_i.

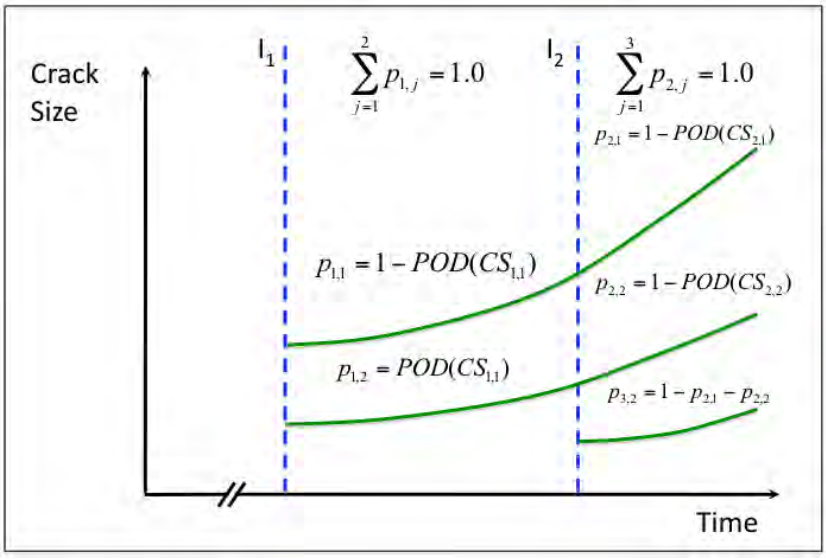

Figure 10. Probability weights for crack paths

At each inspection, two paths are possible (non-detection and detection) based upon the probability-of-detection (POD) value of the crack size at the time of inspection. The probability of being on any branch is given by $p_{i,j}$. After the i^{th} inspection, there are $i+1$ possible paths. The probability of all paths must sum to one based on axioms of probability $\left(\sum_{j=1}^{N+1} p_{i,j} = 1.0\right)$.

Probability calculations are shown in Figure 11. The POF for a path is the POF for a crack on the path times the probability of being on a path. For example, after inspection 1, if a crack is not detected, the probability of being on that path is $1 - POD(a)$. The POF for a crack on that path is calculated as POF_{ORI}, where POF_{ORI} is the POF for the original part. Therefore, the POF for that path is $(1 - POD(a)) \cdot POF_{ORI}$. It is computed similarly for other paths.

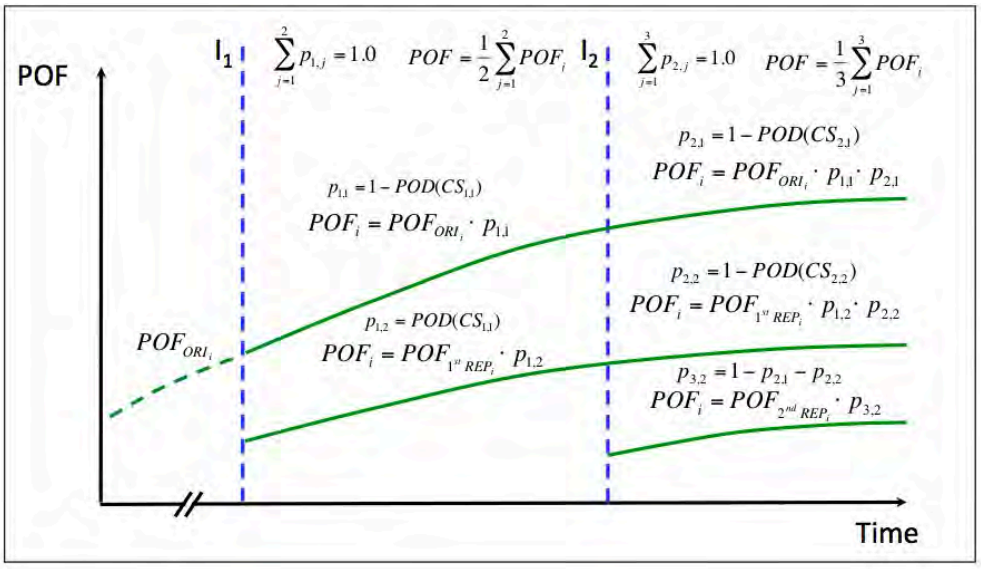

Figure 11. Probability calculations for inspections

2.4.2 Numerical Integration

For numerical integration, after any inspection, some cracks are detected and repaired. The PDF of the crack size after inspection (f_{after}) is composed of a combination of two PDFs: the grown crack size PDF before inspection (f_{before}) and the repair crack size distribution (f_{repair}). The repair crack size distribution is often the same as the initial crack size, but this is not required.

The crack size PDF after inspection is given as:

$$f_{after}(a) = P_{\det} f_{\mathrm{Re}\,pair}(a) + [1 - POD(a)] f_{before}(a) \tag{16}$$

where

$$P_{\det} = \int_0^{\infty} POD(a) f_{before}(a) da \tag{17}$$

is the percentage of detected cracks.

The probability of detecting a crack is determined by the POD curve. The POD is a CDF that varies between 0 and 1 and is a function of crack size. Larger cracks have a higher probability of being detected. After a crack is detected, it is assumed that the crack is repaired. An example of a POD curve is given using a lognormal distribution in Figure 12 (additional POD curves can be found in [13]). Because the crack size cannot be negative, the lognormal distribution is a common choice.

Figure 13 shows an example of different POD effects: when an excellent inspection is conducted (97% of the cracks were detected), the F_{after} CDF appears very close to the F_{repair} CDF. A poor inspection (7% of the cracks were detected) is also shown in Figure 13, where F_{after} CDF appears very close to the F_{before} CDF. The *x*-axis represents crack size and the *y*-axis represents the probability value.

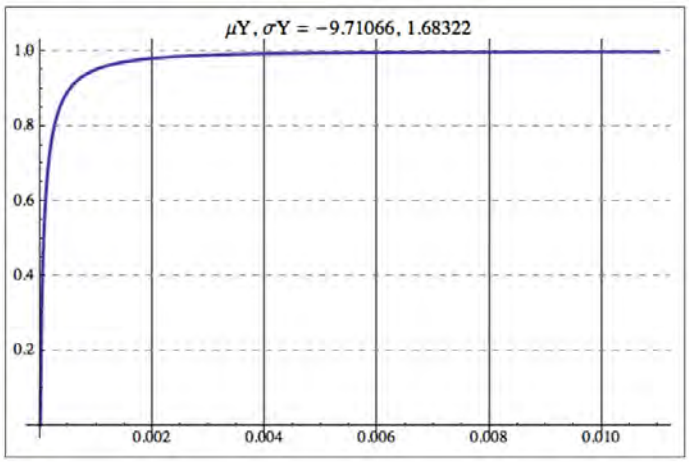

Figure 12. Probability of detecting curve example

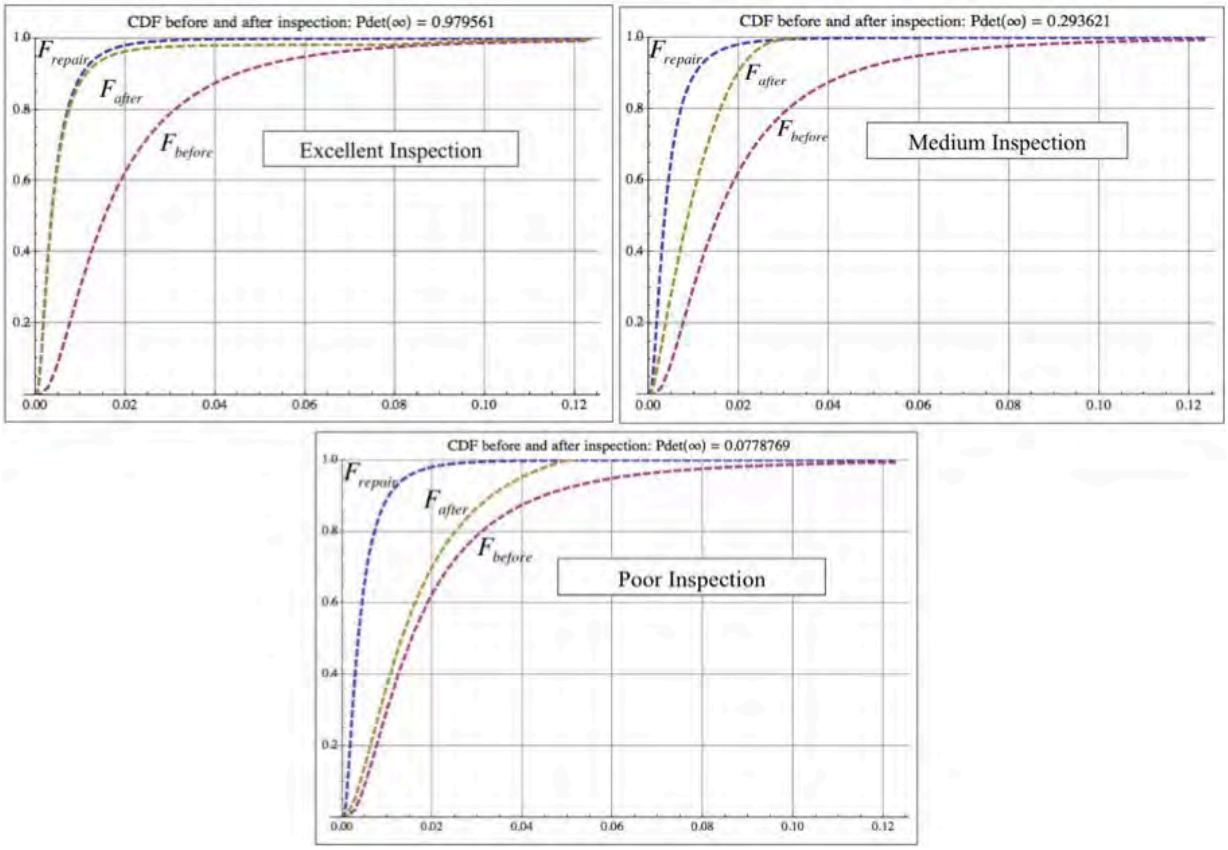

Figure 13. Inspection effect example

2.5 RANDOM VARIABLES

An overview of the random variables is presented in table 2. Further details for each random variable are presented in appendix A.

Table 2. Random variable classification

Variable	Description
Loading	Probabilistic – See Table 1 for more detail
Initial crack size	Probabilistic (lognormal distribution) Probabilistic (Weibull distribution) User input tabular deterministic
Fracture toughness	Probabilistic (normal distribution)
Crack growth parameters (C and m)	Probabilistic (binormal distribution)
Aircraft crack ratio	Probabilistic (normal distribution)
Yield and ultimate stress	Probabilistic (normal distribution)
Edge distance	Probabilistic (normal distribution)
Hole diameter	Probabilistic (normal distribution)
Probability of inspection	Probabilistic (lognormal distribution) User input tabular deterministic
Repair crack size	Probabilistic (lognormal distribution) Probabilistic (Weibull distribution) User input tabular deterministic
Probability of inspection	Deterministic

2.6 CRACK GROWTH OPTIONS

Three different options are available to perform crack growth analysis, as shown in table 3. The crack growth options are explained in detail.

Table 3. Crack growth methods

Method	Description
Master curve	- Representative spectrum - Two random variables can be used (initial crack size and fracture toughness) - Very computationally efficient
NASGRO® direct link	- Representative spectrum - Multiple random variables can be used - Very slow computationally
Kriging	- Representative spectrum - Multiple random variables can be used (initial crack size and fracture toughness) - Computationally efficient

2.6.1 Master Curve Approach

The master curve is a technique used to predict crack growth using a pre-existing crack growth curve and RS curve (master curve). The master curve methodology starts by selecting a very small initial crack size and a very large fracture toughness so that the master curve will span realizations used during the probability calculations (e.g., $a_0 = F_{a_i}^{-1}(0.00001), K_{C_0} = F_{Kc_i}^{-1}(0.9999)$).

Then, for random initial crack sizes and fracture toughness, the master curve can be interrogated to obtain the "*a* vs. *N*" and "*RS* vs. *N*" curves for any set of random initial crack size and fracture toughness. Note, however, that the master curve approach cannot be used if there are any random variables that affect the master curve (e.g., da/d*N* [crack growth rate] data, geometry data, etc.).

Figure 14 shows the basic procedure to establish the master curve and specific crack growth curve for a given realization of initial crack size. The procedure is explained step by step as follows (a similar procedure is used for the RS curve):

- Generate the "*a* vs. *N*" curve, starting with a small initial crack size and extending to a large crack size. This curve is set as the master curve (red curve).
- Generate a random realization for the initial crack size (a_i).
- Interpolate the corresponding value of life (N_i) corresponding to a_i from the master curve.
- Take the values of "*a*" greater than "a_i," with the corresponding values of "*N*" (green values over red curve), and shift the curve to the left (time zero) by subtracting the interpolated value, N_i, from the values of *N* from the master curve.
- The crack growth curve for the random realization, "a_i" is represented by the green dashed curve.

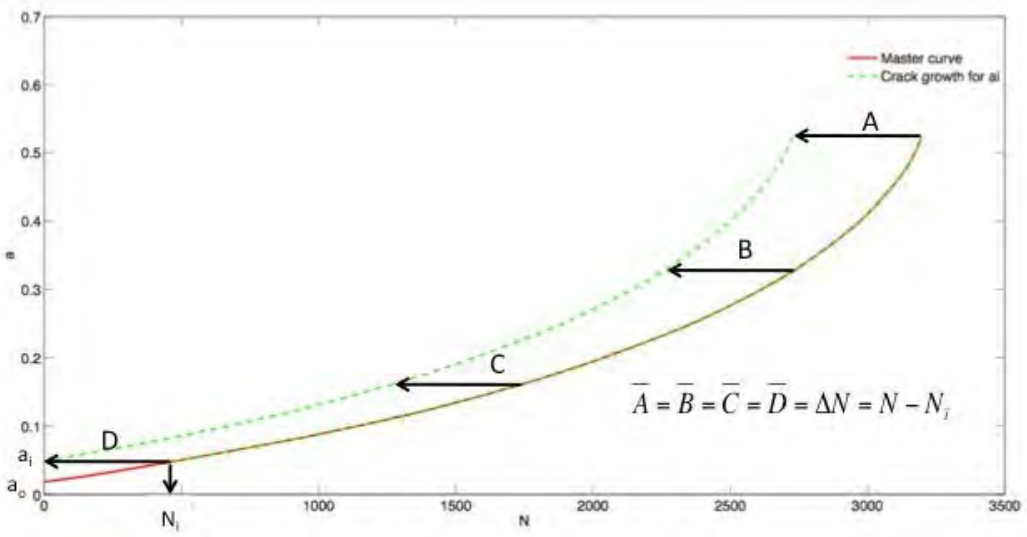

Figure 14. Master curve procedure

2.6.2 NASGRO Link

NASGRO [14] can be used to compute crack growth realizations (RS and crack size). The NASGRO link approach requires one template file (.flabat), one sample file (.sample), and the spectrum file (.spec or .bspec) to perform the crack growth realizations and return an .avsn file.

Four different files are involved with the NASGRO link process. Three of the files are input files to NASGRO (.sample, .spec/.bspec, and .flabat) and one file is an output file from NASGRO (.avsn). Figure 15 shows, schematically, the files involved in the NASGRO runs.

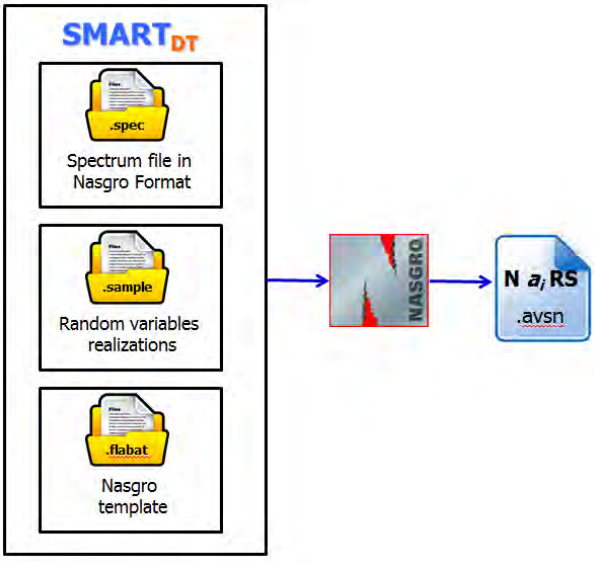

Figure 15. NASGRO link files schematic

Each one of the file types in Figure 15 is explained as follows:

The spectrum file: the loading generated using the methodology explained in section 1.1 needs to be transferred to NASGRO to perform the crack growth realizations. The loading file can be in ASCII format (.spec) or binary format (.bspec). The spectrum file is divided into four sections.
The first contains the file title and description. This section can contain multiple lines. The NASGRO parser scans until it finds the second part, which begins with the first line that contains double quotes (e.g., "S0" in table 4). This line lists the designation of stress quantities corresponding to the columns of data given in the fourth part. The designation is the same as those by NASGRO (i.e., S0, S1, S2, and S3). The stress quantity values are a function of the geometrical model to be analyzed in NASGRO. In general, S0 refers to the tension loading; S1 is the in-plane bending moment; S1 is the out-of-plane bending moment; and S3 is the pin loading [14]. The stress quantities are enclosed in pairs of double quotes. For example, if there is one set of data columns representing S0, then line 2 is listed as "S0." If there are two sets of data columns representing S0 and S3, then line 2 becomes "S0" "S3."

The spacing among the pairs of double quotes can be anything except a double quote. NASGRO determines how many stress quantities, defined by their pairs of double quotes, confirm the content within pairs of double quotes for the NASGRO stress quantities (S0, S1, S2, and S3) and ignores whatever is filled between the sequential pairs. Moreover, this assignment sequence of stress quantities basically defines how the columns of data are provided in the fourth part. So, for example, if two stress quantities are defined, with S3 to be the first and S0 to be the second, the assignment of stress values from the columns of data in the fourth part will become S3 (t1) and S3 (t2), followed by S0 (t1) and S0 (t2).

The third section is one single line with pairs of double quotes. This line describes how to fill in all other stress quantities that are not listed in the second part. The content needs to be enclosed by a pair of double quotes. For example, "S3=0.0" "S1=0.2*S0." If this line is missing, the stress quantities not defined by the second part are assigned with a default value equal to zero.

The content refers to the stress quantities not listed in the second part. For example, if stress quantities S0 and S1 are indicated in the second part, the referred stress quantities should be S2 and/or S3.

The content enclosed in the pair of double quotes must have an equal sign as a separator. The left side of the separator (i.e., the equal sign) designates the stress quantity that has not been listed in the second part. For example, "S1=0.75" assigns 0.75 to the S1 stress quantity and the parser will ensure this stress quantity has not been referred in the second part. The right side of the separator describes the value assigned to the stress quantity on the left side. For example, "S1=0.75" assigns 0.75 to the S1 stress quantity. A simple feature is provided for users to specify the assignment in scale. For example, "S2=0.3*S0" assigns the 30% of S0 to S2.

The scaled assignment needs to be in terms of the stress quantities in the second part. The NASGRO parser recognizes only the symbol "*" for the math/multiplication operation in the scaled assignment. If something else is provided, an error will be issued and the computation will

be terminated. If a fixed value is given on the right-hand side, then this value is assigned to all time points (both max. and min.) for the given stress quantity.

In this part, the sequence of assigning the stress quantities is irrelevant. For example, the assignment from "S2=0.75" "S1=0.1*S3" is the same as this assignment: "S1=0.1*S3" "S2=0.75."

The fourth section contains the columns of data in subsequent lines (one group of lines per flight). That is:

Flight number number of steps in the flight
Number of cycles in step 1 Si (t1) Si (t2) Sj (t1) Sj (t2), etc.
Number of cycles in step 2 Si (t1) Si (t2) Sj (t1) Sj (t2), etc.

where the total number of columns is 1 + (2 × the number of stress quantities listed in the second part), and there is one line for each step in the flight.

Three different example spectra are shown in Table 4–6. The first example, shown in Table 4, uses the first four lines for title and description. The second part indicates that the columns of data defined in the fourth part are for the S0 stress quantity. Because the third part is not defined, the other three stress quantities, S1, S2, and S3, are zero by default.

Table 4. Spectrum file: example 1

```
Example input file #1 with two flights and only one non-zero stress quantity
Example input file #1 with two flights and only one non-zero stress quantity
Example input file #1 with two flights and only one non-zero stress quantity
Example input file #1 with two flights and only one non-zero stress quantity
 "S0"
1       6
2       16.5    10.3
5       20.4    5.5
1       10.4    2.2
10      17.3    3.6
1       11.4    4.4
3       15.2    2.7
2       4
10      13.2    1.1
3       10.6    6.6
1       14.2    5.5
10      13.2    1.1
```

The second example, shown in table 5, uses the first single line for title and description. The second part indicates that the columns of data given in the fourth part are for the S0 and S3 stress quantities—that is, in respective order, S0 (t1), S0 (t2), S3 (t1), and S3 (t2). The third part specifies that all values (both at t1 and t2) for the S2 stress quantity are given by a specific value: 1.1. The S1 stress quantity, because it is not defined, is zero by default.

Table 5. Spectrum file: example 2

```
Example input file #3 with two flights and two non-zero stress quantities
“S0”    “S3”
“S2=1.1”
1       6
2       16.5    10.3    4.4     1.1
5       20.4    5.5     6.6     1.2
1       10.4    2.2     7.1     1.1
10      17.3    3.6     9.3     4.4
1       11.4    4.4     6.6     3.5
3       15.2    2.7     14.1    3.2
2       4
10      13.2    1.1     4.9     0.2
3       10.6    6.6     6.6     1.6
1       14.2    5.5     5.3     1.6
10      13.2    1.1     4.9     0.2
```

The third example, shown in table 6, uses the first three lines for title and description. The second part indicates that the columns of data given in the fourth part are for the S0 and S3 stress quantities. The third part specifies that the value for S2 is always given by a specific value: 1.1. The value for S1 is 70% of S3.

Table 6. Spectrum file: example 3

```
Example input file #4 with two flights and two non-zero stress quantities
Example input file #4 with two flights and two non-zero stress quantities
Example input file #4 with two flights and two non-zero stress quantities
“S0”    “S3”
“S1=0.7*S3” “S2=1.1”
1       6
2       16.5    10.3    4.4     1.1
5       20.4    5.5     6.6     1.2
1       10.4    2.2     7.1     1.1
10      17.3    3.6     9.3     4.4
1       11.4    4.4     6.6     3.5
3       15.2    2.7     14.1    3.2
2       4
10      13.2    1.1     4.9     0.2
3       10.6    6.6     6.6     1.6
1       14.2    5.5     5.3     1.6
10      13.2    1.1     4.9     0.2
```

The sample file: the sample file is generated internally by the SMART code and comprises two sets of data. The first set is for RS computation (the RS computation is explained in detail in the .avsn file section) and the second set lists, line by line, the sampling parameters and their sampled

values. The file is in a text format. The first line in the file is the comment line, which is ignored by the parser. From the second to the ninth lines, data are arranged in two-column format, where the first column, or the keyword column, designates the keyword and the second column specifies its value. Table 7 lists the description of this section. Note the parser is not case sensitive to the keywords or their values.

Table 7. Keywords and their values specified in sample file for RS computation

Line	Keyword	Value Type	Keyword Description
2	NfMax	Real number	Maximum flight number calculation on the .avsn file
3	OpSec	Character string (e.g., T10 or B10)	T10: output interval every 10 flights in text format. B10: output interval every 10 flights in binary format
4	RS	Two characters designating reference stress	Select one from the stress quantities: 'S0', 'S1', 'S2', or 'S3' as reference stress to compute RS in equation 19
5	RSv0	Real number	Value of S0 reference stress
6	RSv1	Real number	Value of S1 reference stress
7	RSv2	Real number	Value of S2 reference stress
8	RSv3	Real number	Value of S3 reference stress
9	NSY basis	Character string designating the basis for Net Section Yielding (NSY)	Select one of the stresses as the basis for NSY computation: Sy (yield stress), Sult (ultimate stress), or Sflow (flow stress)

The second set for sampling parameters starts from the tenth line. It's the label line for sampling parameters. Following that, the data lines list all of the parameterized values corresponding to the labeled columns line by line and one set at a time. The label IDs for the variables that can be parameterized are listed in Table 8 for a two-dimensional crack defined by its depth, "*a*," and length, "*c*". In addition, although the parser is not case sensitive to the label IDs, it is case sensitive to the file names (e.g., the filename for load spectrum).

Table 8. Variables available for parameterization in the interface implementation

Label ID	Description
Run	Sampling number ID; must be in sequence
ai	Initial length of "*a*"
ci	Initial length of "*c*"
aoci	Initial crack shape aspect ratio: aircraft
Paris_m	The slope of Paris type of FCG equation
Paris_C	The coefficient of Paris type of FCG equation
Fract_tough	Plan strain fracture toughness (K1c)
Hole_diam	Diameter of the hole
Edge_Dist	Hole Edge distance
Sy	Yield stress
Sult	Ultimate stress
Spectrum_file	The filename for load spectrum

The template file is a NASGRO FLABAT file and provides the basic parameters required to perform a NASGRO NASFLA analysis deterministically.

The .avsn file contains the results from NASGRO in terms of flight number, crack size, and RS calculations for failure defined by net section yielding and fracture. The following bullets describe the NASGRO .avsn output file that is used in SMART to perform POF calculations with and without inspections.

The crack depths with four crack tips will be included. The four tips are designated as a-, c-, a1-, and c1- based on NASGRO nomenclature, as shown in Figure 16.

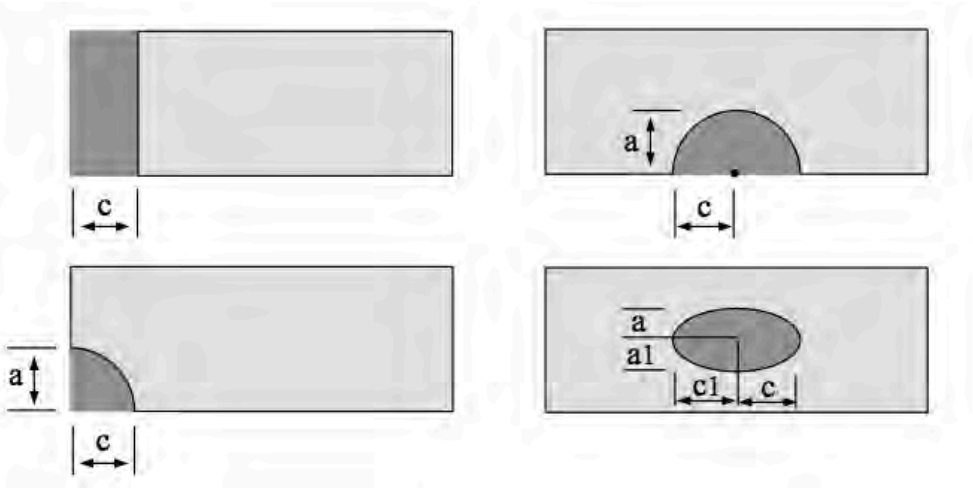

Figure 16. NASGRO crack tips schematic

- The first column designates the flight number, according to user-specified output interval, provided on the .sample file. Its numerical value is an integer and should exist until the last output cycle.
- The second to the fifth columns designate the crack depths with four tips. The crack tips are designated as a-, c-, a1-, and c1-.

    - These parameters are real numbers.
    - For non-applicable crack tips, their crack lengths are denoted by an 'x'.
    - Because of crack transition — for example, from a surface crack to a corner crack — some crack tips may become non-applicable. It means that, although the crack depth of a crack tip may be available at the beginning, after a certain number of flight cycles, some crack tips may become unavailable.

- The sixth column designates the RS. Its numerical value is always in reference to the crack tip(s) that survives to the last flight cycle. If there is more than one crack tip at the last flight cycle, the first survived crack tip from the list of a-, c-, a1-, and c1 -tips will be used. If paired crack tips are available, the averaged crack depths will be used. The following scenarios are used to illustrate how the reference crack depth is selected in determining the RS.

    - Only c-tip survives: The crack depth with this c-tip is used.
    - Only a- and c-tips survive: This is not the paired scenario. The crack depth with the a-tip is used.
    - Only a- and a1- tips survive: This is the paired scenario. The averaged crack depth from a- and a1- tips is used.
    - All four tips survive: The averaged crack depth from a- and a1- tips is used.

The RS calculations contained in the .avsn file are computed by NASGRO using information from two sources. An example of AVSN parameters are also provided in table 9.

Table 9. AVSN, schematically, example

Flt_no	a	c	a1	c1	RS_by_Kc	RS_by_NSY
Integer	Real	Real	Real	Real	Real	Real
Integer	Real	Real	Real	Real	Real	Real
Integer	Real	x	Real	Real	Real	Real
	...	...	...	...	...	...
Integer	Real	x	x	Real	Real	Real
Integer	Real	x	x	x	Real	Real
	...	...	...	...	...	...
Integer	Real	x	x	x	Real	Real
Integer	Real	x	x	x	Real	Real

The first source is from the .OUT2 output file from NASGRO; if the .OUT2 file exits, this signifies that the NASFLA analysis is complete. The information extracted from .OUT2 files is listed as follows:

- F0, F1, F2, and F3 for RS by fracture
- G0, G1, G2, and G3 for RS by NSY

These quantities are determined during FCG analysis for stress intensity factors, K, and net section stress, S, resulting from combined stress quantities. Their respective definitions are given by [14]:

$$K = \left(S_0 F_0 + S_1 F_1 + S_2 F_2 + S_3 F_3\right)\sqrt{\pi c} \tag{18}$$

$$S = S_0 G_0 + S_1 G_1 + S_2 G_2 + S_3 G_3 \tag{19}$$

The second source is from the design or limit values collected from the sample file (Table 7). Respectively, they are:

- The stress quantity to be used as the reference stress. It needs to be one of available stress quantities: S_0, S_1, S_2, and S_3, with the crack model. The computed RSs will be in reference to the specified reference stress quantity.

- The design stress with stress quantities and design toughness for fracture (i.e., $\left(S_0\right)_{design}$, $\left(S_1\right)_{design}$, $\left(S_2\right)_{design}$, $\left(S_3\right)_{design}$, and $\left(K_C\right)_{design}$). These are separate quantities, which are different from those provided in the NASGRO FLABAT file, such as those in the stress spectrum definition. The concept is similar to the design limit stress so that it designates the maximum allowed stress for a component.

- The basis for the NSY criterion. It can be yield stress, flow stress, or ultimate stress, whichever value is available in the FLABAT file. This value is designated by S_n in the following equation for RS_{NSY}, RS by NSY. Therefore, S_n can be σ_y, σ_{flow}, or σ_{ult}.

Using S_0 as a reference stress, the RS defined by fracture is computed using the following equation [14]:

$$RS_{fracture} = \frac{(K_C)_{Design}}{\left(F_0 + F_1 \frac{(S_1)_{design}}{(S_0)_{design}} + F_2 \frac{(S_2)_{design}}{(S_0)_{design}} + F_3 \frac{(S_3)_{design}}{(S_0)_{design}}\right)\sqrt{\pi c}} \tag{20}$$

and the RS by NSY is given by [14]:

$$RS_{NSY} = \frac{S_n}{\left(G_0 + G_1 \frac{(S_1)_{design}}{(S_0)_{design}} + G_2 \frac{(S_2)_{design}}{(S_0)_{design}} + G_3 \frac{(S_3)_{design}}{(S_0)_{design}}\right)} \tag{21}$$

Finally, table 10 lists the crack types supported by the NASGRO interface. Reference [14] shows the different crack-type model geometries.

Table 10. Supported crack types

Crack type	Description
TC: through-thickness crack	
TC01	Through crack at center of plate
TC02	Through crack at edge of plate
TC03	Through crack at hole (offset) in plate
TC04	Through crack at hole in lug
TC05	Through crack(s) at hole in plate with row of holes
TC08	Through crack (circumferential) in hollow cylinder
TC11	Through crack (offset) in plate – univariant weight function
TC12	Through crack at edge of plate – univariant weight function
TC13	Through crack(s) at hole (offset) in plate – univariant weight function
TC17	Through crack at edge notch in plate – univariant weight function
TC18	Through crack(s) at (offset) embedded slot or elliptical hole in plate – univariant weight function
TC19	Through crack at hole (offset) in plate with broken ligament – univariant weight function
TC23	Two unequal through cracks at offset hole
CC: corner crack	
CC01	Quarter elliptical corner crack in plate
CC02	Quarter elliptical corner crack at hole (offset) in plate
CC03	Quarter elliptical corner crack at hole in lug
CC04	Quarter elliptical corner crack(s) at hole in plate
CC08	Quarter elliptical corner crack(s) at hole (offset) in plate – univariant weight function
CC09	Quarter elliptical corner crack in plate – bivariant weight function
CC11	Quarter elliptical corner crack in plate – univariant weight function
CC13	Quarter elliptical corner crack at edge notch in plate
CC14	Quarter elliptical corner crack at (offset) embedded slot or elliptical hole in plate
CC15	Quarter elliptical corner crack at (offset) hole in plate with broken ligament
SC: surface crack	
SC01	Semi-elliptical surface crack in plate
SC02	Semi-elliptical surface crack in plate – univariant weight function
SC05	Semi-elliptical surface crack (circumferential) in hollow cylinder
SC07	Semi-elliptical surface crack (circumferential) in solid cylinder
SC17	Semi-elliptical surface crack (offset) in plate – univariant WF
SC19	Semi-elliptical surface crack (offset) in plate – bivariant WF

Further details about the link between the probabilistic DT code and NASGRO are provided in appendix B.

2.6.3 Kriging Metamodeling

A Kriging surrogate model is incorporated into the code to have multiple random variables and be able to perform POF calculations possessing some level of mathematical efficiency..

Kriging is an interpolation technique that is a type of spatial statistical method that started in the geosciences. This technique was originally developed by a South-African mining engineer named D.G. Krige in the 1950s. Krige improved his method in the 1960s in collaboration with G. Matheron, a French mathematician.

Kriging is a linear approximation method that can provide predictions of unknown values of a random function, field, or process [15]. The predictions are the best linear unbiased estimators under the Kriging assumptions presented later in this section. Moreover, the Kriging predictions are weighted linear combinations of observed data (known as training data or training points). It is assumed by Kriging that the closer the training data are in the random variable space, the more positive correlation exists among the data. Mathematically, the correlation between the data is modeled by a second-order stationary covariance process (the expectations of the observations are constant and do not depend on the location in random variable space). The covariances between the observations depend only on the distances between the corresponding inputs. More specifically, the covariances decrease when the distance between the observations increases. The result is an estimated metamodel, such that observations closer to the prediction point get more weight in the predictor. When predicting the output at the observed (training) point, the prediction equals the observed value [15].

2.6.3.1 Ordinary Kriging

An introduction to ordinary Kriging is presented below. Let $\{x_1, x_2, ..., x_n\}$ be the locations or training points contained in the space R with k dimensions $(\mathbf{x} \in R^k)$, with observed data $\{z(x_1), z(x_2), ..., z(x_n)\}$. It is assumed that the set of data is a realization of a stochastic process $Z(\cdot)$.

In ordinary Kriging, it is assumed that the process generated by the data obeys the relation:

$$Z(\mathbf{x}) = \mu + \delta(\mathbf{x}) \tag{22}$$

where μ is a non-random constant and $\delta(\mathbf{x})$ is a zero-mean spatial stochastic function (i.e., $E(\delta(\mathbf{x})) = 0$). The covariance, $COV(\cdot)$, between two different locations depends only on the distance between the two points through the function $C(\cdot)$, called the covariogram, defined as:

$$COV(\delta(\mathbf{x}_i), \delta(\mathbf{x}_j)) = C(x_i - x_j) \tag{23}$$

Kriging assumes the predictor, $\hat{Z}(x_0)$, at an arbitrary point $x_0 \in R^k$ to be in the form of:

$$\hat{Z}(x_0) = \sum_{i=1}^{n} \lambda_i Z(x_i) \tag{24}$$

where λ_i is the weight for training point i and the weights satisfy the constraint:

$$\sum_{i=1}^{n} \lambda_i = 1.0 \tag{25}$$

where n represents the number of training points. Equation 24 is only true if process Z is intrinsically stationary. "Intrinsically stationary" means that $\Pr(Z(x_i)<z)$ does not depend on x and the variation of the values at two spatial points only depends on the distance between the points.

Under the assumptions presented in equations 24 and 25, the goal of Kriging is to find the best predictor $\hat{Z}(x_0)$. To accomplish this, the weights λ_i are obtained by minimizing the mean square error of the predictions. Defining the mean-squared prediction error as:

$$\hat{\sigma}^2 = E\left[\left(Z(x_0) - \hat{Z}(x_0)\right)^2\right] \tag{26}$$

$\hat{\sigma}^2$ is minimized with the restriction expressed by equation 25.

The Kriging predictions are weighted linear combinations of previously observed (training points) data, as shown schematically in Figure 17.

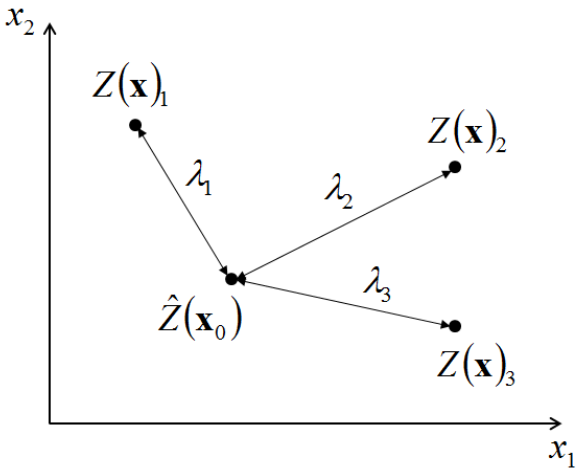

Figure 17. Kriging schematic

The Kriging prediction will, therefore, constitute a BLUE (Best Linear Unbiased Estimator) of the underlying process $Z(\mathbf{x})$. Using a Lagrange's multiplier $2m$, the Lagrange's function, L, is defined as:

$$L(x_0) = E\left[\left(Z(x_0) - \hat{Z}(x_0)\right)^2\right] - 2m\left(\sum_{i=1}^{n}\lambda_i - 1.0\right) \tag{27}$$

Replacing the predictor $\hat{Z}(x_0)$ in equation 27 from equation 24, yields:

$$L(x_0) = E\left[\left(Z(x_0) - \sum_{i=1}^{n}\lambda_i Z(x_i)\right)^2\right] - 2m\left(\sum_{i=1}^{n}\lambda_i - 1.0\right) \tag{28}$$

Equation 28 can be expanded to:

$$L(x_0) = E\left[(Z(x_0))^2\right] - 2\cdot E\left[Z(x_0)\cdot\sum_{i=1}^{n}\lambda_i Z(x_i)\right] + E\left[\left(\sum_{i=1}^{n}\lambda_i Z(x_i)\right)^2\right] - 2m\left(\sum_{i=1}^{n}\lambda_i - 1.0\right) \tag{29}$$

Taking the constants λ_i outside the expected values, equation 29 becomes:

$$L(x_0) = E\left[(Z(x_0))^2\right] - 2\cdot\sum_{i=1}^{n}\lambda_i E\left[Z(x_0)\cdot Z(x_i)\right] + \sum_{i=1}^{n}\sum_{j=1}^{n}\lambda_i\lambda_j E\left[Z(x_i)\cdot Z(x_j)\right] - 2m\left(\sum_{i=1}^{n}\lambda_i - 1.0\right) \tag{30}$$

In Kriging, the covariance is defined as $\mathrm{C}(x_i - x_j) = E\left[\left(Z(x_i)\cdot Z(x_j)\right)\right]$ and the link between the variogram and covariance is given by $2\gamma(x_1 - x_2) = Var(Z(x_1) - Z(x_2)) = 2(C(0) - C(x_1 - x_2)) = 2C(h)$. Using the two statistical definitions above, equation 29 can be written in terms of the semi-variogram as:

$$L(x_0) = \gamma(x_0 - x_0) - 2\sum_{j=1}^{n}\lambda_i\gamma(x_0 - x_j) + \sum_{i=1}^{n}\sum_{j=1}^{n}\lambda_i\lambda_j\gamma(x_i - x_j) - 2m\left(\sum_{i=1}^{n}\lambda_i - 1.0\right) \tag{31}$$

The semi-variogram is discussed in more detail in section 3.1.5.

The $n+1$ unknowns (λ_i, m) can be determined by differentiating equation 31 with respect to $\lambda_1 ... \lambda_n, m$ and equating the results to zero. That is:

$$\frac{\partial L}{\partial \lambda} = 2\sum_{j=1}^{n} \lambda_j \gamma(x_i - x_j) - 2\gamma(x_0 - x_j) - 2m = 0 \tag{32}$$

$$\frac{\partial L}{\partial m} = -2\sum_{j=1}^{n} \lambda_j + 2 = 0 \tag{33}$$

The system of equations can be solved more easily using linear algebra by defining the following vectors and matrices:

$$\lambda_0 = \begin{pmatrix} \lambda_1 \\ \lambda_2 \\ \vdots \\ \lambda_n \\ m \end{pmatrix} \equiv \begin{pmatrix} \boldsymbol{\lambda} \\ m \end{pmatrix},$$
$$\gamma_0 = \begin{pmatrix} \gamma(x_0 - x_1) \\ \gamma(x_0 - x_2) \\ \vdots \\ \gamma(x_0 - x_n) \\ 1 \end{pmatrix} \equiv \begin{pmatrix} \boldsymbol{\gamma} \\ 1 \end{pmatrix}, \tag{34}$$

and

$$\Gamma = \begin{bmatrix} \gamma(0) & \gamma(x_1 - x_2) & \cdots & \gamma(x_1 - x_n) & 1 \\ & \gamma(0) & \cdots & \gamma(x_2 - x_n) & 1 \\ & & \ddots & & 1 \\ & & & \gamma(0) & 1 \\ \text{symm} & & & & 0 \end{bmatrix}. \tag{35}$$

Therefore, the optimal $\lambda_1 ... \lambda_n, m$ can be obtained from solving the equation:

$$\lambda_0 = \Gamma^{-1} \gamma_0 \tag{36}$$

The matrix Γ only depends on the training points and γ_0 depends on the training points and predictor point.

The ordinary Kriging estimate and Kriging variance at x_0 are given by:

$$\hat{Z}(x_0) = \sum_{i=1}^{n} \lambda_i Z(x_i). \tag{37}$$

$$\hat{\sigma}^2 = \lambda_0 \gamma_0 = \sum_{i=1}^{n} \lambda_i \gamma(x_0 - x_i) + m. \tag{38}$$

The 95% confidence bound from the prediction can be computed as:

$$A \equiv (A_{LB}, A_{UB}) \equiv \left(\hat{Z}(x_0) - 1.96\sigma_\varepsilon(x_0), \hat{Z}(x_0) + 1.96\sigma_\varepsilon(x_0)\right) \tag{39}$$

2.6.3.2 Kriging Semi-Variogram

In Kriging, the semi-variogram $\gamma(h)$ is unknown and needs to be estimated from the data, where $h = (x_i - x_j)$ is called the lag. Note that $\gamma(-h) = \gamma(h)$ and $\gamma(0) = 0$. The semi-variogram is the mathematical representation of the relationship between the semi-variogram and lag. The semi-variogram is the measurement of the degree of spatial dependence between the sample points at different locations, whereas the lag is the Euclidean distance between two sample points. A common practice is to estimate the semi-variogram using the equation:

$$2\hat{\gamma}(h) = \frac{1}{|N(h)|} \sum_{N(h)} \left(Z(x_i) - Z(x_j)\right)^2, \quad h \in \mathrm{R}^k \tag{40}$$

where $N(h) \equiv \{(x_i, x_j) : x_i - x_j = h, i, j = 1,2,3,...,n\}$ and $|N(h)|$ is the number of distinct pairs in $N(h)$. We notice that $N(-h) \neq N(h)$, although $2\hat{\gamma}(-h) = 2\hat{\gamma}(h)$.

To compute the variogram, one calculates the lag associated with each of the sample points, groups all the pairings having identical lags, and computes the semi-variance corresponding to each lag grouping using equation 40.

After computing the experimental variogram, one selects and fits the theoretical variogram using a parameter-estimation technique, such as least-squares estimation [16, 17] or the maximum-likelihood estimation (MLE) [16, 17].

There exist several theoretical variograms in the literature. The following equations present some of the variograms available in the literature. The variogram plays an important role in Kriging because the variogram is employed to generate the elements on the semi-variance matrix (Γ) and vector (γ_0). Five common variogram models follow [18]:

$$\text{Exponential}: \quad \gamma(h) = c \cdot \left(1 - \exp\left(-\frac{h}{\theta}\right)\right) \tag{41}$$

$$\text{Gaussian}: \quad \gamma(h) = c \cdot \left(1 - \exp\left(-\frac{h^2}{\theta^2}\right)\right) \tag{42}$$

$$\text{Spherical}: \quad \gamma(h) = c \cdot \left(\frac{3}{2}\frac{h}{\theta} - \frac{1}{2}\frac{h^3}{\theta^3}\right), \text{for } 0 \le h \le \theta \tag{43}$$

$$\text{Cubic}: \quad \gamma(h) = c \cdot \left(7\frac{h^2}{\theta^2} - \frac{35}{4}\frac{h^3}{\theta^3} + \frac{7}{2}\frac{h^5}{\theta^5} - \frac{3}{4}\frac{h^7}{\theta^7}\right), \text{for } 0 \le h \le \theta \tag{44}$$

$$\text{Matern}: \quad \gamma(h) = \frac{1}{2^{\nu-1}\Gamma(\nu)}\left(\frac{2\nu^{1/2}h}{\theta}\right)^{\nu} \kappa_{\nu}\left(\frac{2\nu^{1/2}h}{\theta}\right) \tag{45}$$

In each of the functions above, the parameter θ is called the range parameter or correlation length. It describes the rate of decay of the correlation function with respect to the distances between the locations. A small value of the correlation length, θ, is an indication of small spatial correlation and a rapid spatial variation. The parameter θ is the distance beyond which the responses cease being significantly related. For larger values of the correlation length, predictions are more dependent on the responses of the neighboring points. The parameter *c* represents the limit of the semi-variogram value as the lag increases; it is known as the scaling parameter. Additional theoretical variograms are presented in [19].

The MLE is used to estimate the correlation function parameter $\boldsymbol{\theta}$ that is consistent with the experimental variogram data. MLE assumes that the observations have a known distribution shape (one of the five variogram models given by equations 41–45) [20].

The variogram parameters can be estimated by maximizing the likelihood function shown in equation 46.

$$\ell(\theta \mid \mathbf{Z}) = p(\mathbf{Z} \mid \theta) = \prod_{i=1}^{n} p(z_i \mid \theta) \tag{46}$$

2.6.3.3 Steps to Perform Kriging

The steps to perform Kriging are summarized below:

1. Obtain the training points.
2. Using the training points, create the experimental and theoretical variograms.

    a. Compute the experimental variogram.

        i. The lag $\left(h_{i,j}\right)$ between each training point is computed and the pairs having similar lags are grouped. Mirrored pairs are ignored because $h_{i,j}$ is the same as $h_{j,i}$.

        ii. The semi-variance associated with each group can be computed using equation 40.

    b. Using the experimental variogram data, compute the optimal parameters θ and *c* on a selected theoretical variogram using a parameter estimation technique such as MLE.

3. Compute the lag matrix $\left[\left|\boldsymbol{x}_i - \boldsymbol{x}_j\right|\right]$ and lag vector $\left(\left|x_i - x_0\right|\right)$.
4. Compute the semi-variance matrix $[\Gamma]$ and vector $\left(\gamma_0\right)$.
5. With the semi-variance matrix and vector computed, the Kriging weights can be computed as $\left(\lambda_0 = \Gamma^{-1}\gamma_0\right)$.
6. Predict the values at the unknown points using equation 37.
7. Compute the Kriging variance (error) using equation 38.

2.6.3.4 Adaptive Kriging Surrogate Model for Crack Growth and RS Calculations

The classical statement of the problem is to determine the crack growth as a function of cycles by integrating the equations for the crack growth rate — that is, by solving a set of coupled first-order differential equations [14]:

$$\begin{aligned} \frac{\partial a}{\partial N} &= f\left(\Delta K, R, K_C, K_{th}, a, c\right), \\ \frac{\partial c}{\partial N} &= f\left(\Delta K, R, K_C, K_{th}, a, c\right). \end{aligned} \tag{47}$$

In equation 47, the crack growth rate is a function of the stress intensity factor, ΔK; the stress ratio, R; the fracture toughness, K_C; the stress intensity threshold, K_{th}; the initial crack sizes, a and c; and other random variables, depending on the crack growth model.

To achieve the accuracy and computational speed needed for a probabilistic analysis, fracture mechanics software (e.g., NASGRO), in combination with an error-based Kriging surrogate model, can be used as the crack growth engine.

As explained in the previous section, the formulation of a Kriging approach is composed of several steps. First, sample points (called training points) are selected. A sample point is composed of a specific combination of the random variables as well as their corresponding fracture mechanics results. After the sample points are collected, the corresponding metamodeling coefficients are computed.

Figure 18 shows the surrogate model process schematically. It is explained as follows:

1. Initial realizations of the random variables are produced and the initial training points are generated using the crack growth software.
2. The response surfaces for RS and initial crack size at each of the user-defined times are constructed based on the initial training points.

The following steps are constructed for the Monte Carlo sampling analysis at each time point, *t*. More details about the time dependence are presented in section 2.6.3.5 .

3. A new realization of the random variables is generated.
4. The surrogate models for the RS and crack size are evaluated for the random realizations generated in step 3.
5. The error given by the two Kriging surrogate models (RS and crack size) is compared against a user-defined threshold error (section 2.6.3.6).
6. If either error (RS or crack size) is not acceptable, the random realization generated in step 3 is evaluated using the crack growth software, and the response surfaces are updated with the new training point.
7. If both errors (RS and crack size) are acceptable, the process is repeated for the next realization.
8. Steps 3–5 are repeated for the given number of samples.
9. The SFPOF, hazard, and CTPOF is computed for the total number of samples.

The crack size surrogate models are evaluated only when inspections are required. The crack size responses that have failed are removed from the analysis. Failure is defined as the RS value that is smaller than the maximum applied stress, as explained in section 2.3 . For this reason, the crack size surfaces are evaluated after the RS surfaces to check for the failure points.

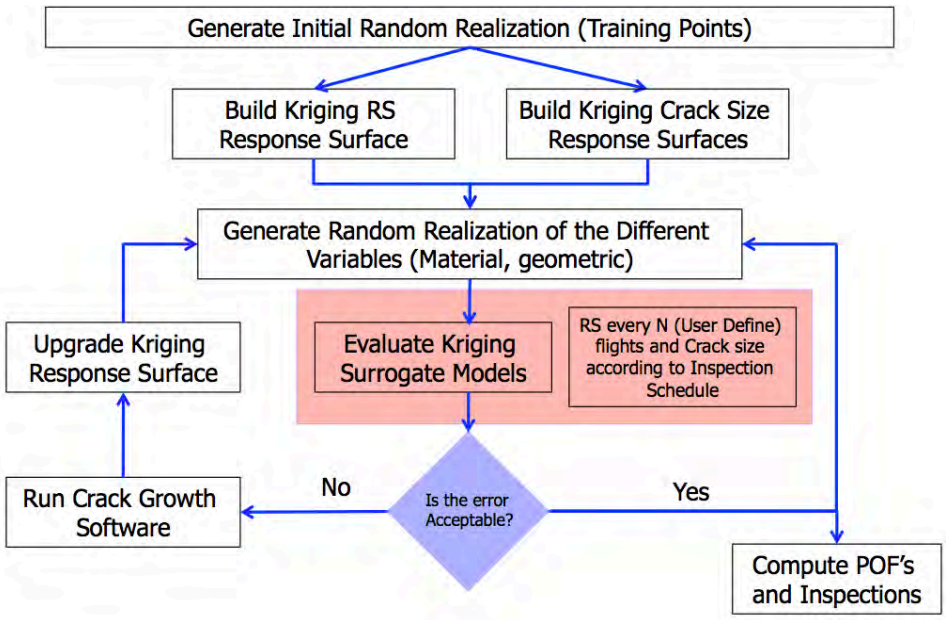

Figure 18. Surrogate model flowchart

2.6.3.5 Kriging and Crack Growth Time Dependency

Crack growth analysis is a time-dependent process. Based on the random variables (initial crack size, fracture toughness, Paris constants, etc.), cracks will grow and the RS will decrease as a function of time. To account for the time dependency in the surrogate model, the code creates different Kriging surfaces through time.

The time-dependent process can be summarized as follows:

1. The Kriging surfaces are created for each time step (the process to create the Kriging surfaces is explained in the previous section):

    a. For the RS, RS Kriging surfaces are created as a function of the random variables at each time step requested by the user (the user selects the time frequency in which the probabilities of failure need to be computed, as explained in section 2.6.2). A schematic is shown in Figure 19, with user-defined time = *2000*).
    b. If an inspection occurs at time, t, crack size Kriging surfaces are created as a function of the random variables at each inspection point, as shown schematically in Figure 20 for two inspections (*t=3000* and *t=10,000*).
    c. The surfaces (crack sizes and RSs) are built using only the samples that survive to that time (samples that failed at a previous time are removed from the surfaces). Figure 21 shows the number of training points for the two Kriging surfaces presented in Figure 19 at the two inspection points. It can be seen in Figure 21 that the green and blue points already failed (see points illustrated with an "x" in Figure 21); therefore, the samples were removed from the Kriging surface at inspection 2 and will not be used to train the surface at inspection 2.

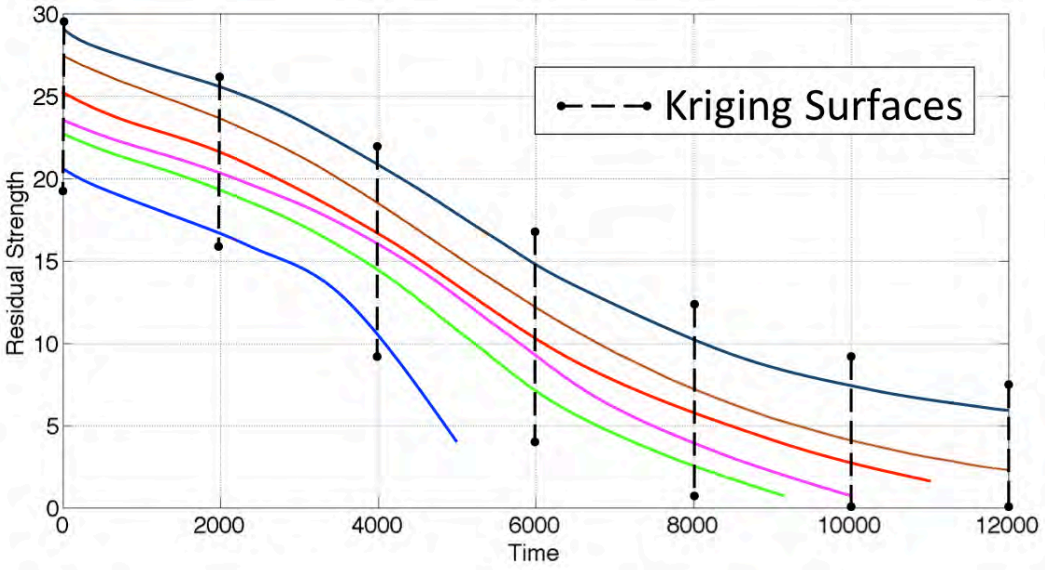

Figure 19. RS Kriging surfaces

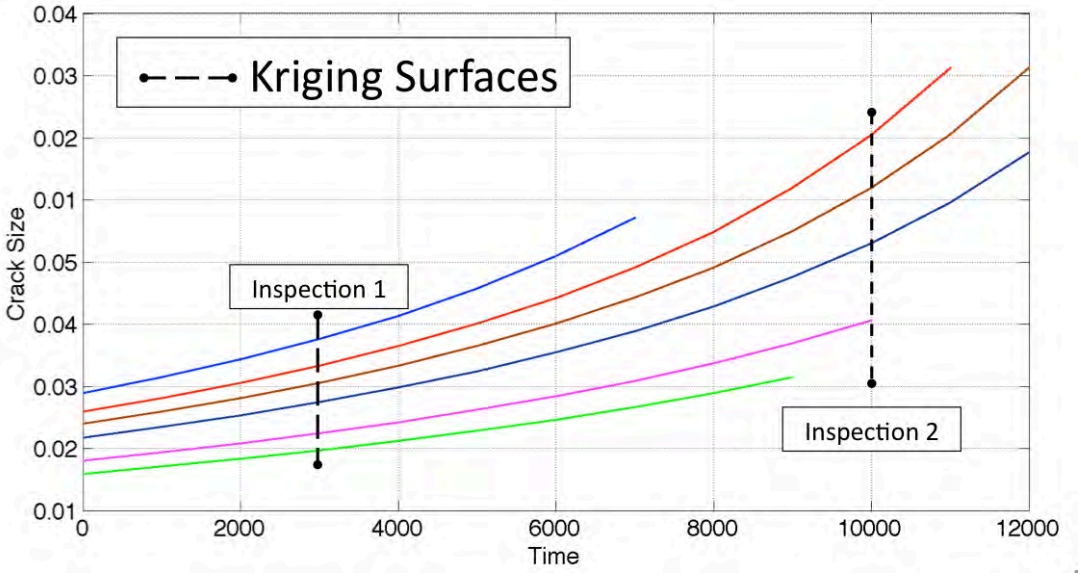

Figure 20. Inspection Kriging surfaces

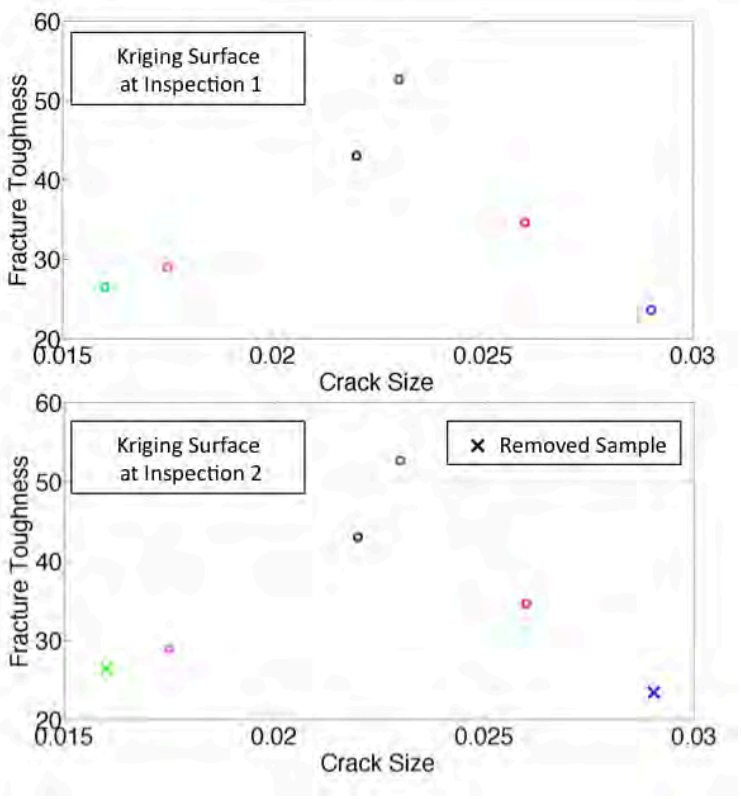

Figure 21. Training point at two different Kriging surfaces

2. Kriging is performed for both surfaces created in step 1 for every random realization.
3. For each random realization, the RS Kriging predictions are tested for failure using the EVD explained in section 2.3 . The sample is assumed failed when the POF exceeds 0.99 ($p_f > 0.99$), as shown in the following equations and, schematically, in Figure 22.

$$p_f = 1 - F_{EVD}(RS_t) \tag{48}$$

$$1 - F_{EVD}(RS_t) = 0.99 \tag{49}$$

$$RS_{CR}(t_I) = F^{-1}{}_{EVD}(0.01) \tag{50}$$

where $RS_{CR}(t_I)$ denotes a critical RS value and t_I denotes an inspection time. Thus, if the RS at t_I is less than $RS_{CR}(t_I)$, the sample is assumed failed.

4. When a failure occurs in the RS surface, it is also assumed that the sample failed in the crack size surface and the failed samples are removed from the analysis.

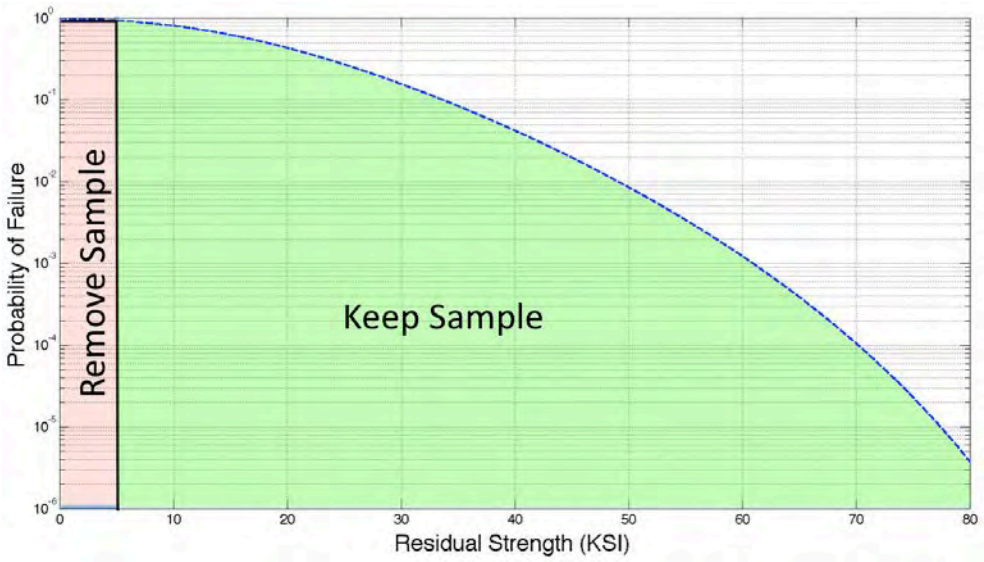

Figure 22. RS failure schematic

The advantages of having independent surfaces through time is that the semi-variance matrices will be smaller (excluding time as a random variable), allowing faster operations and computation time. Moreover, it avoids discontinuities in the surfaces because of already failed samples; further, it adds the ability to better track the failed samples through time.

2.6.3.6 Kriging Surrogate Model Error Calculation

The successful implementation of Kriging to perform DTA depends on the accuracy of the calculations of the prediction errors and their propagation. In this work, the errors are used in the adaptive segment of the algorithm, where the Kriging prediction uncertainty is compared with the user-defined allowed error.

In this report, the error is calculated based on the Kriging variance and the assumption that $Z(\cdot)$ is Gaussian. To compute the 95% or 99% confidence bounds error (uncertainty) due to the Kriging prediction, the prediction interval for $Z(x_0)$ is used as computed in equation 39. Using the prediction interval, the 95% or 99% confidence bounds error for the interval is computed using:

$$error = \frac{\left(A_{LB} - \hat{Z}(x_0)\right)}{A_{LB}} \tag{51}$$

The error computed using equation 51 is compared against the user-defined error tolerance, as described in step 5 in section 2.6.3.3 .

3. GRAPHICAL USER INTERFACE SUMMARY

A graphical user interface (GUI) was developed on visual basic to facilitate the user interaction with the code. The GUI was merged with the fatigue section of the code developed under FAA Grant 09-G-016.

The GUI allows the user to input the different variables that are required to run a PDTA, open existing input files, and visualize output files. The following figures demonstrate the GUI capabilities in more detail.

Figure 23 shows the GUI main screen, the left picture starts the fatigue (linear damage) section of the GUI, and the right picture starts the DT section of the GUI.

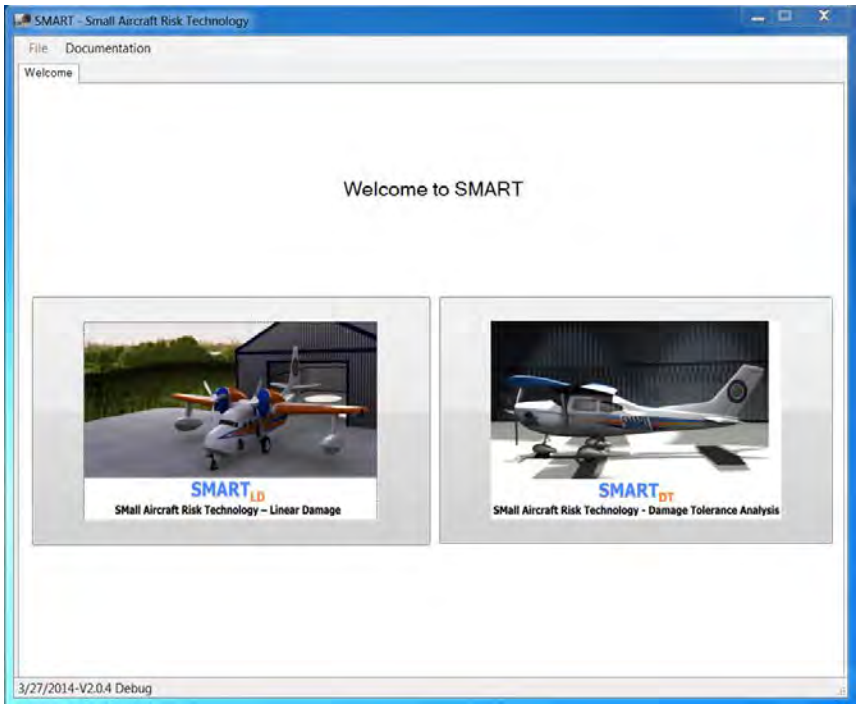

Figure 23. GUI main window

Figure 24 shows the overview tab. The data input here is used to input information that can be used to describe the problem.

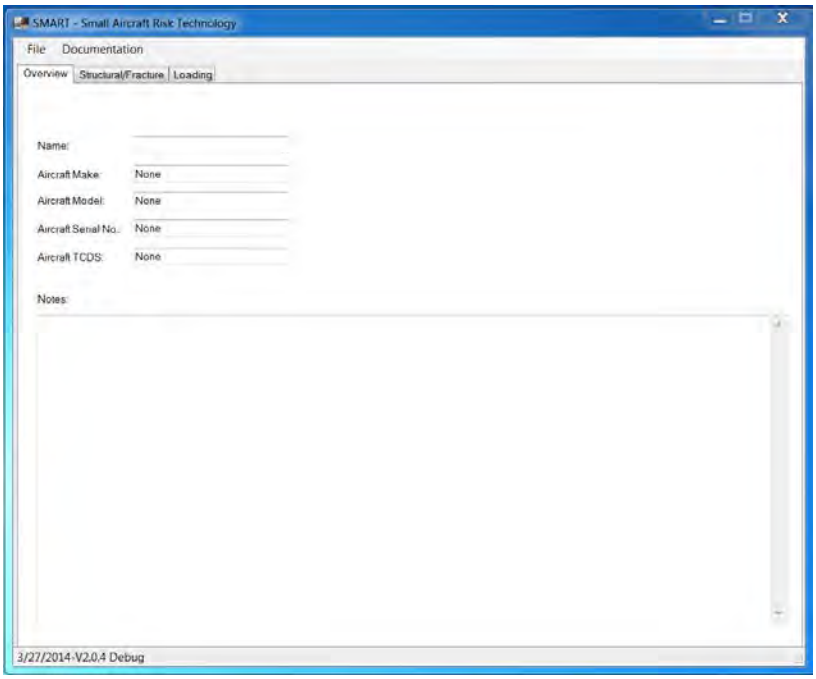

Figure 24. GUI overview tab

Figure 25 shows the structural/fracture tab. In this tab, the user selects the crack growth method (master curve, Kriging, or NASGRO). The random variables required for the analysis are selected in this tab, and the mean and standard deviation are inputted by the user. If the analysis requires NASGRO, the quantities required to compute the RS are entered in this tab.

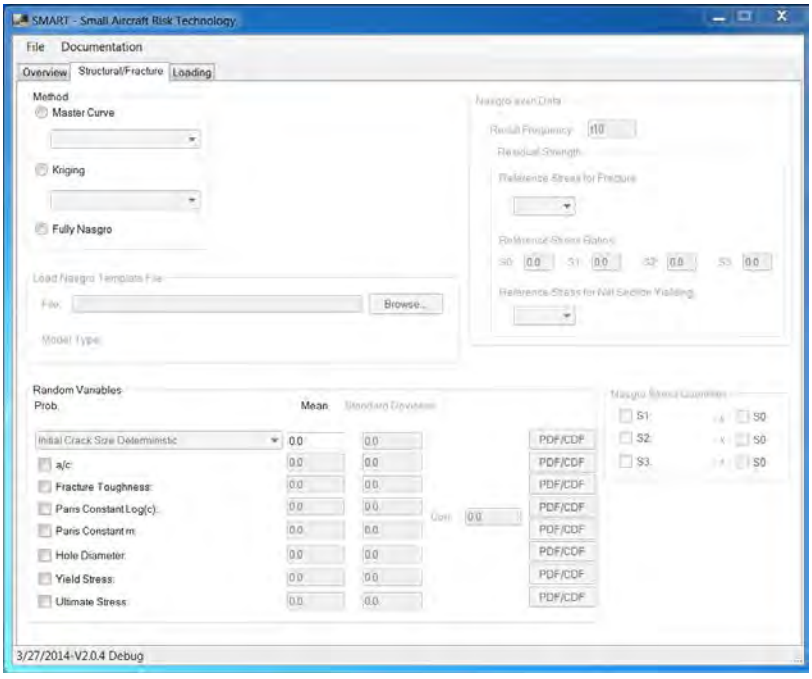

Figure 25. GUI structural/fracture tab

Figure 26 shows the loading tab. Within this tab, the EVD parameters are entered if they are known; if the parameters are unknown, the fitting option can be used and the internal algorithm on the code will find the optimum parameters. The optimum parameters are computed based on the loading information selected by the user within this same tab on the exceedance spectra section.

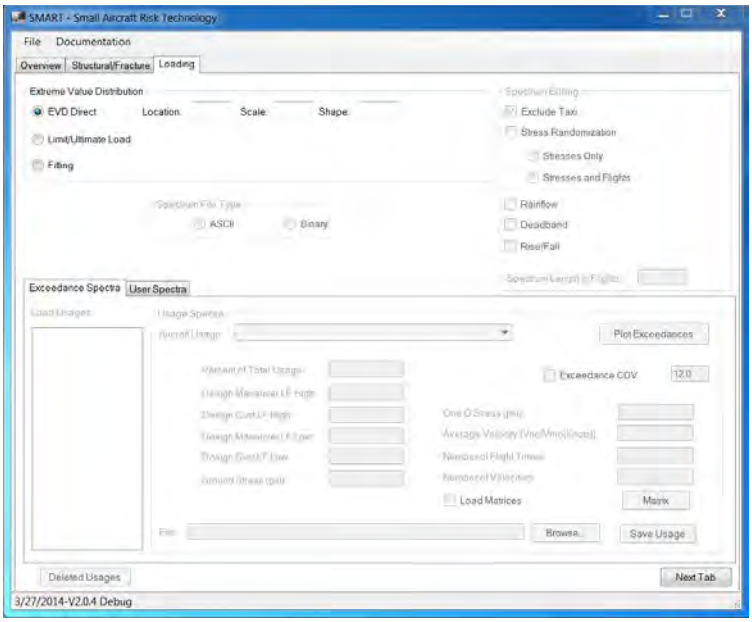

Figure 26. GUI loading tab

Figure 27 shows the inspection tab where all the inspection information can be entered. The GUI allows different types of inspections at different times.

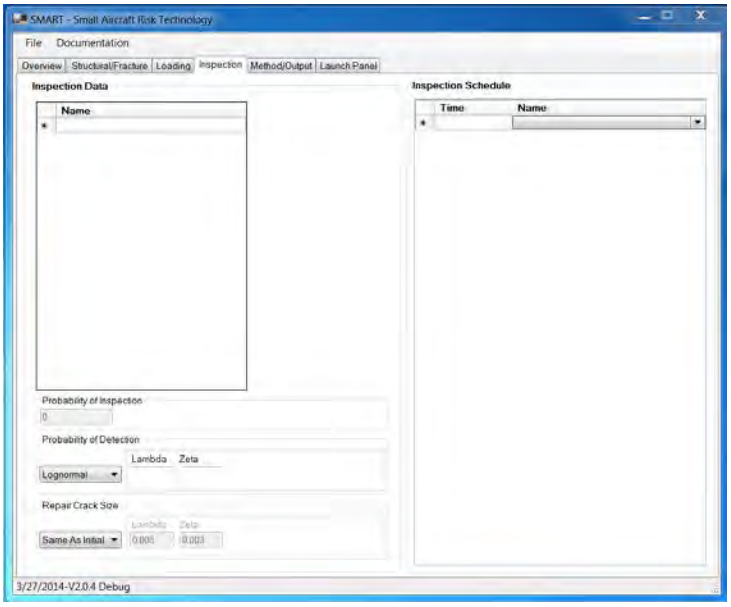

Figure 27. GUI inspection tab

Figure 28 shows the method/output tab; within this tab, the user can select the integration method (numerical integration or Monte Carlo), the output options as evaluation frequency (at what flight numbers to compute the POF), and the maximum number of flights to analyze.

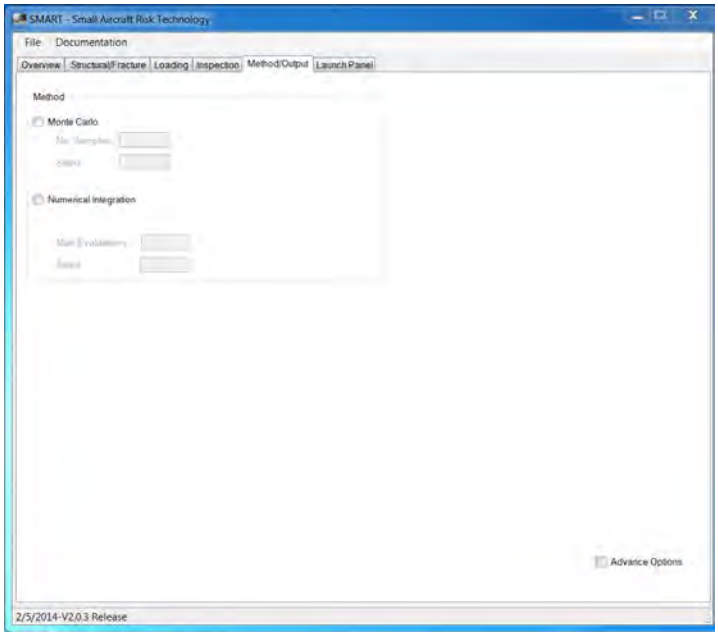

Figure 28. GUI method/output tab

Figure 29 presents the launch panel tab where the input file can be reviewed before running the executable.

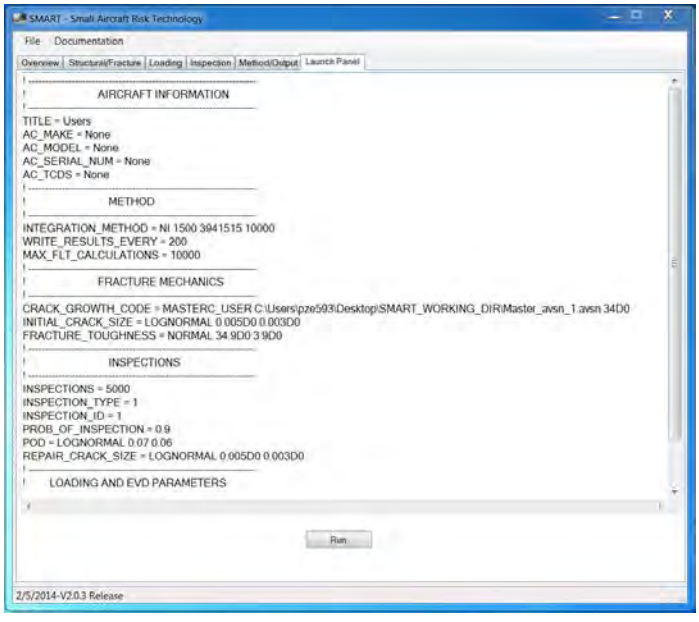

Figure 29. GUI launch panel tab

Figure 30 shows the results tab where the code output files can be visualized and POF plots created.

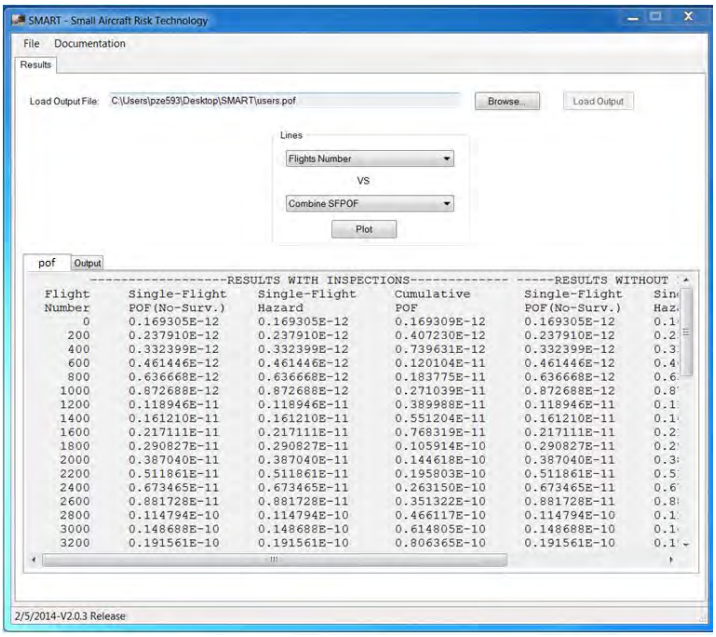

Flight Number	Single-Flight POF(No-Surv.)	Single-Flight Hazard	Cumulative POF	Single-Flight POF(No-Surv.)	Sin Haz
	RESULTS WITH INSPECTIONS			RESULTS WITHOUT	
0	0.169305E-12	0.169305E-12	0.169309E-12	0.169305E-12	0.1
200	0.237910E-12	0.237910E-12	0.407230E-12	0.237910E-12	0.2
400	0.332399E-12	0.332399E-12	0.739631E-12	0.332399E-12	0.3
600	0.461446E-12	0.461446E-12	0.120104E-11	0.461446E-12	0.4
800	0.636668E-12	0.636668E-12	0.183775E-11	0.636668E-12	0.6
1000	0.872688E-12	0.872688E-12	0.271039E-11	0.872688E-12	0.8
1200	0.118946E-11	0.118946E-11	0.389988E-11	0.118946E-11	0.1
1400	0.161210E-11	0.161210E-11	0.551204E-11	0.161210E-11	0.1
1600	0.217111E-11	0.217111E-11	0.768319E-11	0.217111E-11	0.2
1800	0.290827E-11	0.290827E-11	0.105914E-10	0.290827E-11	0.2
2000	0.387040E-11	0.387040E-11	0.144618E-10	0.387040E-11	0.3
2200	0.511861E-11	0.511861E-11	0.195803E-10	0.511861E-11	0.5
2400	0.673465E-11	0.673465E-11	0.263150E-10	0.673465E-11	0.6
2600	0.881728E-11	0.881728E-11	0.351322E-10	0.881728E-11	0.8
2800	0.114794E-10	0.114794E-10	0.466117E-10	0.114794E-10	0.1
3000	0.148688E-10	0.148688E-10	0.614805E-10	0.148688E-10	0.1
3200	0.191561E-10	0.191561E-10	0.806365E-10	0.191561E-10	0.1

Figure 30. GUI results tab

4. NUMERICAL EXAMPLES

Three examples are shown in this section to demonstrate the different capabilities developed under this code.

4.1 EXAMPLE ONE (USER MASTER CURVE)

The first example presents a simple problem for a geometry with a crack in a hole to demonstrate the probabilistic DT methodology. For this example problem, the geometry has a closed-form solution for the stress intensity factor, as shown in equation 52.

$$K = \sigma \cdot \alpha = \sigma \cdot \beta\sqrt{\pi a} \tag{52}$$

where ¶ $\beta = \beta_{hole} \cdot \beta_{width}$, ¶with ¶ $\beta_{hole} = 0.6762 + \dfrac{0.8734}{0.3245 + \left(\dfrac{a}{R}\right)}$ and, $\beta_{width} = \sqrt{\sec\left(\dfrac{\pi(R+a)}{W}\right)}$

The crack growth equation is defined by the exponential function:

$$a = 0.0001 \cdot \exp(0.000293 * T) \tag{53}$$

where a represents the crack size and T is the number of cycles.
Table 11 presents the variable declaration.

Table 11. Probabilistic DT example variables

Variable	Definition
R (Radius)	0.125 in.
W (Width)	10 in.
Fracture Toughness Distribution	Normal: Mean = 34.8 $ksi\sqrt{in}$. Standard Deviation = 3.9 $ksi\sqrt{in}$.
Initial and Repair Crack Size Distribution	Lognormal: Mean = μ_x = 0.003 in. Standard Deviation = σ_x = 0.004 in.
EVD	Gumble: Location = 14.5 Scale = 0.8 Shape = 0.0
POD	Lognormal: Mean = μ_x = 0.08 in. Standard Deviation = σ_x = 0.07 in.
Inspection Times	5000 and 10,000 Flights

The crack growth curve and RS curves are shown in Figure 31 and Figure 32, respectively.

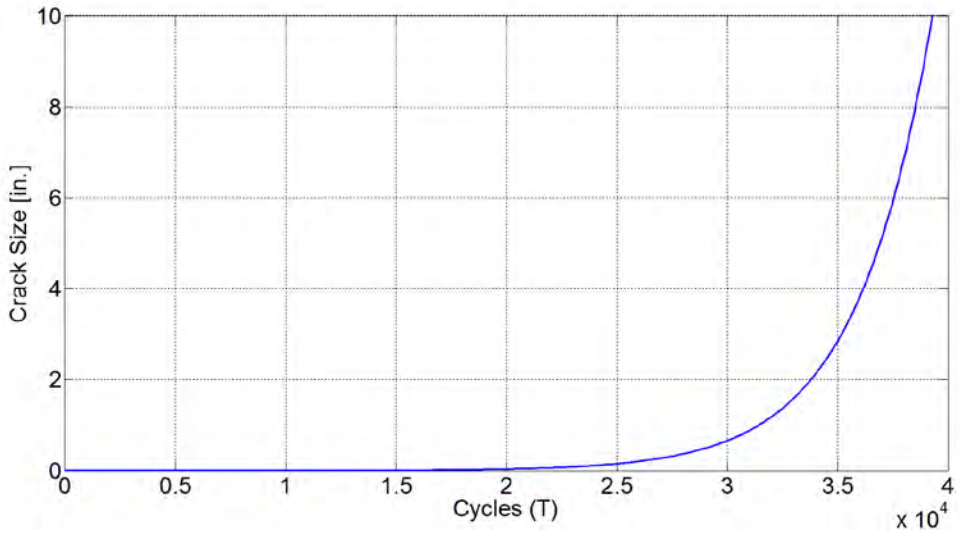

Figure 31. First example: crack growth curve

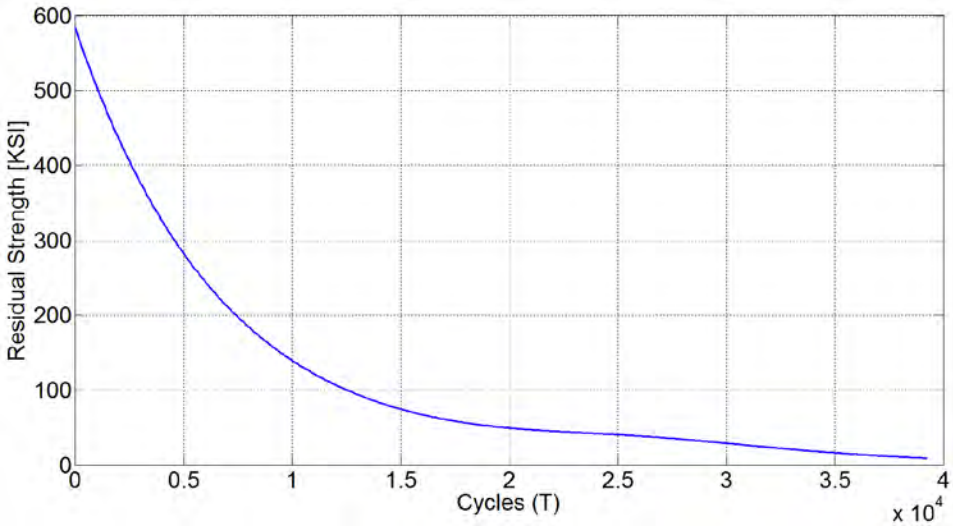

Figure 32. First example: RS curve

This example problem was solved using the master curve approach.

Figure 33 shows the SFPOF with inspections (red line) and without inspections (blue line) using numerical integration and the master curve approach. In Figure 34, the effect of each inspection can be observed by the number of detected cracks on each inspection based on the POD parameters.

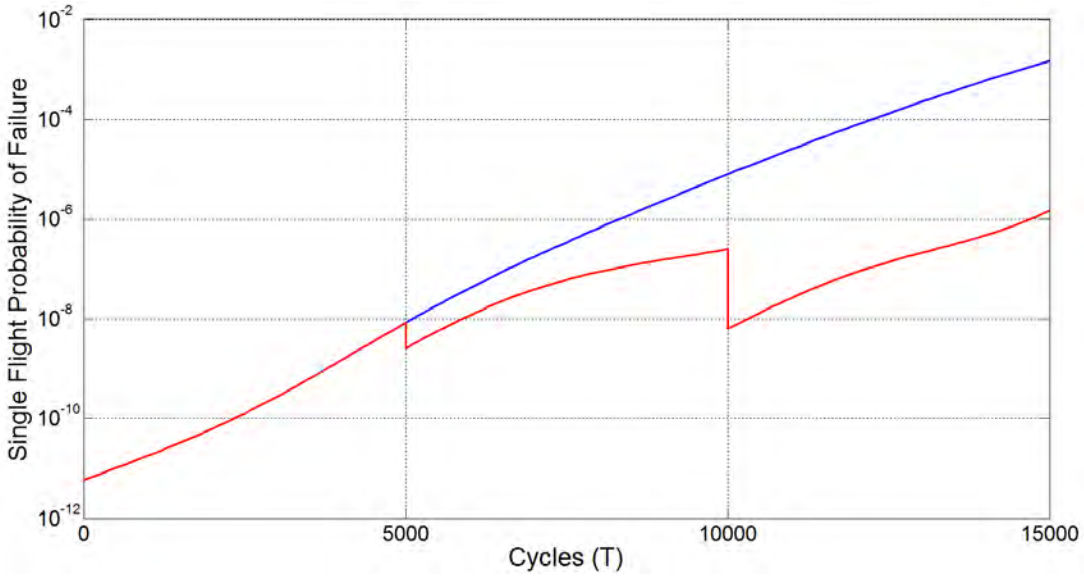

Figure 33. First example: SFPOF calculation results

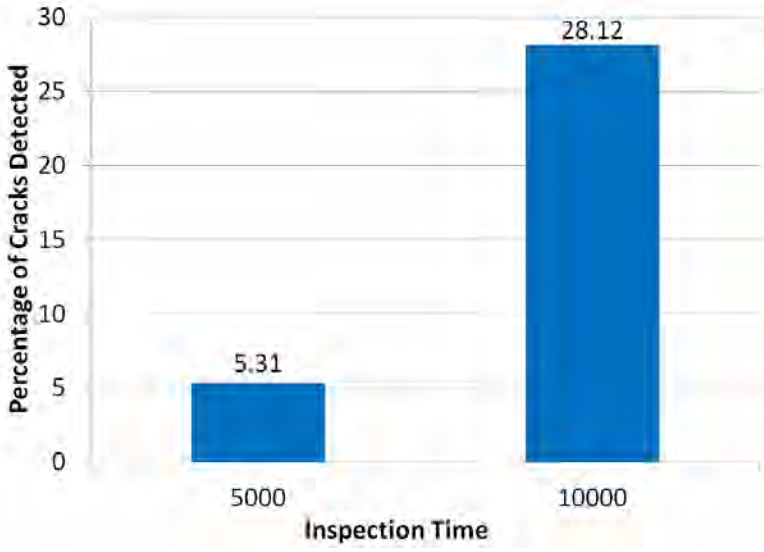

Figure 34. First example: percentage of detected cracks at the inspection points

4.2 EXAMPLE TWO (NASGRO-GENERATED MASTER CURVE)

The second example is an airplane considered with a single usage (i.e., a single-engine unpressurized instructional usage). Table 12 presents the crack growth parameters for a through crack in a hole. The random variables included are initial crack size (lognormal distribution) and fracture toughness (normal distribution).

Table 12. Second example: crack growth problem definition

Quantity	Definition
NASGRO Crack Growth Model	TC03 – Through crack in a hole
Geometric Variables	Width = 2.5 in. Thickness = 0.09 in. Hole Diameter = 0.156 in. Hole Offset = 0.5 in.
Fracture Toughness Distribution	Normal: Mean = 35.0 $ksi\sqrt{in}$. Standard Deviation = 3.0 $ksi\sqrt{in}$.
Initial Crack Size Distribution	Lognormal Median = 0.00163 in. Mean = ln(median) = -6.420 Standard Deviation = 1.113
POD	Lognormal: Mean = μ_x = 0.07 in. Standard Deviation = σ_x = 0.06 in.
Inspection Times	5000 and 8000 Flights

Table 13 presents the loading variables. These variables were used to generate the loading for the crack growth analysis.

Table 13. Second example: loading variables

Variable	Value
Usage	Single Engine Unpressurized Basic Instructional Usage
Design LLF Maneuver	3.2, -1.32
Design LLF Gust	3.4, -1.2
Ground Stress (psi)	-2000
One-g stress (psi)	6500
Flight Length and Velocity Matrix	Deterministic
Flight Length and Weight Matrix	Deterministic
Average Velocity (VNO/VMO [Knots])	165

VMO = maximum operating limit speed; VNO = maximum aircraft safe cruise speed

The EVD was computed using the parameters of Table 13. The results are presented in Figure 35.

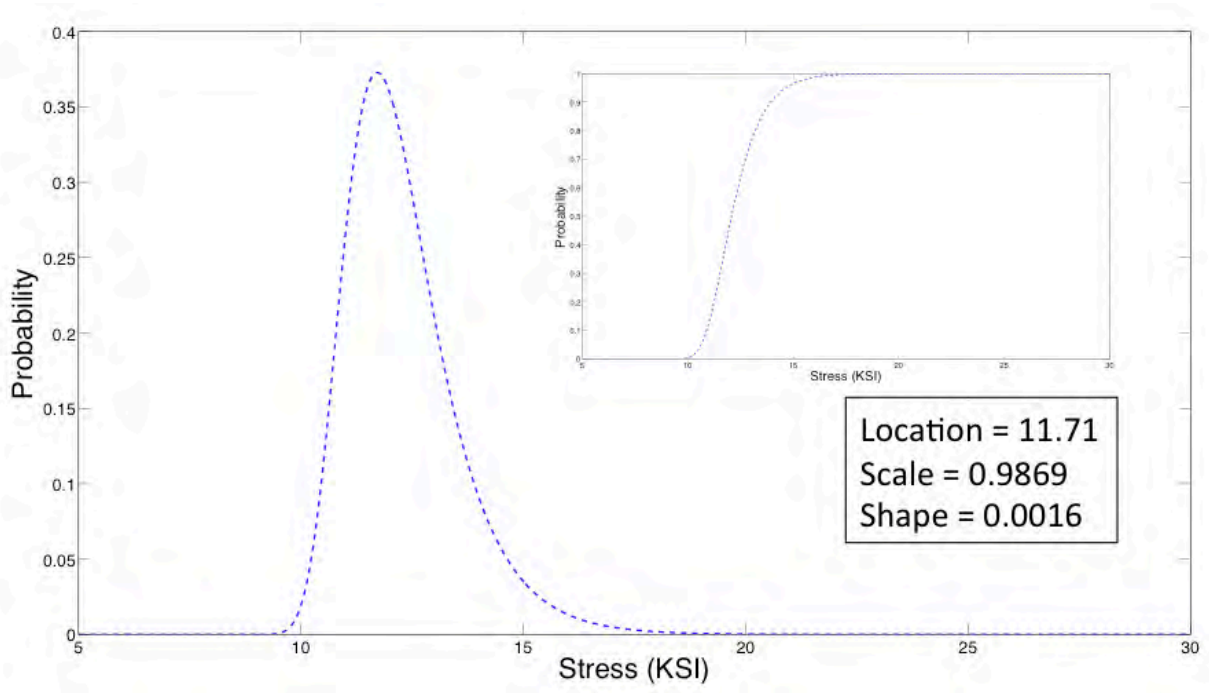

Figure 35. Second example: EVD

Figure 36 shows the SFPOF with inspections and without inspections using numerical integration and the master curve approach. In Figure 37, the effect of each inspection can be observed by the number of detected cracks on each inspection based on the POD parameters.

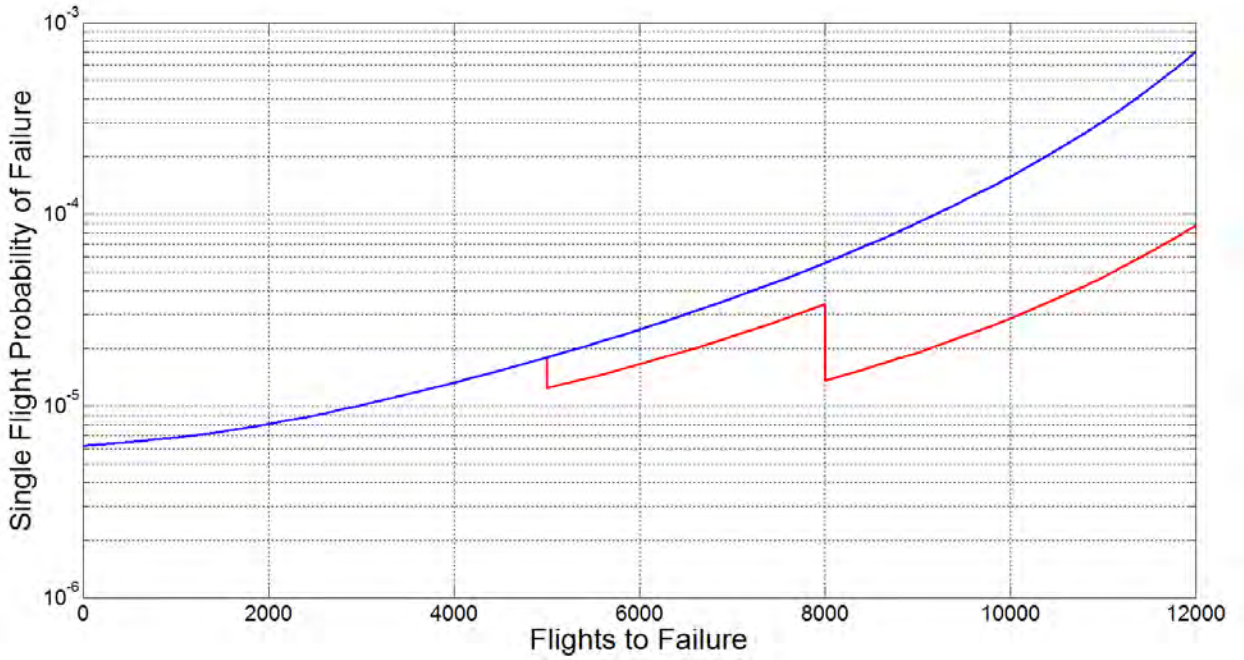

Figure 36. Second example: SFPOF calculation results

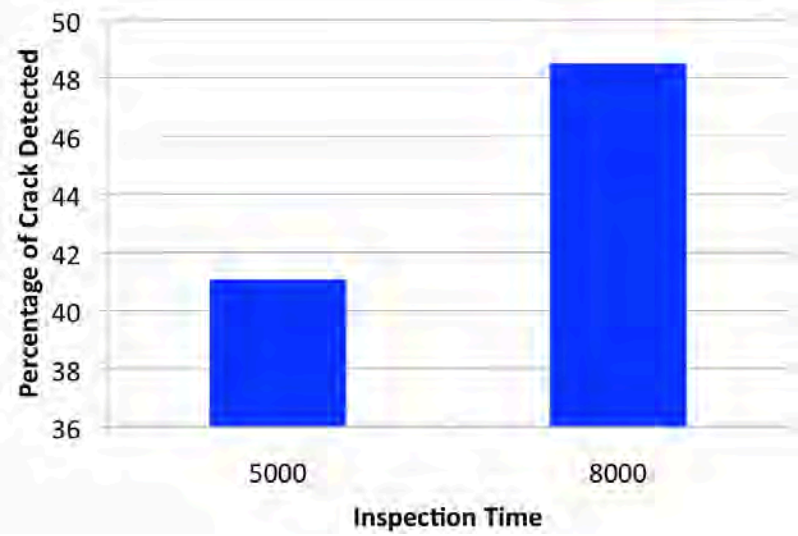

Figure 37. Second example: percentage of detected cracks at the inspection points

4.3 EXAMPLE THREE (KRIGING METAMODELING)

The third example is a single-engine airplane considered with a single usage (i.e., a single engine unpressurized executive usage). Table 14 presents the crack growth parameters for a through crack in a hole. The random variables included are initial crack size (lognormal distribution), fracture toughness (normal distribution), and loading (Gumbel distribution).

Table 14. Third example: crack growth problem definition

Quantity	Definition
NASGRO Crack Growth Model	TC03 – Through crack in a hole
Geometric Variables	Width = 2.5 in. Thickness = 0.09 in. Hole Diameter = 0.10 in. Hole Offset = 0.5 in.
Fracture Toughness Distribution	Normal: Mean = 34.8 $ksi\sqrt{in}$. Standard Deviation = 3.9 $ksi\sqrt{in}$.
Initial Crack Size Distribution	Lognormal Median = 0.00163 in. Mean = ln(median) = -6.420 Standard Deviation = 1.113
EVD (Weibull)	Location = 5.0, Scale = 10.0, and Shape = 5.0
Material	Al-2024

Table 15 presents the loading variables. These variables were used to generate the loading for the crack growth analysis.

Table 15. Third example: aircraft loading variables

Variable	Value						
Usage	Single Engine Unpressurized Basic Executive Usage						
Design LLF Maneuver	3.8, -1.52						
Design LLF Gust	3.155, -1.155						
Ground Stress (psi)	-4550						
One-g stress (psi)	7100						
Flight Length and Velocity Matrix	Dur/Vel		0.80	0.85	0.90	0.95	1.00
	0.50:	0.05	0.05	0.10	0.10	0.10	0.65
	0.60:	0.05	0.05	0.05	0.05	0.15	0.70
	0.70:	0.10	0.00	0.05	0.05	0.15	0.75
	0.80:	0.15	0.00	0.05	0.05	0.10	0.80
	0.90:	0.20	0.00	0.00	0.00	0.10	0.90
	1.00:	0.25	0.00	0.00	0.05	0.05	0.90
	1.10:	0.15	0.00	0.00	0.00	0.05	0.95
	1.20:	0.05	0.00	0.00	0.00	0.05	0.95
Flight Length and Weight Matrix	Dur/Vel		0.80	0.85	0.90	0.95	1.00
	0.50:	0.05	0.05	0.10	0.10	0.10	0.65
	0.60:	0.05	0.05	0.05	0.05	0.15	0.70
	0.70:	0.10	0.00	0.05	0.05	0.15	0.75
	0.80:	0.15	0.00	0.05	0.05	0.10	0.80
	0.90:	0.20	0.00	0.00	0.00	0.10	0.90
	1.00:	0.25	0.00	0.00	0.05	0.05	0.90
	1.10:	0.15	0.00	0.00	0.00	0.05	0.95
	1.20:	0.05	0.00	0.00	0.00	0.05	0.95
Average Velocity (VNO/VMO [Knots])	165						

VMO = maximum operating limit speed; VNO = maximum aircraft safe cruise speed

To calculate the SFPOF, the code was run using 5000 Monte Carlo samples, a surrogate model with 10 initial training points, and a user-defined error threshold equal to 5%.

Figure 38 shows the total number of training points (NASGRO evaluations) used as a function of the total number of Monte Carlo samples. From the Figure 38, it can be observed that for 5000 samples and an error threshold equal to 5%, only 98 NASGRO evaluations were needed, which truly reduces the computational effort.

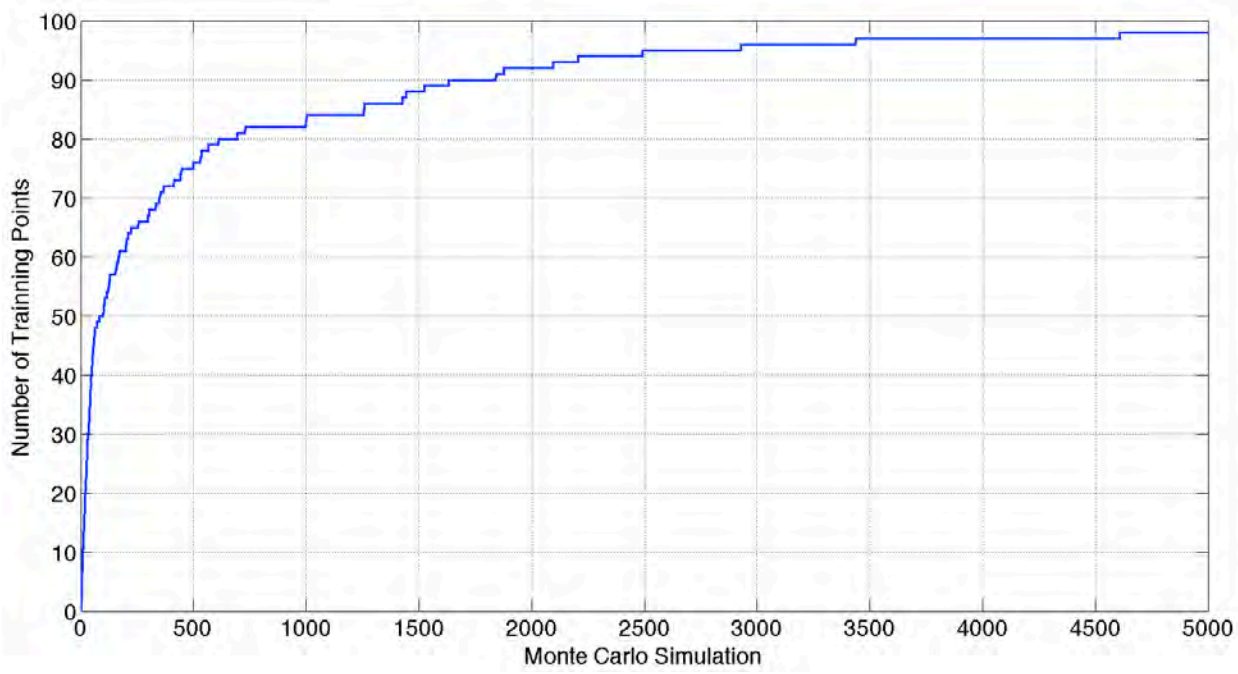

Figure 38. Third example: surrogate model, number of training points vs. number of Monte Carlo evaluations

Figure 39 shows a comparison between the SFPOF if NASGRO is evaluated 5000 times (exact-black line) — running all 5000 evaluations using NASGRO) — and if the surrogate model is used (Kriging-red dots). The total time duration for the full NASGRO run was 18 hours. The total time duration for the Kriging model was 2.3 hours. This demonstrates the computational efficiency of the Kriging metamodeling to perform PDTA.

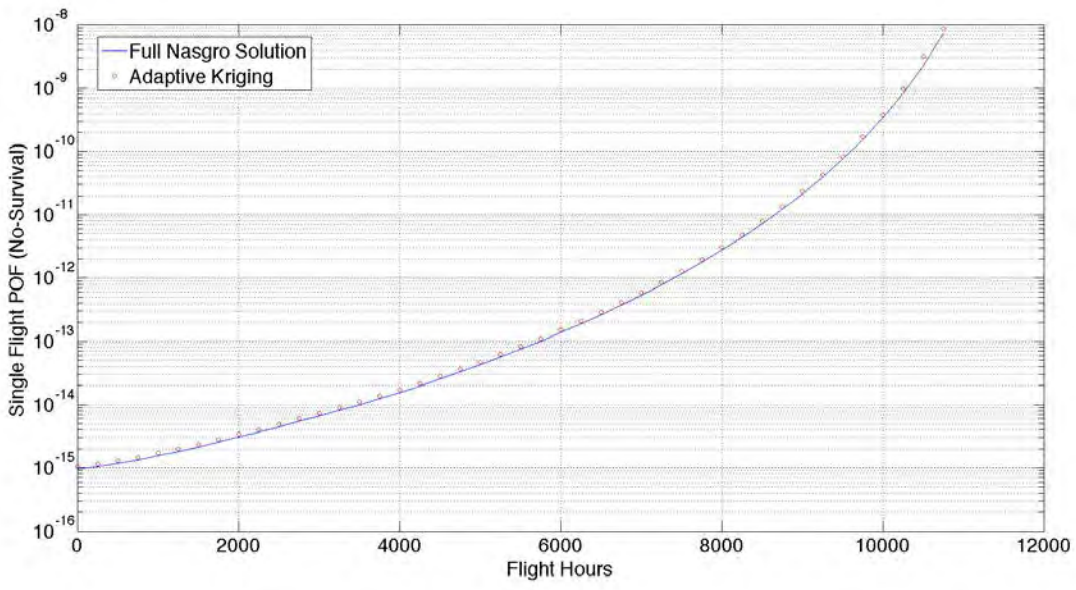

Figure 39. Third example: SFPOF calculation results

5. CONCLUSIONS

The probabilistic fatigue evaluation of GA aircraft is vital for providing important insight into the severity or criticality of a potential structural issue. For this reason, a probabilistic damage tolerance (DT) methodology and computer software were developed for FAA engineers to perform risk assessments of structural issues.

The methodology was programmed into a computer code, "SMART|DT," to quantify the probability of structural failure. This information will provide a proactive approach to enable a nonbiased review of data to ensure airworthiness. The software considers the random variables: loading (gust and maneuver loads, sink rate, flight velocity-duration, flight weight-duration), material behavior (fracture toughness, crack growth parameters, yield stress, ultimate stress), geometric variables (initial crack size, hole diameter, hole edge distance, aircraft ratio), and inspection (repair crack size, POD, probability of inspection). The random variables are used with Monte Carlo simulation or numerical integration algorithms to calculate the airplane probability-of-failure (POF) (SFPOF, cumulative total POF, and hazard function) with and without inspections. SMART has a user interface that creates the input file, runs the executable, creates input/output plots (histograms, probability density functions, cumulative density functions, scatter plots, and 2D line plots), and allows the visualization of the output files. The methodology and software were demonstrated on three different DT examples.

6. REFERENCES

1. FAA. (1998). Advisory Circular 25.571-1C Damage tolerance and fatigue evaluation of structure.

2. Nuss, M., & Shiao, M. (2006). *Probabilistic approach to fleet risk managements of small airplanes*. Proceedings from the 9th Joint FAA/DoD/NASA Aging Aircraft Conference, Atlanta, GA.

3. Reyer W. M. (March, 2006). *Probability basis of safe-life evaluation in small airplanes.* Proceedings From the 9th Joint FAA/DoD/NASA Aging Aircraft Conference. Atlanta, GA.

4. Ocampo, J., Millwater, H. R., Singh, G., Smith, H., Abali, F., Nuss, M., … Shiao, M. (2011). Development of a probabilistic linear damage methodology for small aircraft. *Journal of Aircraft, 48*(6), 2090–2106.

5. LexTech Inc. (2010). AFGROW Fracture Mechanics and Fatigue Crack Growth Analysis Software [Software]. http://www.afgrow.net.

6. Coles, S. (2001) *An introduction to statistical modeling of extreme values*, Berlin, Heidelberg: Springer-Verlag London.

7. Coles, S. & Pericchi, L. (1983). Anticipating catastrophes through extreme value modeling. *Journal of the Royal Statistical Society: Series C (Applied Statistics), 52*(4), 405–416.

8. Nelder, J. A., & Mead, R. (1965). A simplex function minimization. *The Computer Journal, 7*(4), 308–313.

9. Lagarias, J. C., Reeds, J. A., Wright, M. H., & Wright, P. E. (1998). Convergence properties of the Nelder-Mead simplex algorithm in low dimensions. *SIAM Journal of Optimization, 9*(1), 112–147.

10. Air Force Systems Command. (1991). *Risk analysis for aging aircraft fleets* (WL-TR-91-3066). Dayton, OH.

11. Berens, A. P. & Loomis, J. S. (1998). *Update of the PROF computer program for aging aircraft risk analysis.* University of Dayton Research Institute. Dayton, OH.

12. USAF. (2005). *PRobability Of Fracture* (*PROF) Software Version 3* (USAF Contract Number F09650-03-D-0001). University of Dayton Research Institute. Dayton, OH.

13. NTIAC, Texas Research Institute Austin. (1997). *Non-destructive evaluation (NDE) capabilities data book*. Austin, TX: Rummel, W. D., Matzkanin, G. A.

14. SwRI (2009). NASGRO Fracture Mechanics and Fatigue Crack Growth Analysis Software (Version 6.0). http://www.swri.org/4org/d18/mateng/matint/nasgro.

15. Van Beers, W. C. M. & Kleijnen, J. P. C. (2003). Kriging for interpolation in random simulation. *Journal of the Operational Research Society, 54*(3), 255–262.

16. Tobias, P. (2003). Maximum likelihood estimation. In *NIST/SEMATECH e-handbook of Statistical Methods* (Section 8.4.1.2). http://www.itl.nist.gov/div898/handbook/apr/section4/apr412.htm.

17. Aldrich, J. (1997). RA Fisher and the making of maximum likelihood 1912–1922. *Statistical Science*, *12*(3), 162–176.

18. Cressie, N. (1993). *Statistics for spatial data* (Revised ed.). Hoboken, NJ: John Wiley & Sons.

19. Lefebvre, J., Rousell, H., Walter, E., Lecointe, D., and Tabbara, W. (August, 1996). Prediction from wrong models: The Kriging approach. *IEEE Antennas and Propagation Magazine, 38.4*, 35–45.

20. Martin, J. D. & Simpson, T. W. (2004). On using Kriging models as probabilistic models in design. *SAE International, 113*(5). http://papers.sae.org/2004-01-0430.

APPENDIX A—LOAD AND STRESS SPECTRUM GENERATION

A-1. INTRODUCTION

In 1962, at the request of the FAA, and upon recommendation of the NASA Committee on Aircraft Operating Problems, the NASA V-G (velocity, normal acceleration)/VGH (velocity, normal acceleration, pressure altitude) GA Program was established [A-1]. This program recorded gust and maneuver loads, airspeed practices, and other variables for GA airplanes to provide a database of information for use by airplane designers and evaluators. The program recorded more than 42,155 hours of VGH data from more than 105 airplanes. Tabulated data of the exceedance curves can be found in [A-2, A-3]. A probabilistic assessment of exceedance curves can be found in [A-4].

A-2. SPECTRUM GENERATION

A-2.1, MANEUVER AND GUST LOADS

The data for maneuver and gust loads are presented as the cumulative number of occurrences per nautical mile versus the acceleration fraction (an airplane characteristic defined as the incremental normal acceleration divided by the incremental limit factor). Maneuver and gust use the same methodology to generate load data, so only the gust load methodology is discussed.

The gust spectra in the exceedance curves is expressed in terms of the gust load factor ratio:

$$\frac{a_n}{a_{nLLF}} = \frac{\text{Incremental normal acceleration (in delta g)}}{\text{Load limit factor}}. \qquad \text{(A-1)}$$

To develop the gust stress spectrum, a sweep through the exceedance curve of acceleration fraction values (figure A-1) is conducted to account for the possible loads that an airplane faces during a flight. An example is presented for illustration purposes using only four values (0.10, 0.16, 0.22, and 0.28). The values and calculations needed to compute damage due to gust loading are shown in table A-1, with the description in the second column.

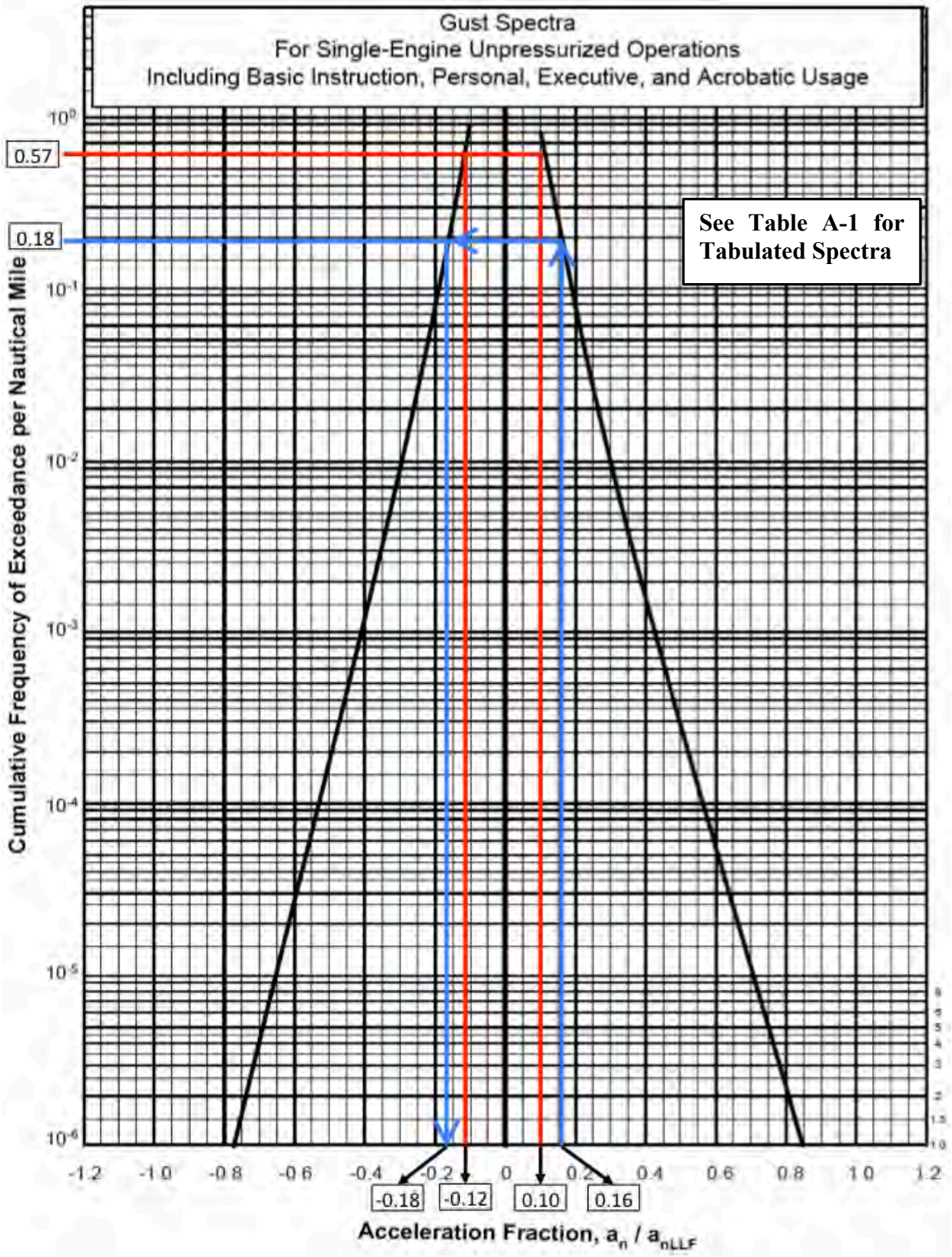

Figure A-1. Exceedance curve for gust

Table A-1. Gust damage calculation

Gust Damage					
1	From the exceedance curve reading the positive values of the gust load factor ratio, a_n / a_{nLLF}.	0.10	0.16	0.22	0.28
		0.16	0.22	0.28	0.34
2	Calculate the average value from the values in Row 1.	0.13	0.19	0.25	0.31
3	From figure A-1, read the different values of cumulative occurrence of gust per nautical mile at a specific gust load factor.	0.57	0.18	0.052	0.013
4	From the exceedance curve, read the negative values of the gust load factor ratio corresponding to Row 2.	-0.12	-0.18	-0.25	-0.32
5	Frequency per nautical mile (no accumulation) is the difference between two successive values in Row 3.	0.39	0.128	0.039	0.0087
6	Number of gust cycles accumulated per hour (Row 5) x 0.9 (Design Cruise Speed, Vc).	57.8	19	5.79	1.292
7	Increment in the stress due to the gusts. To get this value (delta g), multiply Row 2 and Row 4 by $a_{nLLF} = 2.155$.	-0.259	-0.388	-0.539	-0.690
		0.28	0.409	0.539	0.667
8	Maximum and minimum delta stress over and below the maximum stress at the critical component (One-g Stress) – multiply Row 7 by One-g Stress (7410 psi).	-1920	-2870	-4000	-5980
		2070	3030	4000	4940

The steps to calculate gust damage are explained more in detail, as follows:

- Positive and negative acceleration fractions and their corresponding cumulative frequency of exceedance are read from the exceedance curve. Figure A-1 shows the positive values of acceleration fraction (0.1 and 0.16)—see the blue and red lines. Using these values, the respective cumulative frequency values are read (0.57 and 0.18), with the corresponding negative acceleration fraction at the same cumulative frequency level (-0.12 and -0.18).
- The difference between two successive values of cumulative frequency is used to calculate occurrence frequency. Occurrence frequency is the difference between two successive values of cumulative frequency. In this case, the difference between 0.57 and 0.18 results

in 0.39 occurrences per nautical mile. The number of occurrences per hour is calculated by multiplying the cumulative frequency per nautical mile by the aircraft velocity in nautical miles per hour. For this example, the velocity was assumed to be 148.2 nautical miles per hour (90% of the design velocity), resulting in 57.8 occurrences per hour.

- The stresses at this occurrence level (57.8) can be calculated by multiplying the acceleration fractions involved (0.13, the average between two successive positive values of 0.1 and 0.16, and -0.12) by the load limit factor (2.155) to obtain delta g. This delta g value is multiplied by the one-g stress value to obtain the maximum and minimum stress values.

A-2.2. LANDING AND REBOUND LOADS

Using the data presented in [A-2], an average value of 3.0 feet per second was established for the sink rate velocity. Reference [A-3] presents the results from landing gear drop test data, shown in Figure A-2. With the sink rate velocity information, the load factor (g) can be calculated using linear regression as:

$$g = 0.1877 \cdot (\text{Sink Rate Velocity}) + 1.3422. \tag{A-2}$$

where 0.1877 is the slope and 1.3422 is the intercept. After calculating the load factor, the maximum and minimum stresses for landing and rebound are calculated using the following equations:

$$Landing_{\max} = \frac{2}{3}(One - g\_Stress), \tag{A-3}$$

$$Landing_{\min} = (\text{ground\_Stress})g, \tag{A-4}$$

$$Rebound_{MAX} = 0.6 Landing_{MAX}, \tag{A-5}$$

$$Rebound_{MIN} = 0.6 Landing_{MIN}. \tag{A-6}$$

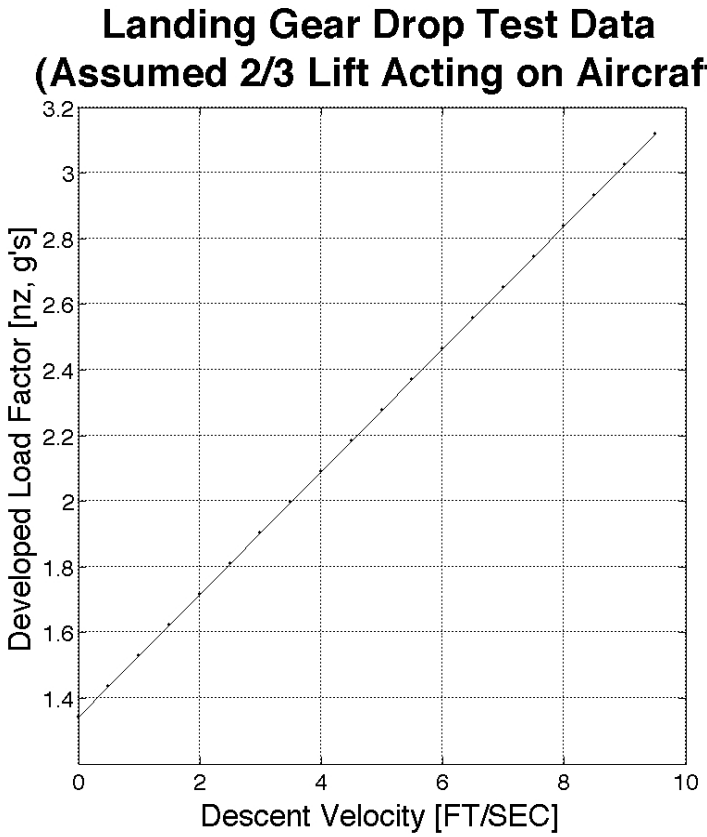

Figure A-2. Landing gear drop test data 0

A-3. TAXI LOADS

The exceedance curve for taxi is shown in Figure A-3. The damage for taxi is determined in an analogous manner to gust loading.

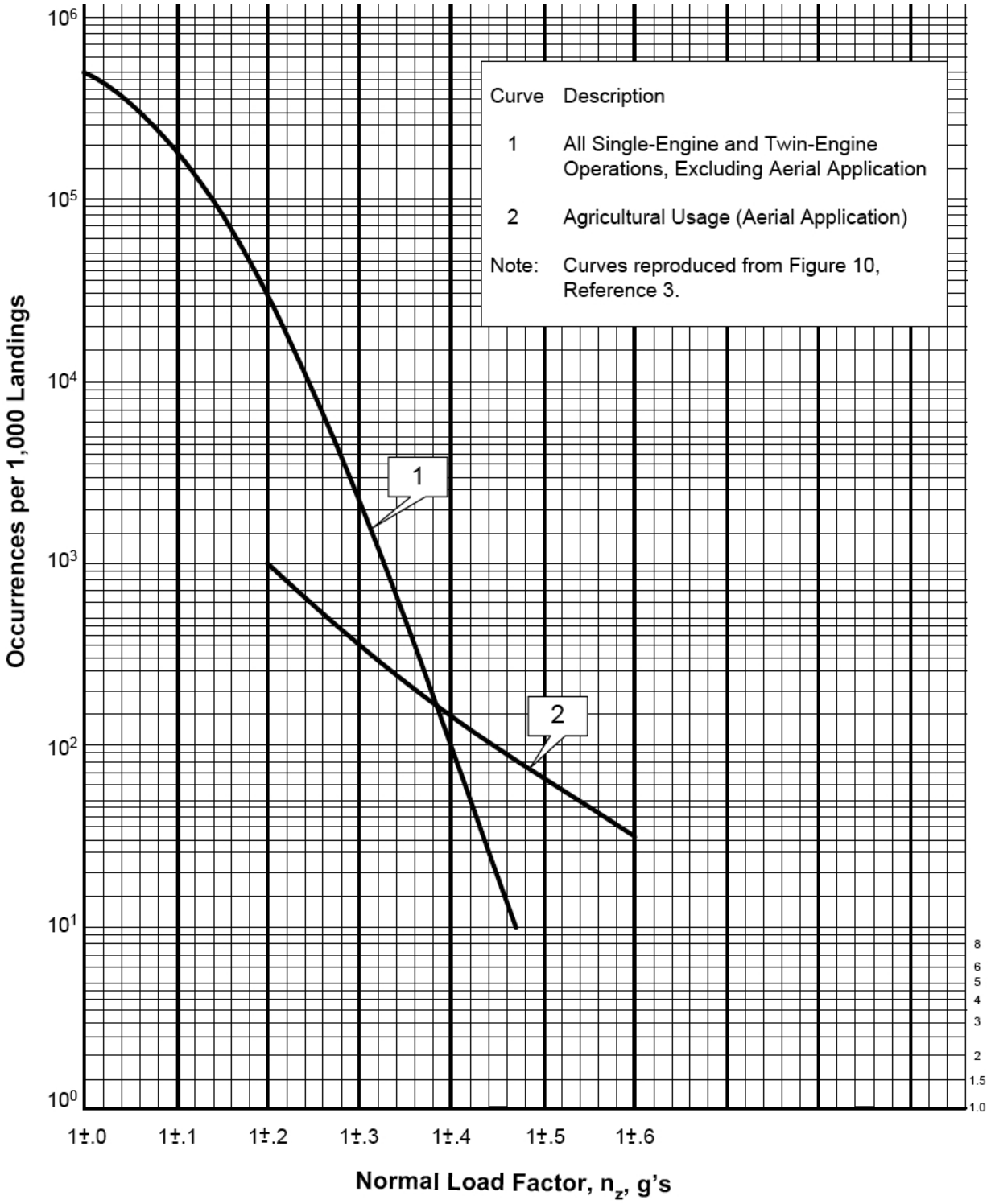

Figure A-3. Exceedance curve for taxi

A-4. GAG LOADS

GAG is a cycle, which is defined by the transition from the minimum ground stress to the maximum stress during a flight. A schematic for the GAG cycle is presented in Figure A-4.

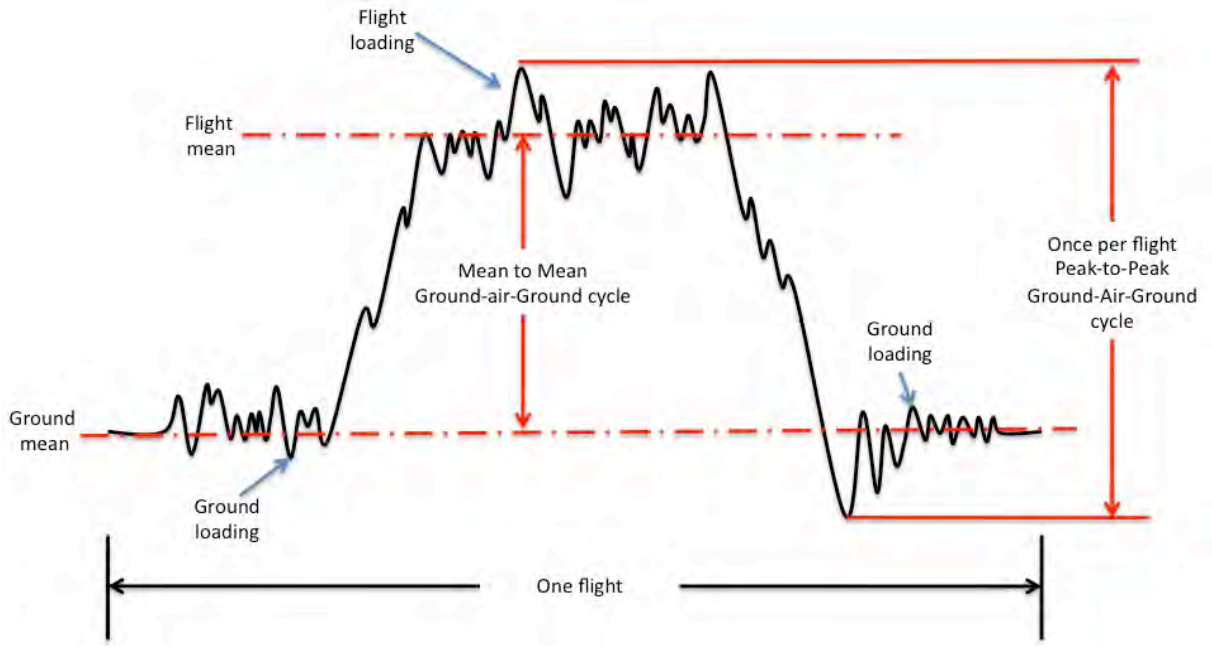

Figure A-4. GAG cycle schematic

The procedure to calculate the once-per-flight, peak-to-peak GAG cycle is explained as follows:

- Using the gust and maneuver exceedances, determine the max stress per flight vs. the number of occurrences (figure A-4).
- Add the number of occurrences in gust and number of occurrences in maneuver to obtain the total number of occurrences at each $max\ GAG\ stress$ (shown as a green line in figure A-5).
- Load the maximum stresses for gust and maneuver, including the corresponding number of occurrences per flight calculated from the exceedance curves.
- Interpolate the max stress to determine the $max\ GAG\ stress$ that occurs at a value of one occurrence per flight (shown as an orange line in figure A-5).
- $min\ GAG\ stress$ is taken from landing, when the minimum stress occurs.

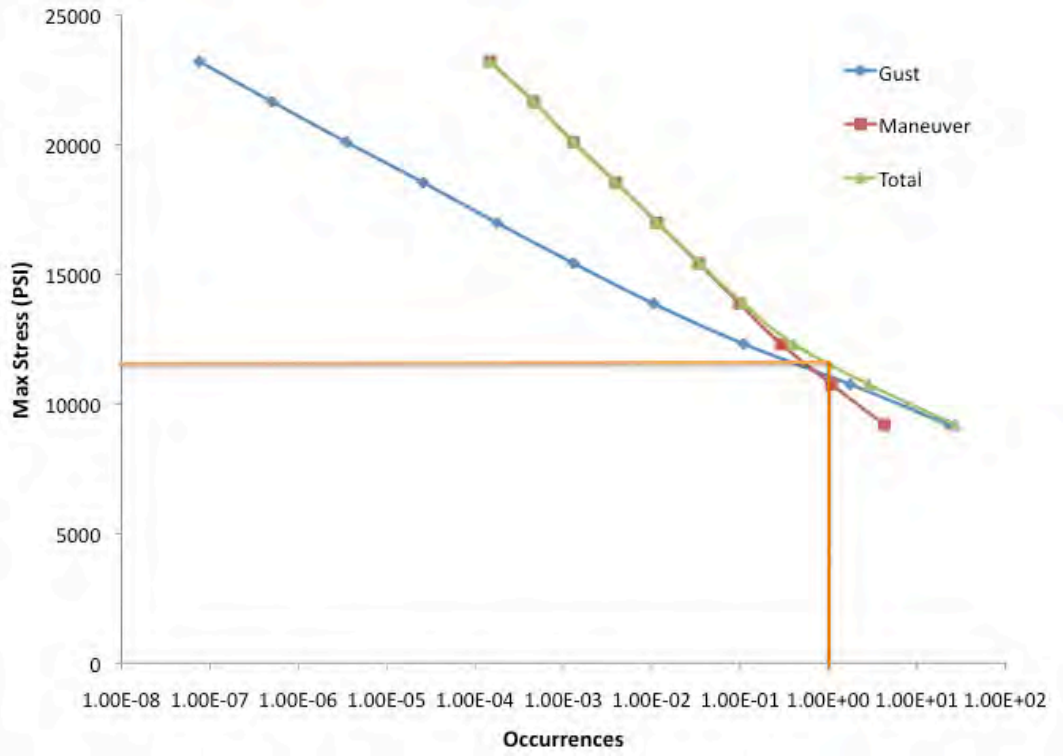

Figure A-5. GAG example

When the entire load pairs for gust, maneuver, taxi, landing and rebound, and GAG have been calculated, the complete number of cycles are taken and assembled into a flight (incomplete cycles are saved to be added to future flights) for the crack growth calculations.

A-5. REFERENCES

A-1. FAA Report. (1993). General Aviation Aircraft—Normal Acceleration Data Analysis and Collection Project (DOT/FAA/CT-91/20).

A-2. FAA Report. (2005). Fatigue Fail-Safe, and Damage Tolerance Evaluation of Metallic Structure for Normal, Utility, Acrobatic, and Commuter Category Airplanes (AC 23-13A).

A-3 FAA Report. (1973). Fatigue Evaluation of Wing and Associated Structure on Small Airplanes (AFS120-73-2).

A-4. Reyer, W. M., (2006). *Probability* Basis of Safe-Life Evaluation in Small Airplanes. Proceedings From Aging Aircraft Conference, Atlanta, GA.

BACKGROUND AND GUIDELINES FOR SPECIFICATION OF RANDOM VARIABLES FOR PROBABLISTIC DAMAGE TOLERANCE ANALYSIS

DRAFT FINAL REPORT

SwRI® Project No. 15609

prepared by

Joseph W. Cardinal
Laura C. Domyancic
Mechanical Engineering Division
Southwest Research Institute
San Antonio, TX

prepared for

The University of Texas at San Antonio
Subcontract No. 220502SWRI

and

The Federal Aviation Administration
Contract No. 09-G-016

October 2013

BACKGROUND AND GUIDELINES FOR SPECIFICATION OF RANDOM VARIABLES FOR PROBABLISTIC DAMAGE TOLERANCE ANALYSIS

DRAFT FINAL REPORT

SwRI® Project No. 15609

prepared by

Joseph W. Cardinal
Laura C. Domyancic
Mechanical Engineering Division
Southwest Research Institute
San Antonio, TX

prepared for

The University of Texas at San Antonio
Subcontract No. 220502SWRI

and

The Federal Aviation Administration
Contract No. 09-G-016

October 2013

Approved:

_____

Timothy A. Fey, P.E., Director
Structural Engineering Department

ACKNOWLEDGEMENTS

The authors of this report would like to acknowledge the University of Texas at San Antonio (UTSA) and the Federal Aviation Administration (FAA) for their support of this work. Dr. Felix Abali of the FAA Technical Center in Atlantic City, NJ was the FAA Program Manager. Mr. Michael Reyer and Mr. Marv Nuss (now retired) from the FAA Small Airplane Directorate in Kansas City, MO have provided key technical guidance. Dr. Harry Millwater and Mr. Juan Ocampo of UTSA were co-Principal Investigators of the overall Probabilistic Damage Tolerance-Based Maintenance Planning for Small Airplanes program and their support is greatly appreciated. Finally, Ms. Deborah Gohmert of SwRI is acknowledged for her preparation of this report.

1.0 INTRODUCTION

The purpose of this document is to provide background information and guidelines to aid in the development and specification of input parameters associated with random variables used in the probabilistic damage tolerance analysis (PDTA) software developed on the Federal Aviation Administration (FAA) research project entitled "Probabilistic Damage Tolerance-Based Maintenance Planning for Small Airplanes." The work reported herein was conducted by Southwest Research Institute® (SwRI®) in San Antonio, TX under subcontract to the University of Texas at San Antonio (UTSA) on FAA Contract No. 09-G-016. The overall project involves the development of a comprehensive probabilistic damage tolerance methodology such that FAA engineers can advise maintenance planning in support of policy decisions in the General Aviation (GA) fleet.

This report is divided into sections that address the different types of random variables (RVs) considered in the PDTA software in the following areas: fatigue crack growth modeling (material properties), geometry models for calculation of stress intensity factors, initial flaw size models, and inspection capability models. Each section of this report presents background information on the models and parameters that are involved, identifies those parameters that are considered as random variables, discusses sources of data and/or methods used to characterize the RVs, and provides guidelines on how to specify their input for use in the PDTA software. References are provided at the end of each major section.

A key aspect of the probabilistic damage tolerance analysis process is the characterization and modeling of the random nature of the aircraft loads. These concepts are not addressed in this report and are documented elsewhere by UTSA in the User's Manual for the PDTA software.

2.0 FATIGUE CRACK GROWTH MODELING

This section first provides a review of fatigue crack growth (FCG) data and how they are modeled using the NASGRO equation [2-1]. This is followed by a discussion of which parameters of the NASGRO equation are considered as random variables within the PDTA software. Guidelines and recommendations for input and use of these random variables are then provided.

1.1 FATIGUE CRACK GROWTH RATE MODELING USING THE NASGRO EQUATION

Fatigue crack growth rate data are generally characterized on log-log plots of growth rate, da/dN (in/cycle) versus stress intensity factor range, ΔK (ksi$\sqrt{}\sqrt{}$in). It is commonplace to consider FCG data to be divided into three regions as shown schematically in Figure 2-1. Region I is the fatigue "threshold" region where cracks propagate very slowly and the data usually exhibit a threshold (ΔK_{th}) below which cracks do not propagate. Region II is the linear or steady-state region where the relationship between da/dN and ΔK is linear on a log-log plot. Region II is also commonly referred to as the Paris region after the power law equation [$da/dN = C(\Delta K)^n$] that has been used to model fatigue crack growth in this region for many years. Region III is the near instability region where rapid unstable crack growth occurs as fracture instability is approached.

Crack growth rate calculations in NASGRO use a relationship called the NASGRO equation given by:

$$\frac{da}{dN} = C\left[\left(\frac{1-f}{1-R}\right)\Delta K\right]^n \frac{\left(1-\frac{\Delta K_{th}}{\Delta K}\right)^p}{\left(1-\frac{K_{\max}}{K_c}\right)^q} \qquad (2.1)$$

where N is the number of applied fatigue cycles, a is the crack length, R is the stress ratio, ΔK is the stress intensity factor range, and $K_{\max} = \Delta K/(1\text{-}R)$. C, n, p, and q are empirically derived constants. The NASGRO equation is a "full-range" crack growth model in that it can represent all three crack growth regions as well as account for the dependence of FCG rate on the stress ratio. Closure is modeled using the Newman crack opening function, f. The critical stress intensity factor or fracture toughness, K_c, influences behavior in the instability region of the curve and controls final failure. For additional detail on the NASGRO equation, the reader is referred to the documentation for the NASGRO software [2-1].

To fit the NASGRO equation to fatigue crack growth rate data, one generally needs multiple sets of data at different R values. Fits to the NASGRO equation for many aerospace materials are available from within the NASGRO software [2-1]. Figures 2-2 and 2-3 illustrate NASGRO equation fits for two common GA aluminum alloys (2024-T3 and 7075-T73511) along with screen captures of the corresponding NASGRO material properties display.

1.1.1 Degeneration of the NASGRO Equation into the Paris Equation

If desired by the user, the NASGRO equation can be simplified to the traditional Paris equation [$da/dN = C(\Delta K)^n$] by judicious choices of NASGRO equation parameters and options on the

material screen in the NASGRO GUI. In order to accomplish this, set $p = q = 0.0$ and check the box to suppress closure (see the NASGRO GUI screen in Figures 2-3 and 2-4). These choices remove the threshold and instability influences on the NASGRO equation (Regions I and III become linear extensions of Region II) and the effect of the load ratio, R, is no longer accounted for resulting in a conservative high-R crack growth equation.

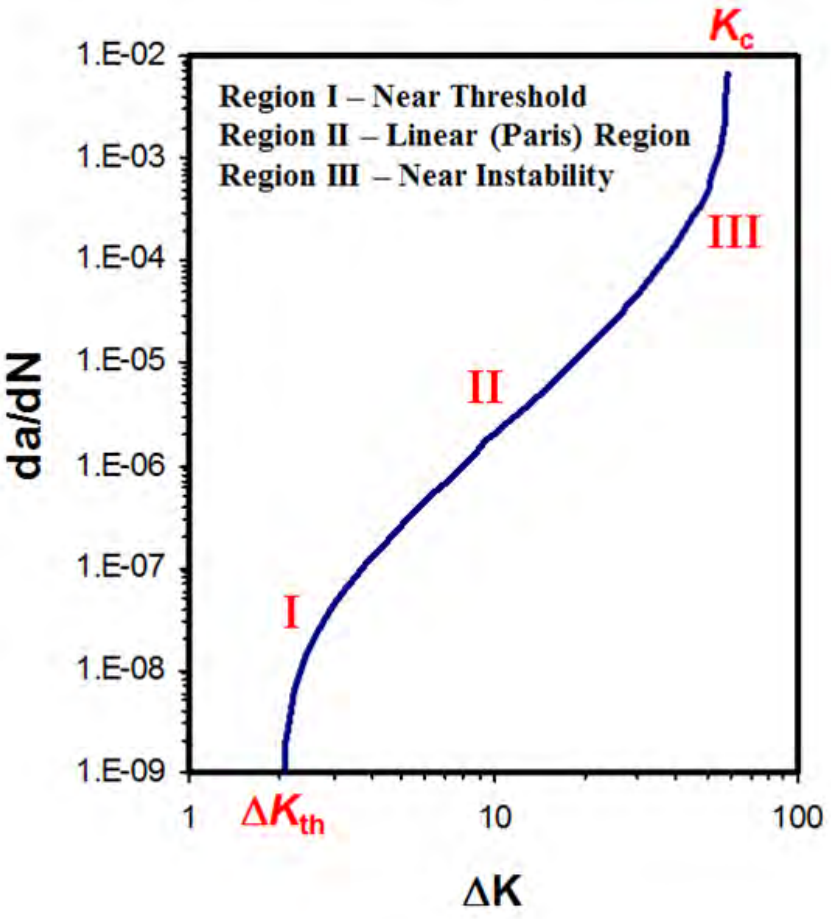

Figure 2-1 Schematic of Fatigue Crack Growth Behavior Illustrating the Three Regions of Fatigue Crack Growth

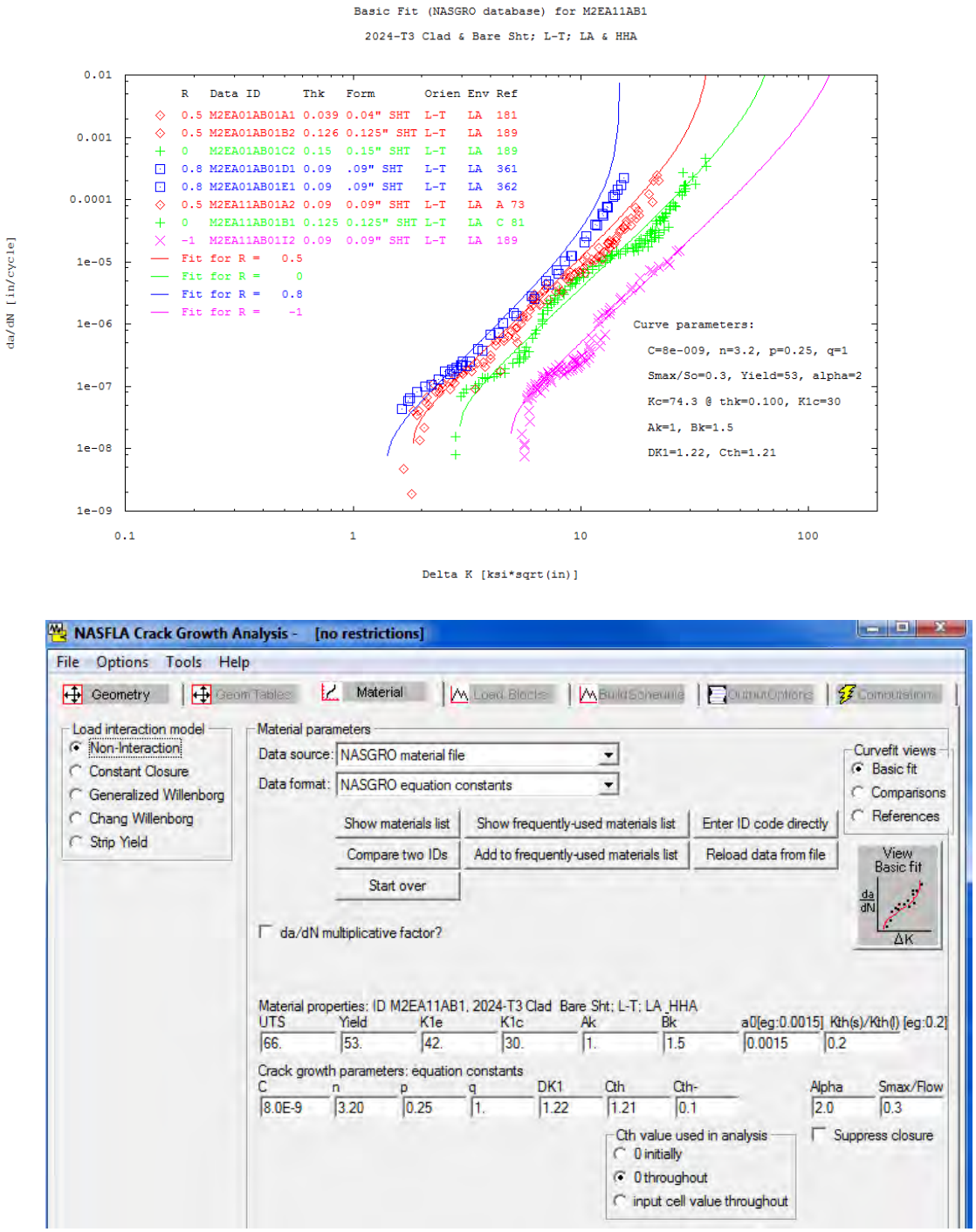

Figure 2-2 NASGRO Equation Fit and Material Screen for 2024-T3 Aluminum Sheet

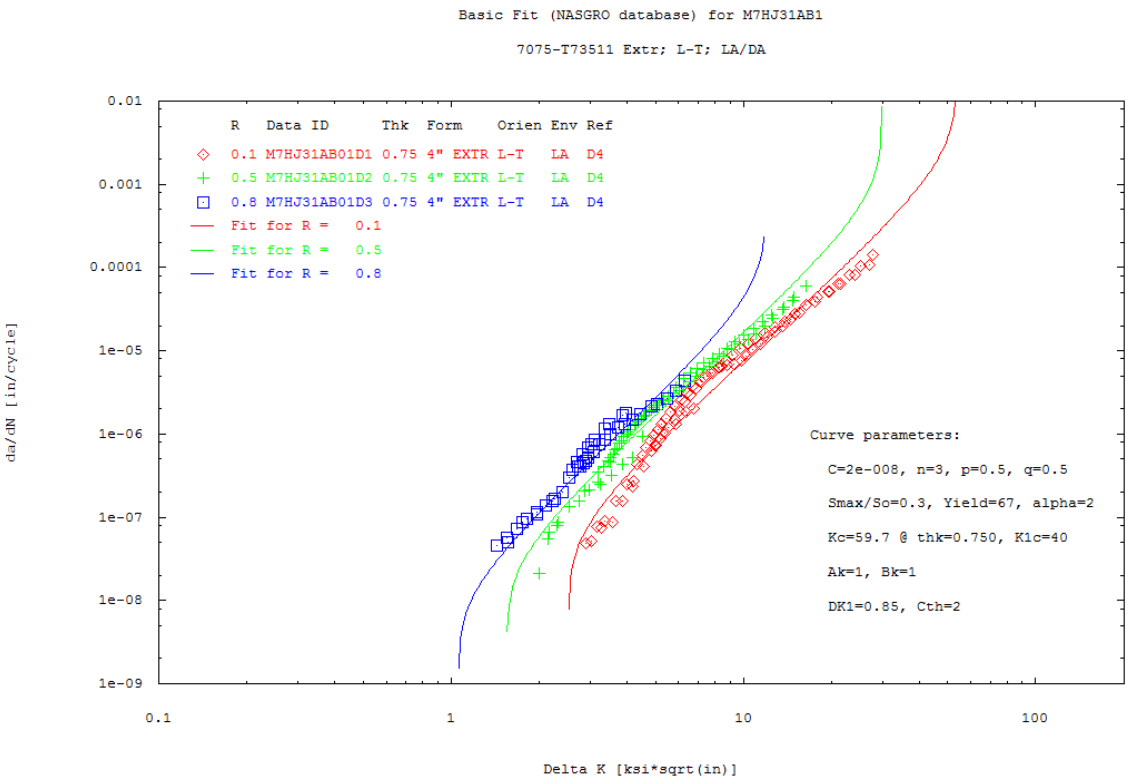

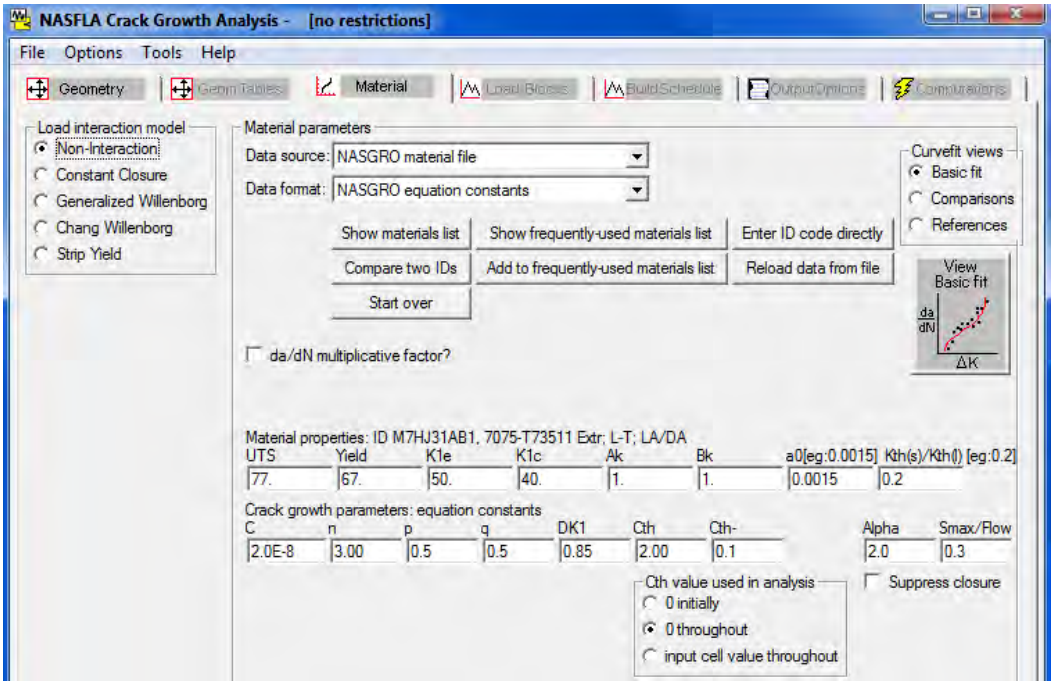

Figure 2-3 NASGRO Equation Fit and Material Screen for 7075-T73511 Aluminum Extrusion

1.2 RANDOM VARIABLES USED IN THE NASGRO EQUATION FOR THE PDTA SOFTWARE

The NASGRO equation contains a number of parameters or material properties as briefly described above. However, it must be recognized that a number of these parameters (f, ΔK_{th}, and K_c) are really not single-valued parameters themselves; rather, they represent sub-models in NASGRO comprised of their own set(s) of equations with their own parameters to model closure behavior, threshold behavior, and toughness, respectively. Therefore, within the NASGRO equation, there are at least fifteen parameters that are used to model fatigue crack growth. These sub-models are described in detail in the NASGRO User's Manual [2-1]. When the NASGRO user selects a material from the NASGRO database of NASGRO equation curve fits, the full set of NASGRO equation parameters for that material is specified as shown in Figures 2-2 and 2-3.

Conceivably, all of the parameters contained in the NASGRO equation could be considered as random variables; however, for the purposes of the PDTA software this was impractical and also unnecessary. The following parameters and material properties can be considered as random variables for the NASGRO analyses performed within the PDTA software:

Paris constant, C
Paris exponent, n
Yield stress, S_y
Ultimate stress, S_u
Fracture Toughness, K_c

Therefore, in the PDTA software, all other parameters related to the NASGRO equation are considered deterministic (e.g., the exponents p and q as well as those parameters that go into the threshold model and the toughness model). In general, for the use of the PDTA software with the full NASGRO option, it is assumed herein that the user would use either the NASGRO database of material properties for a given material ID, edit those database properties if he desires, or provide his own set of user-defined NASGRO equation parameters.

When using the material properties and equation parameters contained in the NASGRO database, it is important to be aware that these data are considered "typical" in the context of MMPDS (formerly MIL-HDBK-5) terminology [2-2]. That is, they are average values that have no statistical assurance associated with them. They are not S-basis, B-basis or A-basis values. Usually they are the values that have been obtained from the test reports referenced by the NASGRO database.

Guidelines and recommendations for input and use of these five random variables are provided below in Sections 2.3 to 2.5.

1.3 PARIS PARAMETERS, C AND N

1.3.1 Sources of Fatigue Crack Growth Data

The NASGRO database [2-1] contains curve fit parameters to the NASGRO equation for many aerospace alloys and therefore is an excellent source of values for these parameters. For a given material, in many cases NASGRO contains multiple sets of crack growth data; however, in general

there are not enough data sets to compute the standard deviations (or coefficients of variation) for these parameters and the NASGRO database does not provide a statistical characterization of *C* and *n* or any of the other parameters. The USAF Damage Tolerant Design Handbook [2-9] presents mean FCG rate data in both tabular and graphical form for many aerospace structural alloys but does not provide fits for *C* and *n*. The MMPDS [2-2] does not contain much FCG data and for what it contains, curve fits are not provided.

1.3.2 Characterization of *C* and *n* as Random Variables

It has been well known for many years that fatigue crack growth data can exhibit considerable variability [2-3, 4]. Furthermore, log *C* and *n* are each normally distributed and a strong negative correlation exists between the Paris equation parameters *C* and *n* [2-5, 6, 7]. The correlation coefficient, ρ, between *C* and *n* is commonly assumed to be on the order of -0.9 to -0.99 [2-7, 8].

In the PDTA software, log *C* and *n* are treated as correlated normal random variables with required inputs being the mean (μ) and standard deviation (σ) along with the correlation coefficient ρ. In the absence of other data, the mean values of *C* and *n* can be taken to be the parameters from the NASGRO database. A coefficient of variation (COV = σ/μ) of 0.10 is a reasonable choice to assume when specifying the standard deviation for each of these parameters in the absence of test data.

Alternatively, as an option, *n* can be assumed to be deterministic (i.e., a constant slope for the FCG curve) and allow all of the variability in *da/dN* to be modeled by the intercept *C*. This would be accomplished by setting the standard deviation of *n* to be zero along with setting the correlation coefficient ρ equal to zero.

1.4 YIELD AND ULTIMATE STRENGTH

The material yield and ultimate strengths are used by NASGRO to compute failure by net section yielding [2-1]. The NASGRO database [2-1] contains values of yield and ultimate strength for many aerospace alloys. However, as discussed above, these values should be considered as "typical" values. The MMPDS [2-2] provides allowable strength values on an S-basis, B-basis or A-basis, where an S-basis value is a minimum value, a B-basis value is exceeded 90% of the time with a 95% confidence and an A-basis value is exceeded 99% of the time with a 95% confidence.

1.4.1 Characterization of Yield and Ultimate Strength as Random Variables

Generally, yield and ultimate strengths are considered to be normally distributed and the PDTA software requests the mean and standard deviation for each. In the absence of test data or other information, a reasonable estimate of the COV for material strengths is 5-10%. A study performed by RAE Farnborough reviewed thousands of material test results and found that the yield strength tends to exhibit a larger variation than the ultimate strength, and cast materials tend to exhibit a larger variation than wrought materials [2-11].

An estimate of the mean and standard deviation can also be obtained from the MMPDS A- and B-basis values. Using Chapter 9 of Ref. 2-2, A- and B-basis allowables are calculated from test data according to the following equations:

$$A = \mu - \sigma k_{99}$$
$$B = \mu - \sigma k_{90}$$

where μ and σ are the sample mean and standard deviation, respectively. Assuming the data is normally distributed, $k_{99}k_{99}$ and $k_{90}k_{90}$ are one-sided tolerance limit factors for the distribution, calculated by:

$$k_{99} = 2.326 + \exp\left[1.340 - 0.522\ln(n) + \frac{3.87}{n}\right]$$
$$k_{90} = 1.282 + \exp\left[0.958 - 0.520\ln(n) + \frac{3.19}{n}\right]$$

where *n*-1 is equal to the degrees of freedom. Since the degrees of freedom are not reported in the MMPDS tables, it is advisable to use $n = 30$, which is the recommended minimum sample size. This would also lead to a more conservative distribution. Using this value, $k_{99}k_{99}$ and $k_{90}k_{90}$ reduce to 3.062 and 1.776, respectively. Thus, the A- and B-basis allowable equations become:

$$A = \mu - 3.062\sigma$$
$$B = \mu - 1.776\sigma$$

Solving this system of equations gives the mean and standard deviation of the normal distribution:

$$\mu = 2.38B - 1.38A$$
$$\sigma = (B - A)/1.286$$

As an example of this method, consider the steel alloy AerMet 100, a common material for landing gear. The A- and B-basis allowables for the yield strength are 235 ksi and 247 ksi, respectively. Thus, using the above equations, the values for the mean and standard deviation would be 263.57 and 9.33, respectively.

Note that this method should only be used when no other data or information for the material is available.

1.5 FRACTURE TOUGHNESS

Prediction of failure by fracture requires specification of the material fracture toughness. In fracture mechanics, the plain strain fracture toughness (K_{Ic}), is the lower limiting toughness for a material; however, it is generally much too conservative to implement into a damage tolerance analysis. In actual structures, the thickness dependent fracture toughness (K_c) or effective fracture toughness (K_{Ie}) are more commonly used to represent the fracture failure criteria. The thickness dependent fracture toughness provides larger toughness values than the plane strain fracture toughness because of constraint loss driving up the fracture toughness values. The NASGRO material database [2-1] contains values of K_{Ic} and K_{Ie} for each material and computes K_c (a function of thickness, *t*) using the following equation:

$$K_c / K_{Ic} = 1 + B_k e^{-\left(A_k t/t_0\right)^2} \tag{2.2}$$

where

$$t_0 = 2.5\left(K_{Ic} / \sigma_{ys}\right)^2$$

and A_k and B_k are fit parameters contained in the NASGRO database. These equations are used by NASGRO to calculate a K_c value to substitute into the NASGRO equation (Equation 2.1) for all through crack geometries. For the part-through crack geometries, K_c in Equation 2.1 is set equal to a constant value of K_{Ie}, taken from the NASGRO material properties files.

If the user wants to conservatively use K_{Ic} throughout the analysis, this can be achieved by setting B_k equal to zero on the NASGRO material screen (see Figures 2-2 and 2-3) resulting in K_c being set equal to K_{Ic} in Equation 2.2.

1.5.1 Sources of Fracture Toughness Data

In addition to the NASGRO material database of curve fits to the NASGRO equation, the NASMAT module of NASGRO contains a large database of toughness values for each material ID, tabulated as a function of thickness [2-1]. NASMAT also has a handy tool that allows the user to select sets of toughness data (e.g., for a specific thickness) and compute the average toughness and the corresponding standard deviation.

The USAF Damage Tolerant Design Handbook [2-9] is also a very good source of fracture toughness data in that it provides fracture toughness values and standard deviations as a function of thickness for many aerospace structural alloys. Additionally, the MMPDS [2-2] also provides plane strain toughness values (min/avg/max) and COVs for different thicknesses.

1.5.2 Characterization of Fracture Toughness as a Random Variable

Fracture toughness is usually assumed to be characterized by a normal distribution in aircraft risk analyses [2-10] and the PDTA software follows this approach requiring the input of a mean and standard deviation for the toughness. Generally, a DTA will only use a single (mean) value for K_c and does not consider the variability in toughness. Therefore, choosing the toughness used in the DTA as the mean value for the probabilistic analysis is a good approach.

The COVs for fracture toughness (σ/μ) can vary considerably for aerospace aluminums. The MMPDS shows a range of about 3 to 25 percent depending on the alloy, product form, thickness and orientation. Common choices for the fracture toughness COV used in probabilistic risk analyses are usually about 5 to 10 percent. The analyst should make an effort to investigate the references cited herein [2-1, 2 and 9] to obtain data to determine a COV and standard deviation appropriate for the component geometry and material being analyzed.

1.6 REFERENCES

2-1. NASGRO® Fracture Mechanics and Fatigue Crack Growth Analysis Software, Version 7.0, Southwest Research Institute and NASA Johnson Space Center, November 2012.

2-2. Metallic Materials Properties Development and Standardization (MMPDS), MMPDS-07, Federal Aviation Administration, April 2012.

2-3. Clark, W.G., Jr. and Hudak, S.J., Jr., "Variability in Fatigue Crack Growth Rate Testing," *J. of Testing and Evaluation*, Vol. 3, No. 6, pp. 454-476, 1975.

2-4. Virkler, D.A., Hillberry, B.M., and Goel, P.K., "The Statistical Nature of Fatigue Crack Propagation," *Journal of Engineering Materials and Technology, ASME*, Vol. 101, April 1979.

2-5. Ostergaard, D.F. and Hillberry, B.M., "Characterization of the Variability in Fatigue Crack Propagation Data," *Probabilistic Fracture Mechanics and Fatigue Methods: Applications for Structural Design and Maintenance, ASTM STP 798*, J.M. Bloom and J.C. Ekvall, Eds., American Society for Testing and Materials, 1983, pp. 97-115.

2-6. Ichikawa, M., "Probabilistic Fracture Mechanics Investigation of Fatigue Crack Growth Rate," *Statistical Research on Fatigue and Fracture, Current Japanese Materials Research – Vol. 2*, T. Tanaka, et al, Eds., Elsevier and the Society of Materials Science, Japan, 1987.

2-7. Annis, C., "Probabilistic Life Prediction *Isn't* as Easy as It Looks," *Probabilistic Aspects of Life Prediction, ASTM STP-1450*, W.S. Johnson and B.M. Hillberry, Eds., ASTM International, West Conshohocken, PA, 2003.

2-8. Cremona, C., "Reliability Updating of Welded Joints Damaged by Fatigue," *Int. J. of Fatigue*, Vol. 18, No.8, pp567-575, 1996.

2-9. Skinn, D.A., Gallagher, J.P., Berens, A.P., Huber, P.D., Smith, J., "Damage Tolerant Design Handbook – A Compilation of Fracture and Crack Growth Data for High Strength Alloys," Vols. 1-5, WL-TR-94-4052, USAF Wright Patterson AFB, OH, May 1994.

2-10. Smith, F.R., et al., "PROF v3.1 Probability-of-failure User's Manual," UDR-TR-2011-15, University of Dayton Research Institute, Dayton, OH, February 2011.

2-11. Clifton, F., "Strength Variability in Structural Materials," Aeronautical Research Council Reports and Memoranda No. 3654, February 1969.

3.0 GEOMETRY MODELING

This section provides a review of geometry parameters used in the stress intensity factor (SIF) models contained in the NASGRO software [3-1]. This is followed by a discussion of which parameters of the NASGRO SIF models are considered as random variables within the PDTA software. Guidelines and recommendations for input and use of these random variables are then provided in the final subsection.

3.1 OVERVIEW OF NASGRO STRESS INTENSITY FACTOR GEOMETRIES AND NOMENCLATURE

The NASGRO software has a large library of SIF solutions (models) that are available to the analyst and the reader is referred to the NASGRO manual [3-1] for a detailed description of each. These models are named by the type of crack: TCxx (through cracks), CCxx (corner cracks), and SCxx (surface cracks). Table 3-1 lists the NASGRO SIF models that are currently supported by the PDTA software. Note that this list is a large subset of the overall NASGRO SIF solution library.

The nomenclature used by NASGRO to define the geometric parameters of the various stress intensity factor models is listed as follows:

- a = crack depth, in the through-thickness, t, direction
- c = crack length, or half crack length, along the surface, in the width, W, direction
- c is used for through-crack lengths
- Crack aspect ratio = a/c
- Width must generally be greater than thickness, $W \geq t$
- D = hole diameter, cylinder diameter
- B = hole edge distance (hole center offset); measured from hole center to edge of plate

As an example, Figure 3-1 shows the geometry for a commonly used corner crack at a hole model (CC02) illustrating the definition of the geometric parameters. Sketches like this are provided in the NASGRO manual and are displayed in the NASGRO GUI for each SIF model.

Table 3-1 NASGRO Stress Intensity Factor Models Supported in the PDTA Software

Crack type	Description
TC01	Through crack at center of plate
TC02	Through crack at edge of plate
TC03	Through crack at hole (offset) in plate
TC04	Through crack at hole in lug
TC05	Through crack(s) at hole in plate with row of holes
TC08	Through crack (circumferential)in hollow cylinder
TC11	Through crack (offset) in plate – univariant WF
TC12	Through crack at edge of plate – univariant WF
TC13	Through crack(s) at hole (offset) in plate – univariant WF
TC17	Through crack at edge notch in plate – univariant WF
TC18	Through crack(s) at (offset) embedded slot or elliptical hole in plate – univariant WF
TC19	Through crack at hole (offset) in plate with broken ligament – univariant WF
TC23	Two unequal through cracks at offset hole
CC: corner crack	
CC01	Quarter elliptical corner crack in plate
CC02	Quarter elliptical corner crack at hole (offset) in plate
CC03	Quarter elliptical corner crack at hole in lug
CC04	Quarter elliptical corner crack(s) at hole in plate
CC08	Quarter elliptical corner crack(s) at hole (offset) in plate – univariant WF
CC09	Quarter elliptical corner crack in plate – bivariant WF
CC11	Quarter elliptical corner crack in plate – univariant WF
CC13	Quarter elliptical corner crack at edge notch in plate
CC14	Quarter elliptical corner crack at (offset) embedded slot or elliptical hole in plate
CC15	Quarter elliptical corner crack at (offset) hole in plate with broken ligament
SC: surface crack	
SC01	Semi-elliptical surface crack in plate
SC02	Semi-elliptical surface crack in plate – univariant WF
SC05	Semi-elliptical surface crack (circumferential) in hollow cylinder
SC07	Semi-elliptical surface crack (circumferential) in solid cylinder
SC17	Semi-elliptical surface crack (offset) in plate – univariant WF
SC19	Semi-elliptical surface crack (offset) in plate – bivariant WF

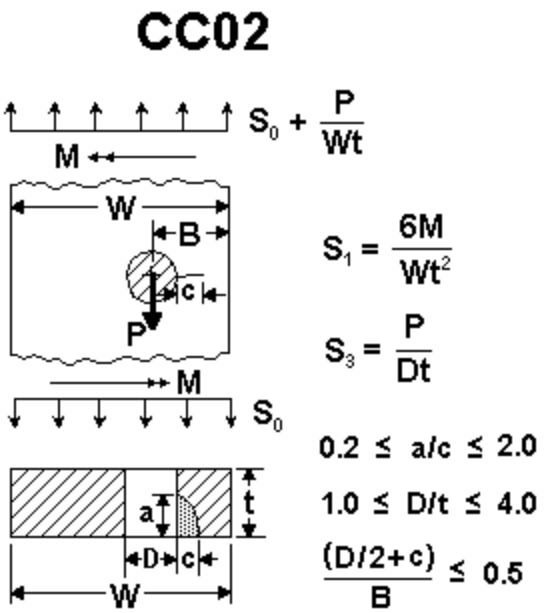

Figure 3-4 NASGRO SIF Model for a Quarter-Elliptical Corner Crack at an Offset Hole in a Plate (CC02)

3.2 GEOMETRIC RANDOM VARIABLES USED IN THE PDTA SOFTWARE

The initial crack size and shape are well known to be perhaps the most significant random variables in probabilistic damage tolerance analyses and Section 4.0 of this report is devoted to modeling initial crack size distributions. The other geometric random variables that the PDTA software can consider are the hole diameter, *D*, and the edge distance (or hole offset), *B*. See Figure 3-1. The PDTA software requires that the mean and standard deviation for each of these random variables be specified, assuming a normal distribution.

3.3 CHARACTERIZATION OF GEOMETRIC RANDOM VARIABLES

The variability of hole diameters and edge distances within an aircraft structure depend mainly on the manufacturing quality of the airframe. Since fastener holes are drilled with the same tool used repetitiously, the COV for the hole diameter is typically very small. Generally, the nominal hole diameter is used as the mean and the standard deviation is dependent on the tolerance values. Edge distance COV can depend on whether the fastener holes were hand-drilled or machine-drilled, leading to high and low COVs, respectively.

A few studies give insight into the uncertainty quantification of geometric random variables. Millwater and Wieland [3-2] studied the sensitivity of the probability-of-failure to various PDTA random variables and characterized the hole diameter and edge distance variability on a certain fastener hole location in the T-38 lower wing skin. The mean and standard deviation of the hole diameter was 0.26 and 4.2E-4 inches, respectively, giving a COV of 0.16 percent. However, it was stated that the measurements of the hole diameter were only accurate to 5E-4 inches; thus, the true COV is likely smaller than that which was measured. Fastener holes at this location were hand drilled and edge distances had a COV of 2.69 percent.

A similar study recorded the edge distance variation of fastener holes on a splice joint which was part of a modification for a military aircraft [3-3]. After taking edge distance measurements of eight similar locations on 24 aircraft, it was determined that this particular structural detail exhibited a COV of 38 percent. However, this large variation did not seem to have a significant effect on the probability-of-failure. Figure 3-2 shows how a lognormal distribution was fit to the data using a histogram of values.

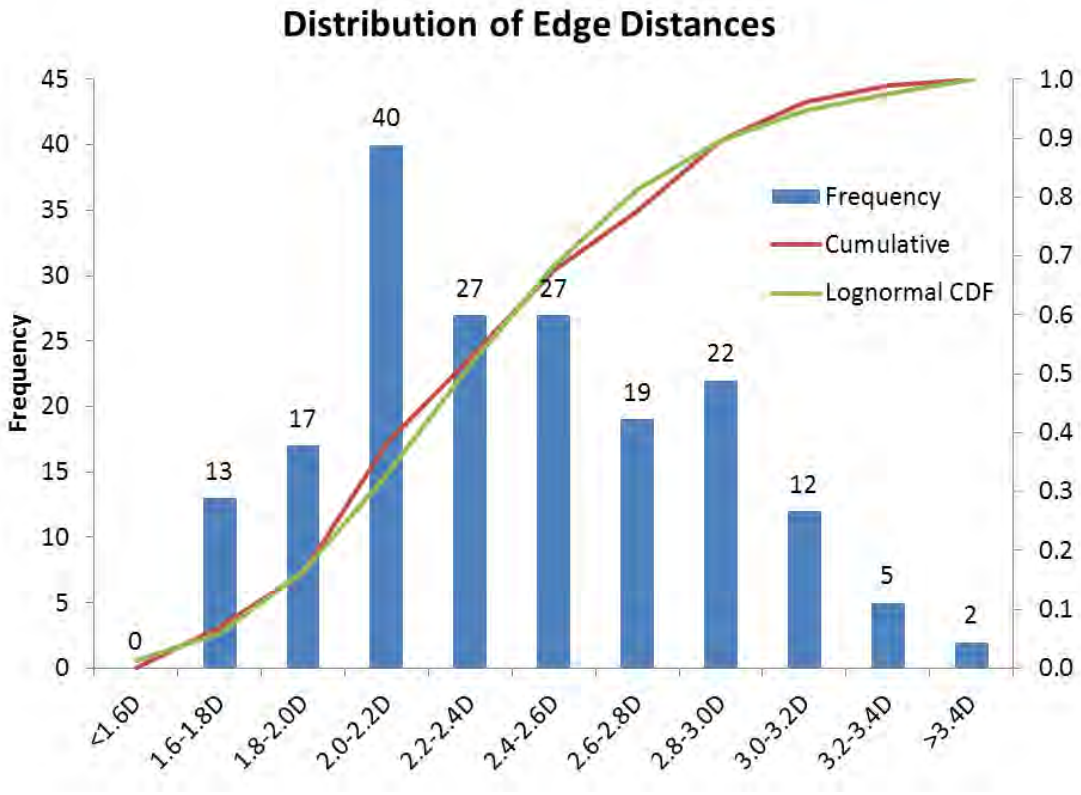

Figure 3-5 Edge Distance Measurements Fit to a Lognormal Distribution [3-3].

3.4 REFERENCES

3-1. NASGRO® Fracture Mechanics and Fatigue Crack Growth Analysis Software, Version 7.0, Southwest Research Institute and NASA Johnson Space Center, November 2012.

3-2. Millwater, H.R., and Wieland, D.H., "Probabilistic Sensitivity-Based Ranking of Damage Tolerance Analysis Elements," *Journal of Aircraft*, Vol. 47, No.1, pp. 161-171, 2010.

3-3. Domyancic, L.C., et al., "Sensitivity Analysis for Risk Assessment of an Aircraft Fatigue Critical Location," *53rd AIAA/ASME/ASCE/AHS/ASC Structures, Structural Dynamics, and Materials Conference*, Honolulu, HI, 2012

4.0 INITIAL FLAW SIZE MODELING

4.1 BACKGROUND

The PDTA methodology uses results from linear elastic fracture mechanics computations for the growth of fatigue cracks in critical structural components. In contrast to US Air Force damage tolerance requirements, the FAA does not specify an initial crack size to be used for these analyses. It is the analyst's responsibility to characterize the state of flaws or cracks at some initial time, which is usually at the time of manufacture.

This need to characterize the initial structural condition has led to the development of the concept of the equivalent initial flaw size (EIFS) [4-1]. The EIFS is a hypothetical crack, assumed to exist in the structure, which characterizes the equivalent effect of the actual flaws in the structural detail. As such, if the distribution of equivalent initial flaw sizes was used as initial crack sizes in fracture mechanics crack growth analyses, results would predict the crack sizes found in a durability test article or destructive teardown inspections. Because of the variable nature of fatigue, there is a distribution of crack sizes found during these inspections, such as shown at time t_1 in Figure 4-1. Using this distribution of crack sizes at time t_1, along with the deterministic crack growth curve, the distribution of crack sizes at some initial time, t_o, can be determined as illustrated in Figure 4-1.

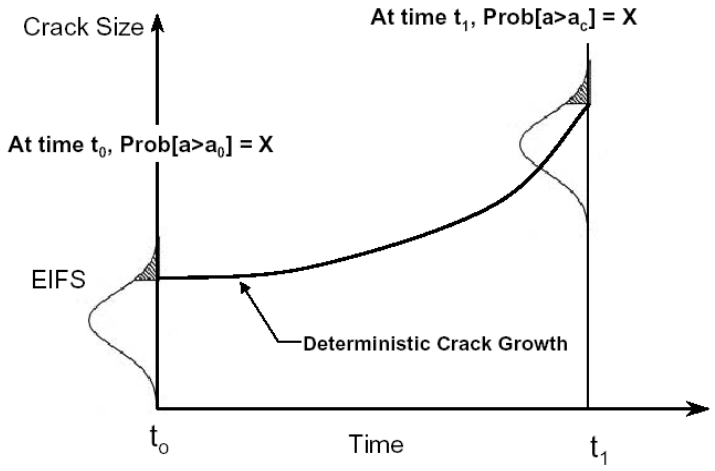

Figure 4-6 Concept to Determine the Equivalent Initial Flaw Size (EIFS)

Section 4.2 discusses how to obtain EIFS data and reviews some commonly used statistical distributions. An example is also presented to demonstrate how discrete EIFS data and corresponding statistical distributions can be approximated from field inspection information. The following Section 4.3 reviews existing EIFS distributions for aircraft materials. Finally, a description of the post-repair flaw size distribution is presented in Section 4.4.

4.2 PROCESS TO DETERMINE EIFS DISTRIBUTION FROM INSPECTION DATA

The ideal method of developing an EIFS distribution is to collect data from an inspection of the entire fleet. This allows for a full characterization of the state of the fleet, whereas a teardown inspection will only give a small sample of data.

For each location that is inspected, the detected crack length and flight history are needed. It is very important that non-detections – i.e. inspections that found no cracks – are also included in the dataset. In this way, an EIFS distribution which is grown forward in time will be representative of the actual state of the fleet, and not just the cracked locations. These non-detections should be considered suspended data points and can be assigned a "missed" crack size based on either a minimum detectable crack size, a POD curve of the inspection method, or engineering judgment.

Once the data set is collected, each point must be translated back to time zero in order to determine the equivalent initial flaw size. This is done in the following manner. First, the "equivalent" current time is found for the data point by interpolation of the current crack size on the deterministic crack growth curve. Second, the actual flight hours of the location is subtracted from the equivalent current time. This will give the crack size at time zero, known as the EIFS. Note that this process can be complicated if the aircraft sees varying usage; the crack growth curve must be representative of the actual aircraft usage.

An EIFS distribution can be constructed after this process is completed for the entire data set. Common distribution fitting techniques can be used, such as ranking, regression, and maximum likelihood estimation. Ref. 4-3 discusses the process and gives examples. Also, statistical software that specializes in fitting data to distributions is widely available. Due to the high sensitivity of the output to the EIFS distribution, the lognormal and Weibull distribution options in the PDTA software should only be used if a close fit can be obtained. Otherwise, tabular input should be used to provide the best representation of data.

Many existing EIFS distributions use the Weibull three-parameter model, where the cumulative distribution function F(c) is written as:

$$F(c) = 1 - exp\left(-\left(\frac{c - c_0}{\eta}\right)^{\beta}\right)$$

Where:

c = crack size (inches)
c_0 = distribution origin (inches)
η = scale parameter (inches)
β = shape parameter

To fit empirical EIFS data to a Weibull distribution, the CDF function F(c) above is transformed to a Weibull scale and the Weibull parameters (c_0, η, and β) are determined by a "best fit" linear regression process.

As a general observation, EIFS curves that are shifted to the right, especially at higher cumulative probability levels, will result in greater probability-of-failure.

4.2.1 Example

As an example of creating an EIFS distribution from inspection data, consider a fleet of 69 aircraft with a wing fastener hole fatigue critical location (FCL) under analysis. Given that each half of the wing has one FCL, there are a total of (69 x 2) 138 inspected locations. For simplicity, assume that the crack growth curve can be modeled analytically using an exponential function:

$$C(t) = 0.005 \exp(0.000379\mathrm{t})$$

where C(t) is the crack size as a function of flight hours, and t is the time in flight hours. The crack length at zero flight hours (t = 0) is taken as 0.005 inches.

During a fleet inspection, 71 locations had flaws which were found and recorded, and 67 locations did not have detected flaws. Figure 4-2 shows the distribution of 71 flaws found at the FCL on a population of 69 inspected aircraft. Flaw sizes were generally not directly measured but estimated by the oversize of the reamer needed to remove the flaw indication. Note the vertical steps at 0.015, 0.03 and 0.06 inches in Figure 4-2. These correspond to oversize values of 1/64, 1/32, and 1/16 inch on the radius. Also noted on this figure are the two large 0.21-inch and 0.36-inch flaws found on separate aircraft at 4,619 and 4,519 flight hours, respectively.

These "inspected" flaw sizes were used in conjunction with the given crack growth curve to estimate the EIFS. The analysis assumes that the inspected flaws are sharp fatigue cracks, and linear elastic fracture mechanics, as represented by the crack growth curves, can be used to backtrack the crack size.

As a specific example of how to backtrack the size of a single crack, assume that a 0.032-inch crack was found at the FCL at 6,909 flight hours. Using the analytical crack growth equation the number of flight hours from the 'initial time' is calculated as 4,898. Note that the crack length at the 'initial time' (i.e., at zero flight hours) is 0.005 inches from the crack growth equation. However, the aircraft was inspected at 6,909 hours and has flown 2,011 hours (6,909 – 4,898) prior to the 'initial time.' Using the analytical crack growth equation at –2,011 flight hours gives a crack size of 0.00233 inches. This is the EIFS for the particular flaw indication found during inspection.

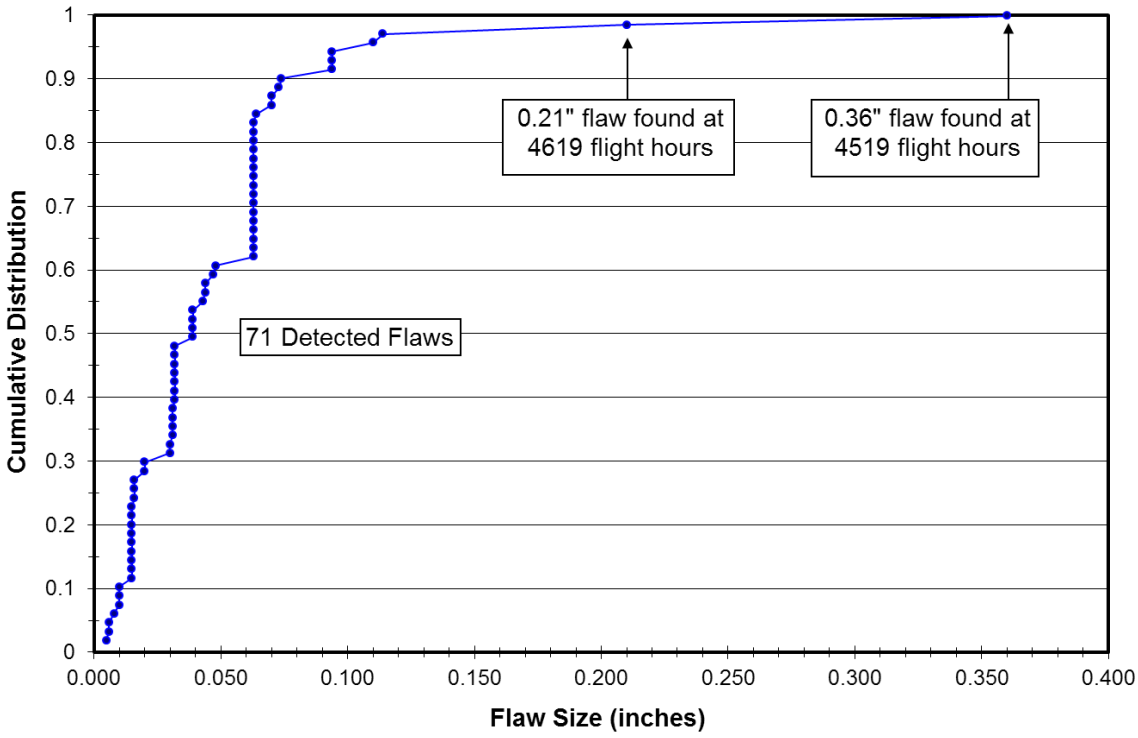

Figure 4-7 Distribution of Flaw Sizes (Detected Only) at the Example FCL.

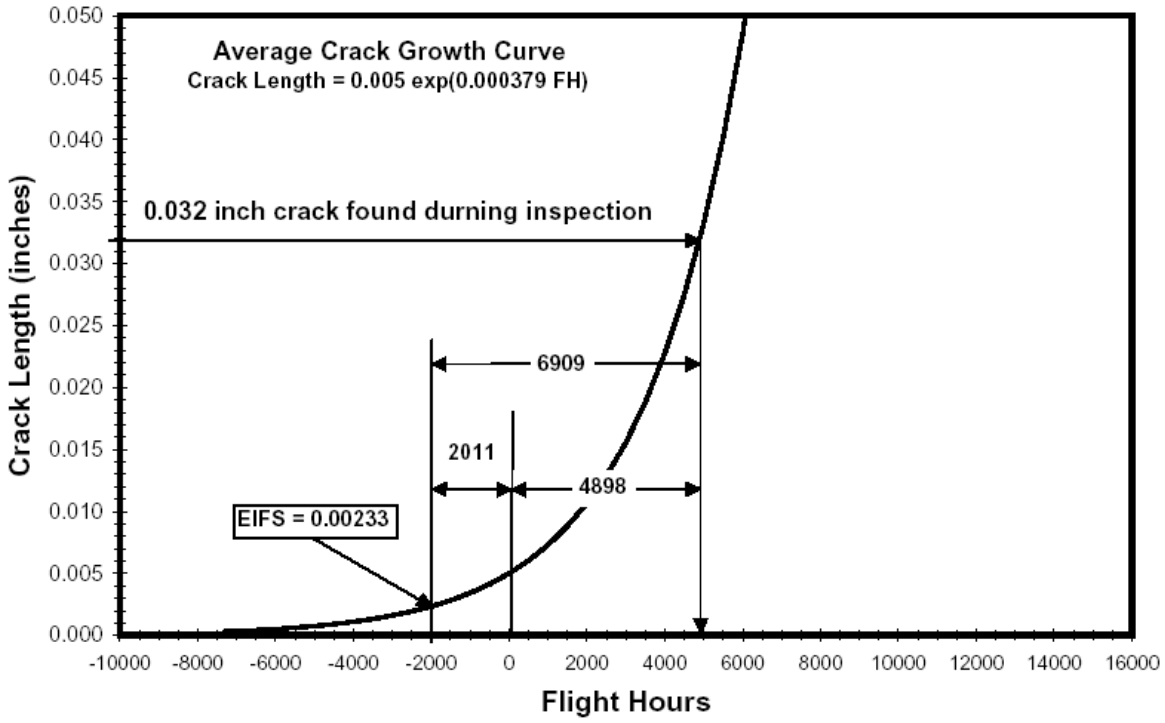

Figure 4-8 Process to Determine EIFS from Inspection Data

Using the process illustrated in Figure 4-3, two EIFS distributions were created. The first, called "Detected Flaws Only," uses only the 71 data points of the detected flaws. The second assumed that for the 67 remaining locations, a flaw existed which was below the minimum detectable flaw size. This analysis assumes that each of these holes contains a flaw equal to the size of the smallest flaw found (0.005 inch). This means that flaws are assumed at all holes, either those 71 flaws detected or the 0.005 inch flaw assumed to exist in the remaining 67 holes. This should give a lower bound to the discrete EIFS distribution using the inspection data.

The two EIFS data sets are plotted in Figure 4-4. The dataset using only the detected flaws best fit a lognormal distribution, while the dataset assuming flaws at all holes best fit a Weibull distribution. These curves collectively show the large difference that can occur when suspended data points (non-detections) are included in the EIFS construction. Also plotted are curves for the 2024-T851 [4-2] and 7075-T73 [4-4] distributions for comparison.

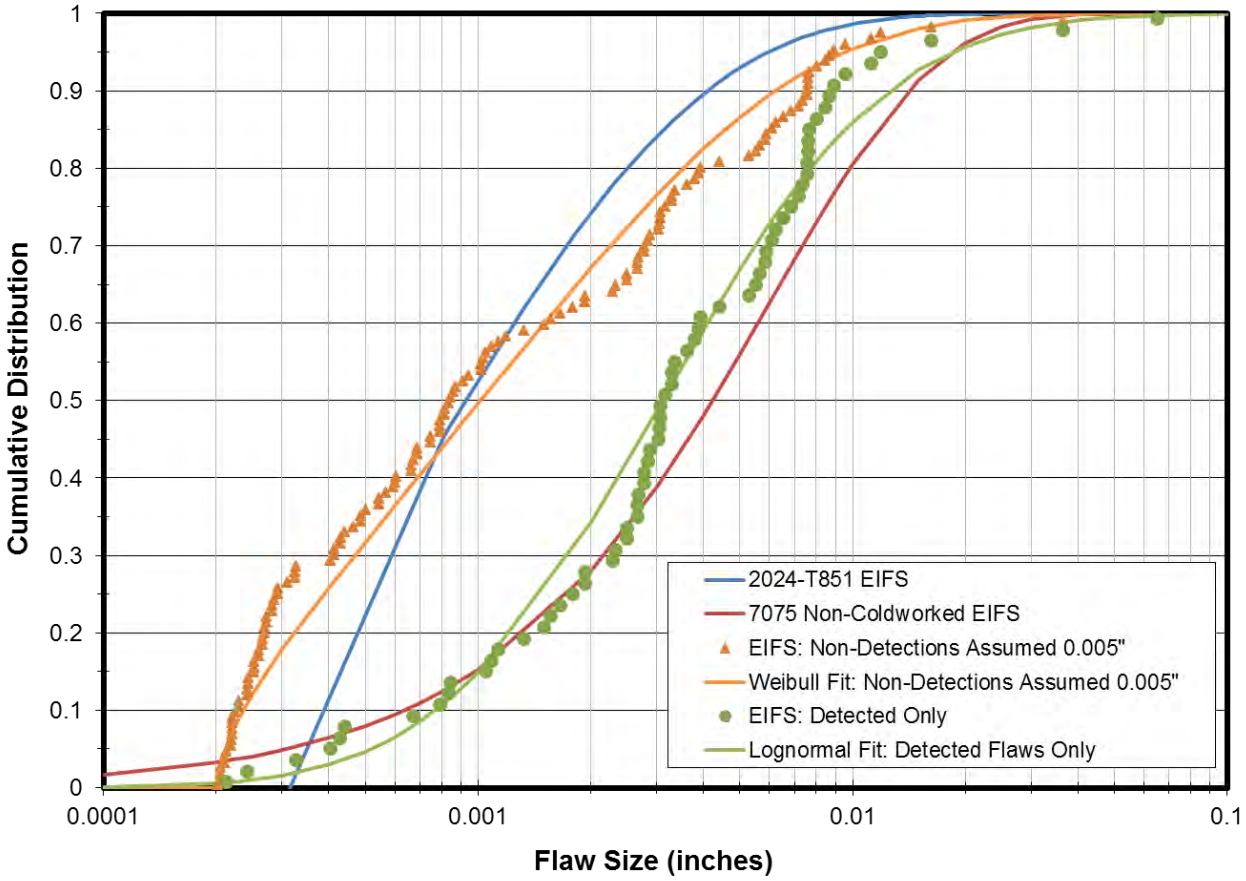

Figure 4-9 Comparison of EIFS Distributions

4.3 EXISTING EIFS DISTRIBUTIONS

Since the probability-of-failure is highly sensitive to the EIFS distribution, every effort should be made to create this distribution from inspection or teardown data that is specific to the structural detail under analysis. However, there are cases where this information does not exist and best engineering judgment must be used instead. The following section lists EIFS distributions that are available in the literature and can be used as a guide for EIFS inputs.

In 1996, SwRI conducted a full-scale durability fatigue test followed by a destructive teardown inspection as part of an economic life evaluation of the T-38 –29 wing [4-4]. The T-38 wing skin material was 7075-T73 plate, and contained both coldworked and non-coldworked fastener holes. The holes were distributed over the lower wing skin and each was subjected to its own stress field, had a unique wing skin thickness, and used varying fracture mechanics models. This resulted in 24 separate fracture mechanics analyses that included crack growth retardation. The resulting EIFS distributions are considered conservative since the data set did not include suspended data.

In 1999, Lincoln and Melliere published a paper [4-2] addressing the economic life of a military aircraft. That paper presented EIFS distributions, based upon Weibull models, for several 2000 and 7000 series aluminum and titanium alloys obtained from durability tests conducted by McDonnell Aircraft for the USAF F-15E.

Table 4-1 gives the Weibull parameters for the EIFS distributions that were documented in the above studies.

Table 4-2 Weibull Parameters for Aluminum and Titanium EIFS Distributions

Material	Shape β	Scale η (inches)	Location c_0 (inches)	Source
2024-T851	0.659	0.00106	0.000315	4-2
7075-T73 (Non-coldworked hole)	0.996	0.0061	0.0	4-4
7075-T73 (Coldworked hole)	0.939	0.0025	0.0	4-4
7075-T7352	0.763	0.00016	0.00024	4-2
7075-T76	1.519	0.00189	0.0	4-2
7175-T7452	1.056	0.00130	0.00071	4-2
Ti-6Al-4V	1.434	0.00279	0.00012	4-2
Ti-6Al-6V-2Sn	0.730	7.87E-5	3.94E-5	4-2

For 4340 steel, test results from Purdue University [4-5] were used as a basis for assuming an initial crack size distribution. That research developed a three-parameter (shifted) lognormal fit based on “crack forming inclusion” measurements obtained from 4340 SENT specimen fracture surfaces. This distribution is plotted in Figure 4-5 as a function of crack length.

The distribution reported in [4-5] is a function of area. Due to the exclusion of crack forming inclusions below a threshold size, a shifted lognormal distribution was used, whose cumulative distribution function, f(X), is given by

$$f(X)=\Phi\left[\frac{\ln(X-\tau)-\mu}{\sigma}\right]$$

where

X = crack inclusion area, (in^2)
μ = scale parameter, -16.8422 ($\ln(in^2)$)
σ = shape parameter, 1.0658
τ = threshold parameter, 3.9541E-8 (in^2)

To obtain an EIFS distribution from the inclusion area distribution, the corresponding crack sizes were extracted from the areas by assuming a semi-circular crack. This transformation is given by

$$X=\frac{\pi c^2}{2}$$

The total length of the crack is equal to 2c and corresponds to the x-axis of Figure 4-5.

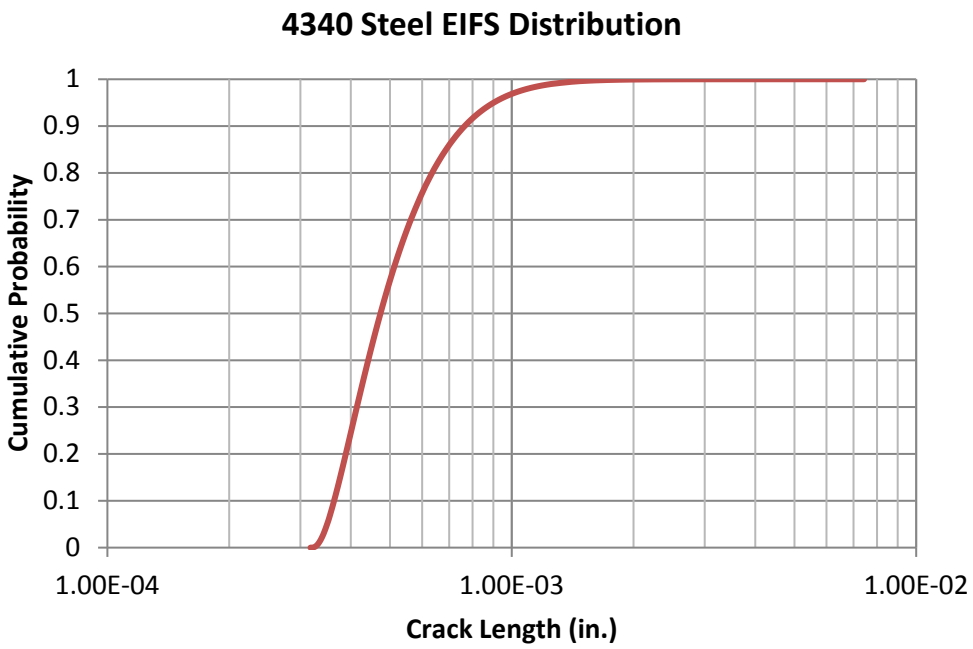

Figure 4-10 EIFS Distribution for 4340 Steel

4.4 POST-INSPECTION AND POST-REPAIR INITIAL FLAW SIZE DISTRIBUTION MODELING

The repair crack size distribution models the cracks present in a location after a repair has been performed. Very rarely does sufficient data exist to properly model this variable. Analytical models (e.g. lognormal, Weibull) for this distribution are the same as those used for the EIFS distribution; however, the parameters may be different depending on the type of repair. For instance, if a repair consists of replacing a used part with one of equivalent initial quality, then the same EIFS distribution can be used as the repair crack size distribution.

Alternatively, a repair may consist of slight modification to the original structure, such as oversizing a fastener hole. In these types of repairs, a location with a crack indication is modified until the NDI method no longer detects a crack. However, cracks may still exist in the structure which are smaller than the detection size threshold. Thus, engineering judgment should be used to make assumptions of crack sizes by taking into account the type of repair and the minimum detectable flaw size of the NDI method. The repair crack sizes generally will be much smaller than the cracks that are detected during an inspection cycle and will not affect the failure probabilities until multiple inspection cycles have been completed.

4.5 REFERENCES

4-1. "Durability Methods Development," AFFDL-TR-79-3118, Volumes I-IX, Air Force Flight Dynamics Laboratory, Wright-Patterson Air Force Base, OH, April 1978-January 1984.

4-2. Lincoln, J.W., and Melliere, R.A., "Economic Life Determination for a Military Aircraft," *AIAA Journal of Aircraft*, Vol. 36, No. 5, September-October 1999.

4-3. Abernathy, R.B., *The New Weibull Handbook*, Fourth Edition, published by Dr. R.B. Abernathy, 536 Oyster Road, North Palm Beach, Florida, 33408, February 2005.

4-4. Burnside, H., Wang, W. and Dubke, J., "Economic Life Evaluation of the T-38 –29 Wing," Proceedings of the 1996 USAF Aircraft Structural Integrity Program Conference, San Antonio, Texas, December 1996.

4-5. Sharpe, P.S., Hillberry, B.M., and Craig, B.A., "Fatigue Life Variability Prediction Based on Crack Forming Inclusions in a High Strength Alloy Steel," ASTM STP 1450, Probabilistic Aspects of Life Prediction, W.S. Johnson and B.M. Hillberry, Eds., ASTM International, West Conshohocken, PA, 2004.

5.0 INSPECTION CAPABILITY MODELING

5.1 ANALYTICAL MODELS FOR POD CURVES

Inspection capability in the PDTA software is modeled using a probability of detection (POD) curve as a function of crack size. However, there are limited sources of POD data since the number of tests required to obtain a full POD curve is very large. As an alternative, the capability of an inspection system can also be quantified (albeit to a lesser extent) by defining the crack length for which the probability of detection is 0.9. This crack length is known as a_{90}.

For a lognormal distribution, the parameters that define the POD curve are the median detectable crack size, $a_{50} = \mu$, and the POD standard deviation, defined in this report as σ. If only the a_{90} value is available rather than a full POD curve, engineering judgment can be used to determine a standard deviation, σ. A larger σ implies a "flatter" POD curve, meaning lower detectability at larger crack sizes. The following relation can be used to determine μ from a_{90} [5-1]:

$$\mu = \frac{a_{90}}{\exp(1.282\sigma)}$$

Fully automated eddy current inspection systems conducted with the part removed from the aircraft can have σ values in the range of 0.2 to 0.7, depending on the material and geometry of the parts [5-2]. Less controlled inspections using manual or semi-automated eddy current can have σ values greater than 1.0 [5-3, 5-4].

5.2 SOURCES OF POD DATA

An effort should be made to define a POD curve or a_{90} value that is specific to the structural detail under analysis. If this is not possible, there is a short list of documents that are available to use as a reference for NDI capabilities. US Air Force Structures Bulletin EN-SB-08-012 [5-5] defines the recommended nondestructive inspection (NDI) capability flaw sizes (a_{NDI}) that should be assumed when computing the re-inspection intervals for structures managed by the Air Force Aircraft Structural Integrity Program (ASIP) when no other supporting data is available. Both a_{90} and $a_{90/95}$, the 90 percent detectable crack length with 95 percent confidence, values are given for aluminum, steel, and titanium for various inspection methods.

The Nondestructive Evaluation (NDE) Capabilities Data Book [5-4] contains 423 POD curves from tests using different inspection methods, materials, and geometries. Also available are standard NDE capability flaw sizes used for NASA applications. However, it is emphasized that this data is for reference only and that POD curves should be developed for critical parts under analysis.

5.3 REFERENCES

5-1. Smith, F.R., et al., "PROF v3.1 Probability-of-failure User's Manual," UDR-TR-2011-15, University of Dayton Research Institute, Dayton, OH, February 2011.

5-2. Berens, A.P., "Analysis of the RFC/NDE System Performance Evaluation Experiments," *Review of Progress in Quantitative Nondestructive Evaluation 6A*, Edited by Donald O. Thompson and Dale E. Chimenti, Plenum Press, New York, 1987.

5-3. Lewis, D.P., et al., "Reliability of Nondestructive Inspection – Final Report," SA-ALC/MME 76-6-38-1, San Antonio Air Logistics Center, Kelly Air Force Base, TX, December 1978.

5-4. Rummel, W.D., and Matzkanin, G.A., *Nondestructive Evaluation (NDE) Capabilities Data Book*, 3rd Ed., NTIAC:DB-97-02, November 1997.

5-5. EN-SB-08-012, Rev. C, "In-Service Inspection Flaw Assumptions for Metallic Structures," US Air Force Structures Bulletin, AFLCMC/EZ, May 2013.

6.0 CONCLUSIONS

The purpose of this document was to provide background information and guidelines to aid in the development and specification of input parameters associated with random variables used in the probabilistic damage tolerance analysis (PDTA) software developed to assist the FAA in maintenance planning for small airplanes.

Section 2.0 of this report provided background on the NASGRO equation for fatigue crack growth and guidelines regarding choices for parameters that are considered as random variables in the NASGRO equation. It is noted, however, that the PDTA software has options other than the NASGRO equation (i.e., the master curve approach) that also use some of these parameters, in particular, yield strength and fracture toughness. In these cases the discussions in Section 2.4 and 2.5 would also apply to this alternate approach.

In Section 3.0, examples were provided on how to obtain data to categorize the variability of select geometry parameters (hole diameter, edge distance) that would be used in the stress intensity factor model of a fatigue critical location. The variability of these types of data can be aircraft dependent and depend on the initial manufacturing process, quality and vintage of the airframe. If repairs and/or modifications were performed at a given fatigue critical location, the variability may be significant, particularly if different repair shops were used across the fleet. Therefore, if the analyst is concerned with how differences in geometry may affect life and risk, there really is no substitute for obtaining a sample of measurements of these quantities from the fleet. In the absence of such data, the analyst should perform a sensitivity study on his geometry modeling assumptions to determine if they have a significant effect on life and risk. In many cases, the influence of these parameters is minor when compared to other factors such as material properties and equivalent initial flaw size.

The use of the equivalent initial flaw size (EIFS) distribution to characterize the initial condition of a fatigue critical location was reviewed in Section 4.0. While the EIFS distribution is often the most influential random variable in a probabilistic DTA (with the possible exception of the loadings), it should be realized that it is not based on a measurement of initial material quality; rather, it is based on extrapolated values of crack sizes which when grown forward produce crack sizes consistent with those observed in fatigue tests and/or actual aircraft structure. Therefore, EIFS distributions cannot in general be considered a material property and it must be recognized that the EIFS distribution parameters listed in the Section 4.0 examples were obtained for specific materials, geometries and aircraft usage (spectra). Ideally, fleet inspection and/or teardown data for a specific aircraft and usage should be used in the determination of the EIFS distribution at a given fatigue critical location. The EIFS distribution parameters listed in Section 4.0 provide an illustration of typical values based on data in the literature and previous SwRI research experience; they were not obtained for general aviation aircraft. Therefore, their use in general aviation probabilistic DTAs is problematic and the analyst must recognize that they may not be representative of general aviation materials and usages.

Inspection capability in probabilistic DTAs is usually modeled with a POD curve and ideally this curve would be developed specifically for each structural detail and NDI method; however, in practice many times all that is available is the crack length that is detectable 90 percent of the time. Section 5.0 discusses approaches to develop a lognormal POD curve; however, considerable

engineering judgment may be involved and consultation with NDI experts familiar with the methods being used and the locations being inspected may be warranted in order to develop a credible POD curve for use in a probabilistic DTA.

APPENDIX C—DEVELOPMENT OF NASGRO® ALTERNATIVE INTERFACE FOR PROBABILISTIC DAMAGE TOLERANCE ANALYSIS

C-1. INTRODUCTION

The purpose of this document is to provide detailed information on an alternative input interface developed for the NASGRO software that facilitates the large number of repetitive crack growth calculations required by the probabilistic damage tolerance analysis (PDTA) software developed as part of the FAA research project entitled "Probabilistic Damage Tolerance-Based Maintenance Planning for Small Airplanes." It is presumed that the readers of this report are familiar with the use of both NASGRO and PDTA software.

The work reported herein was conducted by Southwest Research Institute® (SwRI®) in San Antonio, TX, under subcontract to the University of Texas at San Antonio (UTSA) as part of FAA Contract No. 09-G-016. The overall project involves the development of a comprehensive probabilistic damage tolerance methodology, such that FAA engineers can advise maintenance planning in support of policy decisions in the general aviation fleet.

C-2. SUMMARY

An alternative interface for NASGRO has been developed to facilitate the large amount of repetitive NASGRO fatigue crack growth (FCG) analyses demanded by PDTA applications. With this approach, more than 400 application program interface (API) functions were developed in support of this new interface. Separate driver routines, specifically for PDTA, were implemented to use one template file to define the analysis problem and one sample file to obtain parameterized variables from randomization.

A software package is supplied on a CD along with this report. The package contains software routines and binary executable code developed specifically for the PDTA applications. The listing of the routines contained on the CD can be found in appendix A. Bearing in mind that the NASGRO core application is distributed in terms of a binary library format, a procedure for constructing the NASGRO workspace, as described in appendix B, is provided to the user in the event of a need to rebuild the NASGRO application. The software driver is derived from the driver routines for PDTA, whose content can be identified in the included text-formatted driver routines. Additional "dummy" routines are provided in case modifications to the driver routines, resulting in a rebuild, are needed.

For future development, it is suggested that the output capability based on this new alternative interface be enhanced. With such a new effort, a new compact and more structured format for the output database will need to be defined and a separate set of output API functions implemented. This would eliminate the computation lag as a result of writing output inside NASGRO and lead to more effective control over the output functionality through API function calls.

C-3. INTERFACE DEVELOPMENT PROCESS

With the development of an alternative interface for NASGRO to facilitate the UTSA/FAA PDTA applications, driver routines and internal NASGRO restructuring were required. The restructuring

established a clean interface, enabling the user to use NASGRO as an individual software module. It also provides an alternative interface, in addition to the conventional one, tightly associated with the released NASGRO GUI that generates text-based batch files required by the conventional NASGRO interface. The NASGRO program containing the new alternative interface is generated based on a separate set of compiler macro directives. The objective of this new interfacial approach is to facilitate the computational effort to perform large amounts of repetitive NASGRO analyses demanded by PDTA applications. The approach replaces the traditional NASGRO batch file-based data passing mechanism with a more efficient approach: API function calls. The advantage becomes obvious when considering the time-consuming and error-prone shortcomings involved with generating text-based batch files.

Using this new approach, the input process for the analysis problem is conducted at the very beginning inside the driver routines by scanning through the template file. This step defines the basic required parameters such as those grouped by GUI tabs for geometry, material, loading, schedule, and output options. Next, a loop of repetitive processes—consisting of scanning each parameterized set of randomized variables in the sample file, replacing template values by parameterized values, and conducting NASGRO FCG analysis—is performed up to completion. The scanning and updating is done in the driver routines and the updated numerical data by parameterized values are passed through the alternative interface to NASGRO libraries.

As evident in the data-passing mechanism described above, the program structure can be roughly described into two classes. One class is the driver, the other is the main core of the NASGRO program. The driver is an executable generated from the driver routines. Its main function is to drive repetitive NASGRO FCG computations while obtaining a new set of parameterized variables. The NASGRO main core is distributed by SwRI as binary dynamically linked libraries (whose file extension is .dll). The libraries are provided on the CD and is delivered to the FAA with this report. Respectively, they are "nasgro_context.dll" and "nasgro_dll.dll." Note that they are accessible only within the Microsoft® Windows® environment.

The crack cases (stress intensity factor models) applicable for parametric computations in this specific version of NASGRO are listed in table C-1. This list has three new crack models—CC17, SC30, and SC31—in addition to those in the previous version provided to UTSA. As can be seen, almost all the important crack models in NASGRO for aircraft damage tolerance analyses are contained in this list. Both SC30 and SC31 are to replace SC17 and SC19, and CC17 has the new capability to compute stress intensity factors for two dissimilar corner cracks at a hole.

Table C-1 Applicable NASGRO crack models* for parameterized computation

CC (corner crack model)	TC (through-thickness crack model)	SC (surface crack model)
CC01	TC01	SC01
CC02	TC02	SC02
CC03	TC03	SC05
CC04	TC04	SC07
CC08	TC05	SC17
CC09	TC08	SC19
CC11	TC11	SC30
CC13	TC12	SC31
CC14	TC13	
CC15	TC17	
CC16	TC18	
CC17	TC19	
	TC23	

* Refer to the NASGRO user's manual for a detailed description of each model.

C-4. EXECUTION OF INTERFACE

Interactive execution of the program is straightforward. To start with, the program can be launched either in command prompt or in Microsoft Windows. Once the program is launched, three consecutive questions will be asked. For illustration, an interactive session is provided to outline these steps:

Step 1: Start the analysis either by double clicking on the program icon or by providing the program name in a new interactive session using the command prompt. For example, the following single command line shows how to provide the program name right after the system prompt to start the analysis. The program name is the same as the NASGRO program with this document:

dosSystemPrompt > nasgro_using_api

Step 2: Specify the analysis type after the on-screen prompt by the program. For PDTA, this should be for multiple analyses (two) that require a sample file.

1. Single (no sampling file) analysis
2. Multiple (using sampling file) analyses

Step 3: Provide the name of the master file or the template file after the on-screen prompt by the program.

What is the master file?
Cc01_tst1.flabat

Step 4: Provide the name of the sample file after the on-screen prompt by the program.

What is the file containing randomized variables?
Cc01_tst1.sample

Once the above information is provided, the program will start the parameterized computation. Each parameterized run designated in the sample file will have its own result file group in connection with the root name given by the template file. The root name is the name of the template file without the extension. The results of parameterized runs will be associated with file groups having indices corresponding to the IDs in the sample file. For example, the root name of the template file "cc01_tst1.flabat" is "cc01_tst1", and the parameterized analysis will generate groups of result files of which file names are expressed in terms of the following root names:

"cc01_tst1-r1," "cc01_tst1-r2," …, etc.

The interface is current with and compatible with NASGRO version v7.1. This application can be invoked as described previously.

C-5. FUTURE DEVELOPMENT

Current API functions support only the construction of the input database. A separate set of API functions would need to be generated to support the output database, such that a streamlined approach solely through API functions can be established. This would require a new definition of the data structure (in contrast to current NASGRO OUT2 file text format) consisting of all output variables, such that the integrity of the output can be retained in a compact structured binary format for quick access by the user through output API function calls.

Significance of Including Missed-Detections in Structural Reliability Updating

By

Justin Y-T. Wu

CompRel, Inc., Raleigh, NC

Feb. 2014

1.0 EXECUTIVE SUMMARY

This investigation is the continuation of an FAATC research effort, which aimed at managing aircraft structural reliability by using damage tolerance (DT) methodology combined with nondestructive inspections. The effort was largely in response to the DT requirements in FAR 29.571, Fatigue Evaluation of Rotorcraft Structures (Rotorcraft Working Group Report, 1999; 2001), which were based on the recommendations by the Technical Oversight Group for Aging Aircraft.

The DT methodology accepts the possible existence of initial flaws in structures and incorporates inspection and subsequent risk mitigation strategies to sustain structural reliability and safety. In the last decade, the above research effort has been focusing on two major areas: the advancement of the reliability-based damage tolerance (RBDT) methodology, and the addressing of the lack-of-data issue to build credible probabilistic distributions for DT analysis. It has resulted in the development of a highly efficient computational methodology for estimating reliability with or without inspections as well as the development and demonstration of a reliability-based maintenance optimization (RBMO) methodology (Ref. 1).

To address the lack-of-data issue, another research was conducted recently to target the characterization of the initial flaw size (IFS) distribution, which had been widely recognized as an important random parameter in the DT methodology. Applying the Bayes' theorem to update IFS using inspection data is a well-used approach to address the data issue. However, in the application of the Bayes' theorem, it normally requires a substantial amount of inspection data to create the likelihood function.

In order to remove the constraint, a model-based methodology which employs DT model and the probability of detection (POD) function to create likelihood functions was developed recently (Ref. 2). It proposed that the DT model could provide a foundation to build a Bayesian updating framework capable of incorporating inspection results from multiple locations and points of time. Built on this framework, a tailored computational method was subsequently developed to compute the likelihood functions and update the IFS efficiently. The two approaches have been integrated and tested by selected fracture mechanics examples. The result was encouragingly promising.

However, the above research did not fully address the situations when inspections miss either the hard-to-detect small flaws or the larger ones with a slim, but non-zero, probability to be detected. Because non-detections suggest negligible risks, it is possible that such inspection records may be overlooked when conducting Bayesian updating. Subsequently the updated IFS would reflect only the larger defects. The result could become overly conservative, especially when there are numerous misses. It is essential to investigate the importance of including the missed detections - the objective of the current project.

This report presents a DT-based Bayesian updating framework which includes both the detected and the missed detections. To demonstrate the methodology, a tailored sampling-based approach has been developed to compute likelihood functions for all the inspection results. Using a DT example, the result suggests that (1) a good POD with sizing information have a useful dominating effect for updating, (2) the non-detection results from a bad POD can provide misleading evidence

and should not be used for Bayesian updating, (3) when the inspection POD is reasonably effective, the inclusion of the count of non-detections can provide useful information for Bayesian updating.

In summary, this study shows that, with a reasonably effective POD, recording and utilizing complete inspection results, i.e., including non-detections, can be important and beneficial for aircraft reliability and risk management, including RBMO applications. The study also suggests that future research should investigate the effect of uncertainty in POD model, because of the important role POD played in DT and also the fact that POD can be highly uncertain.

2.0 INTRODUCTION

This study is the continuation of an FAATC research effort, which aimed at managing aircraft structural reliability by using damage tolerance (DT) methodology combined with nondestructive inspections. The effort was largely in response to the DT requirements in FAR 29.571, Fatigue Evaluation of Rotorcraft Structures (Rotorcraft Working Group Report, 1999; 2001), which were based on the recommendations by the Technical Oversight Group for Aging Aircraft.

The DT methodology accepts the possible existence of initial flaws in structures and incorporates inspection and subsequent risk mitigation strategies to sustain structural reliability and safety. In the last decade, the above research effort has been focusing on two major areas: the advancement of the reliability-based damage tolerance (RBDT) methodology, and the addressing of the lack-of-data issue to build credible probabilistic distributions for DT analysis. It has resulted in the development of a highly efficient RBDT computational methodology for predicting reliability with or without inspections. The RBDT methodology covers a wide range of uncertainties including the following:

- Random or uncertain parameters in material (e.g., threshold of the stress intensity factor, modulus of elasticity)
- Defect or flaw parameters (including size, shape, and location, and the frequency of occurrence)
- Loading, type of usage (with frequency of occurrence)
- Finite element model (including modeling error)
- Crack growth model (including modeling error)
- Maintenance (including inspection schedules, frequency of inspections, probability of detection curves, repair/replacement methods and effect

In order to realize the full values of the DT approach, the RBDT methodology was extended for reliability-based maintenance optimization (Refs. 1, 4). The RBMO methodology was built on an efficient and robust random simulation framework which featured three integrated efficient methods: (1) a meta-modeling approach to create fast-running DT model, (2) a stratified importance sampling method for computing reliability and generate failure-conditioned random realizations, and (3) a recursive probability integration (RPI) method for computing reliability with inspections and repairs (Ref. 3).

The remaining issues for DT applications center on the modeling of the following uncertainties:

- Probabilistic characterizations of initial flaw sizes (IFS), probability of detection (POD), and other significant uncertainties in the DT models
- Other uncertainties associated with maintenance effects, such as the quality of the repaired parts

The uncertainty modeling issues remain challenging because the needed data could be costly to obtain. It is even more so in the case of the IFS since all the NDI devices have limitations in detecting very small IFS. One solution is to measure flaws at a later time, such as from a tear-down inspection, and apply fracture mechanics crack growth models to back-extrapolate the defect sizes. The resulting IFS is commonly called Equivalent Initial Flaw Size (EIFS). However, since

the EIFS is derived under certain specific conditions, its use is limited to structural geometries and loading conditions. And because the material properties related to crack growth are random, the back-extrapolate process itself is imprecise. In actuality, the EIFS should be regarded as a rough approximation of the true IFS.

To address the lack-of-data issue, another research was conducted recently to target the characterization of the IFS distribution, which had been widely recognized as an important random parameter in the DT methodology. Applying the Bayes' theorem to update IFS using inspection data is a well-used approach to address the data issue. However, in the application of the Bayes' theorem, it normally requires a substantial amount of inspection data to create the likelihood function.

In order to remove the constraint, a model-based methodology which employs DT model and the probability of detection (POD) function to create likelihood functions was developed recently (Ref. 2). It proposed the use of the DT model to build a Bayesian updating framework capable of incorporating inspection results from multiple locations and points of time. Built on this framework, one tailored computational method was subsequently developed to compute the likelihood functions and update the IFS efficiently. The two approaches have been integrated and tested by selected fracture mechanics examples. The result was encouragingly promising.

However, the above research did not fully address the situations when inspections miss either the hard-to-detect small flaws or the larger ones with a slim, but non-zero, probability to be detected. Because non-detections suggest negligible risks, it is possible that such inspection records may be overlooked when conducting Bayesian updating. Subsequently the updated IFS would reflect only the larger defects. The result could become overly conservative, especially when there are numerous misses. It is essential to investigate the importance of including the missed detections - the objective of the current project.

In the proposed methodology, the POD plays an important role in modeling the likelihood function. In general, the parameters in a POD model should be treated as random variables that should be updated. To simplify the investigation and focus on the main objective, a range of deterministic POD curves are assumed in this study.

In the long history of the application of the Bayes' theorem for fracture mechanics (e.g., Ref 5), the likelihood functions has mostly been based on data. While the formulation to include a time-dependent likelihood function existed (e.g., Ref. 6), no implementation was available because of the difficulty in computing the likelihood functions. Most recently, the limit-state reliability method and the response surface approach was proposed to compute the crack size PDF and the likelihood function (Ref. 2). However, it has been found that that the method is not sufficiently robust or efficient.

This report presents a DT-based Bayesian updating framework which includes a complete formulation of the likelihood functions for both the detected and the missed detections. The report also includes an improved sampling-based method to replace the limit-state reliability approach for computing the crack size PDF and the likelihood function. Most importantly, the report applies

the method to investigate the significance of incorporating the number of non-detections. A representative fracture mechanics example is selected for the investigation.

3.0 METHODOLOGY

Based on the Bayes' theorem, the prior PDF distribution of a set of random variables θ, denoted as $q^-(\theta)$, is updated to a posterior PDF, $q^+(\theta)$, by using:

$$q^+(\theta \mid a_D) = C \cdot L(a_D \mid \theta) \cdot q^-(\theta) \tag{1}$$

in which a_D represents detected crack sizes, $L(a_D \mid \theta)$ a likelihood function, and C is a normalization factor defined as:

$$C = \frac{1}{\int \cdot\cdot \int L(a_D \mid \theta) \cdot q^-(\theta) \cdot d\theta} \tag{2}$$

For damage tolerance applications, the variables θ include multiple statistical parameters (e.g., mean, standard deviations) of initial flaw size, POD, applied load, and other DT modeling parameters.

Due to technology limitations or human errors, NDI devices may or may not be able to detect all defects. To include all the inspection results, the likelihood function can be modeled as a product of "detected" and "missed" likelihood functions (Ref. 7):

$$L(\theta) = L_D(\theta) \cdot L_M(\theta) \tag{3}$$

In general, inspection devices may provide flaw indications with or without crack size measurements. For simplicity, but without losing generality, this study assumes that sizing errors can be neglected. A study of the measurement uncertainty is not within the scope of the current study, but can be treated by introducing additional θ-variables to model measurement errors.

Given a detected crack of size a_{D_j} at location j, at time of inspection time, t_i, the likelihood function can be formulated as:

$$\begin{aligned} L_{D_j}(\theta) &= f_{D_i}(a_{D_j}(t_i) \mid \theta) \\ &= POD(a_{D_j}(t_i)) f_a(a_{D_j}(t_i) \mid \theta) \end{aligned} \tag{4}$$

When the crack sizing data is not available, the unknown crack size cab be treated as a random variable and the likelihood function can be formulated by integrating equation 4 over all the possible crack sizes, i.e.,

$$L_{D_j}(\theta) = \int POD(a(t_i)) \cdot f_a(a(t_i) \mid \theta) da \tag{5}$$

which can be simplified by using the expectation function E[.] as:

$$L_{D_j}(\theta) = POD_{All}(\theta) = E[POD(a(t_i)) \mid \theta] \tag{6}$$

Equation 6 suggests that the likelihood function can be estimated by taking a sample average using samples from the distribution of $f_a(a(t_i) \mid \theta)$, which can be analyzed using a DT model.

Similarly, when there is no indication of a crack, the PDF of the missed flaw can be assumed to be proportional to the PDF of the grown crack at t_i and the probability of non-detection (PND), and the likelihood function of missing the detection can be formulated by integrating over all the possible crack sizes, i.e.,

$$L_{M_k}(\theta) = \int PND(a(t_i)) \cdot f_a(a(t_i) \mid \theta) da \tag{7}$$

which can be expressed as:

$$L_{M_k}(\theta) = PND_{All}(\theta) = E[PND(a(t_i)) \mid \theta] \tag{8}$$

which can be estimated by taking a sample average using samples from the distribution of $f_a(a(t_i) \mid \theta)$.

Assume that there are I inspections at $t_{Insp} = \{t_1, t_2, .., t_I\}$, and that for each t_i there are N_i inspected locations with N_{D_i} positive indications and N_{M_i} misses, i.e.,

$$N_i(t_i) = N_{D_i}(t_i) + N_{M_i}(t_i) \tag{9}$$

The combined likelihood function for the cumulative inspection results, from multiple locations and points of time, can be summarized as:

$$L(\theta) = \prod_{i=1}^{I} \left\{ \prod_{j=1}^{N_{D_i}} L_{D_j}(\theta) \cdot \prod_{k=1}^{N_{M_i}} L_{M_k}(\theta) \right\} \tag{10}$$

WITH CRACK SIZE MEASUREMENTS

If NDI can provide sizing measurements, the likelihood function can be expressed as, by substituting equations 4 and 8 into equation 10,

$$L(\theta) = \prod_{i=1}^{I} \left\{ \left(\prod_{j=1}^{N_{D_i}} POD(a_{D_j}(t_i)) \cdot f_a(a_{D_j}(t_i) \mid \theta) \right) \cdot \left(\prod_{k=1}^{N_{M_i}} E[PND(a(t_i)) \mid \theta] \right) \right\} \tag{11}$$

in which the indices *j* and *k* are associated with inspection locations for an inspection time t_i. In equation 11, $\prod POD(a_{D_j}(t_i))$ is independent of θ, and can be taken out of the group of products and treated as part of the normalization constant in equation 2. However, in general, POD can include additional θ variables to model POD uncertainty. When a DT problem involves a single inspection location, which will be assumed in the example presented below, $E[PND(a(t_i)\,|\,\theta)]$ is the same for $k = 1$ to N_{M_i}. For this special case, the likelihood function can be abbreviated as:

$$L(\theta) = \prod_{i=1}^{I} \left\{ \left(\prod_{j=1}^{N_{D_i}} f_a(a_{D_j}(t_i)\,|\,\theta) \right) \cdot \left(E[PND(a(t_i))\,|\,\theta] \right)^{N_{M_i}} \right\} \tag{12}$$

WITHOUT CRACK SIZE MEASUREMENTS

For the cases when flaws are detected but without sizing information, the likelihood function is:

$$L(\theta) = \prod_{i=1}^{I} \left\{ \prod_{j=1}^{N_{D_i}} E[POD(a(t_i)\,|\,\theta)] \cdot \prod_{k=1}^{N_{M_i}} E[PND(a(t_i)\,|\,\theta)] \right\} \tag{13}$$

When a DT problem involves a single inspection location, $E[POD(a(t_i)\,|\,\theta)]$ is the same for $j = 1$ to N_{D_i}. For this special case, equation 13 can be abbreviated as:

$$L(\theta) = \prod_{i=1}^{I} \left\{ \left(E\left[POD(a(t_i)\,|\,\theta)\right] \right)^{N_{D_i}} \cdot \left(E\left[PND(a(t_i)\,|\,\theta)\right] \right)^{N_{M_i}} \right\} \tag{14}$$

Consider an extreme case in which the crack sizes are very small such that the POD(*a*) is nearly zero resulting in no detections, i.e., $N_{D_i} = 0$. Equation 13 can be simplified further to:

$$L(\theta) = \prod_{i=1}^{I} \left\{ \left(E\left[PND(a(t_i)\,|\,\theta)\right] \right)^{N_{M_i}} \right\} \tag{15}$$

If there is only one inspection, $I = 1$, the maximum likelihood of non-detection will occur when $E\left[PND(a(t_i)\,|\,\theta)\right]$ is at the maximum. This maximum is associated with a θ that characterizes the smallest possible crack sizes that are hard to detect. In fact, if θ is not constrained, the maximum would occur when there are no cracks at all such that PND = 1. In reality, however, θ is constrained by material characteristics and manufacturing qualities.

COMBINATION OF WITH-AND-WITHOUT CRACK SIZE MEASUREMENTS

A situation may arise when a portion of the detected flaws has sizing measurements but the remaining detections have indications but no sizing information. For this scenario, it is

straightforward to establish $L_D(\theta)$ by creating a product of likelihood functions using equations 4 and 6.

LIKELIHOOD FUNCTION COMPUTATIONAL METHODS

By using a sampling-based method, the main computational challenge is to calculate $L(\theta)$ efficiently for a large number (e.g., thousands or more) of θ samples/realizations. For each realization, the crack size PDF, $f_a(a(t_i)|\theta)$, is needed at each time of inspection, t_i, for all the inspection results, with or without detections.

To minimize the computational effort, three approaches have been developed. The first two approaches were investigated earlier (Ref. 2). The third approach, developed and used for this study, has been found to be numerically more robust and more suitable for the current study. However, the three approaches have their pros and cons and should be selected based on several factors including speed, accuracy, robustness, and computational implementation issues.

Approach 1: Limit-State Based CDF Analysis

This approach evaluates the PDF of the crack at $a = a_D$, where a_D denotes the detected sizes or the sizes needed to compute $L_D(\theta)$ and $L_M(\theta)$. The PDF can be computed using a numerical differentiation scheme such as:

$$f_a(a_D \mid \theta) = \lim_{\Delta a \to 0} \frac{\Delta F(a_D(t_i) \mid \theta)}{\Delta a} \tag{16}$$

where $F_a(a_D \mid \theta)$ is the CDF of the defect at $a = a_D$ and can be computed by a conventional limit-state reliability analysis method based on the following formulation:

$$F_a(a_D(t_i) \mid \theta) = \Pr[a(\boldsymbol{X} \mid \theta,\ t_i) \le a_D] \tag{17}$$

where $a(\boldsymbol{X} \mid \theta,\ t_i)$ is the crack growth function in which $\boldsymbol{X}$ is a set of random variables such as crack growth material parameters.

When a commonly used sampling method, such as Markov chain Monte Carlo (MCMC), is selected to update the posterior PDF (Ref. 2), the total number of times the CDF function, $F_a(a_D \mid \theta)$, needs to be calculated is proportional to the number of samples as well as the number of CDF analysis needed to compute $L(\theta)$. Therefore, Approach 1 is suitable if $F_a(a_D \mid \theta)$ can be computed analytically or numerically easily.

Approach 2: CDF Response Surface

Prior to the Bayesian-updating sampling process, a single "global" response surface (a surrogate model) of $F_a(a_D \mid \theta)$ can be created, for a range of θ, to replace the original CDF. Aside from the initial "pre-processing" time to create a proper response surface, the subsequent CDF analysis time for Bayesian updating can be drastically reduced. However, building a sufficiently accurate response surface model could be challenging, especially if the

CDF function is highly nonlinear or ill-behaved. Additionally, the analysis errors from the limit-state reliability analyses must be carefully controlled to reduce the modeling error.

Alternatively, multiple "local" response surfaces of $F_a(a_D \mid \theta)$ can also be created during the Bayesian-updating sampling process, for each θ realization.

Creating a global response surface entirely during a pre-processing stage is a useful advantage, but constructing a sufficiently accurate response surface can be challenging because the global response surface must cover a sufficient range of θ. Conversely, creating local response surfaces must be done "on demand", for each θ realization, and will slow down the Bayesian-updating sampling process, although the computational task of response surface model-building may be drastically simplified.

In principle, the response surface approach can be applied directly to the crack size PDF function. However, this alternative method is not recommended because the CDF function is, by definition, a monotonic function, which is relatively easier to fit with a lower-order response surface.

Approach 3: CDF Fitting

In this new approach, a selected number of random samples of $a_l(t_i) \mid \theta$ are generated for each θ and used to establish an empirical CDF function, $F_a(a(t_i) \mid \theta)$. A numerical differentiation method is then used to compute $f_a(a_D(t_i) \mid \theta)$. From $F_a(a(t_i) \mid \theta)$, separate sets of random crack sizes are generated to compute $E[POD(a_l(t_i) \mid \theta)]$ and $E[PND(a_l(t_i) \mid \theta)]$.

The created $F_a(a(t_i) \mid \theta)$ can be used for a wide range of crack sizes. The efficiency of the approach is proportional to the computation time for generating random samples $a(t_i) \mid \theta$ from the crack growth model. In the demonstration example, this approach will be selected because generating random samples $a(t_i) \mid \theta$ from the crack growth model is simple and fast.

Unlike the above two approaches, Approach 3 does not require numerous direct computations of $F_a(a(t_i) \mid \theta)$ by using a limit-state reliability method. Therefore, this approach is preferred if generating random crack sizes for CDF fitting is faster than constructing a CDF response surface by the limit-state reliability method. This approach is also easier to apply and more robust because the CDF curve-fitting involves a single response variable.

SAMPLING METHODS FOR BAYESIAN UPDATING

MCMC is a method widely used to avoid the tedious calculation of the normalization factor (Refs. 8-9) and was used in the precious Bayesian-updating research (Ref. 2). In this study, constructing the posterior PDF is not needed. Instead, the problem has been simplified to locate the optimal θ to maximize $L(\theta)$. This optimization problem can be solved by a numerical procedure without resorting to using MCMC or other sampling methods. However, in general, MCMC is recommended in order to view the entire posterior distribution.

4.0 FRACTURE MECHANICS EXAMPLE

ANALYTICAL MODEL

The selected problem is a fatigue reliability model originally developed for a ship-structure application (Ref. 10) and was used in the previous Bayesian-updating research (Ref. 2). The limit-state function is:

$$g(t) = \int_{a_o}^{a_f} \frac{da}{\left(\varepsilon_Y Y(a)\sqrt{\pi a}\right)^m} - C\upsilon t \varepsilon_S^m A^m \Gamma\left(1+\frac{m}{B}\right) \tag{18}$$

where

$a_o a_o$ = Initial crack depth
$a_f a_f$ = Final crack depth at failure
Y(a)Y(a) = Geometry function of the crack shape
C, m = Crack growth parameters
υ = Stress range annual frequency (cycles/year)
tt = Time under consideration (year)
ε_Y = Model uncertainty for geometry
A, B_oA, B_o = Weibull parameters for stress range

The defect is modeled as a surface crack on a plate with a width of 10,000 mm and a thickness of 30 mm. The random variables and fixed parameters are listed in Table 1. For m = 3, the defect-growth function can be derived analytically as:

$$a(t) = \frac{1}{\left[\frac{1}{\sqrt{a_o}} - \frac{C\upsilon t \varepsilon_S^3 A^3 \Gamma(1+\frac{3}{B})}{2/\varepsilon_Y^3 (1.12)^3 \pi^{1.5}}\right]^2} \tag{19}$$

which can be used to generate random crack sizes easily and quickly – which leads to the selection of Approach 3 as the best computational method.

The probability-of-failure is defined as p_f = P[g < 0] where g = Plate depth – $a(t_s)$, in which t_s = 10 years. By using a reliability analysis software with a specified 5% error bound, the probability-of-failure was p_f = 0.01225.

Table 3. Input Data for the Test Example

Name	Description	Distribution	Mean	Std. Dev.
ai	Initial crack depth (mm)	Exponential	0.11	0.11
C	Crack growth parameter (lnC)	Normal	-29.7	0.29997
ln_A	Weibull stress parameter (lnA)	Normal	2.26	0.14916
Inv_B	Weibull stress parameter (1/B)	Normal	1.43	0.1001
es	Stress modeling error	Normal	1	0.1
ey	Random geometry factor	Normal	1	0.1
Name	Description	Fixed Values		
vo	Average stress cycles per year	2.50E+06		
m	Crack growth parameter	3		
r	Crack aspect ratio (a over C)	0.15		
z	Plate thickness (mm)	30		
b	Plate width (mm)	10000		
T	Time (years)	5		
af	Final crack depth (mm)	30		
am	Measured crack depth (mm)	10		

The POD has an exponential distribution with a mean value of $1/\lambda$. The POD and the PND curves for a baseline value of λ =1.279 mm are plotted in Figure 1.

$$POD(a) = 1 - \exp(-\lambda a) \tag{20}$$

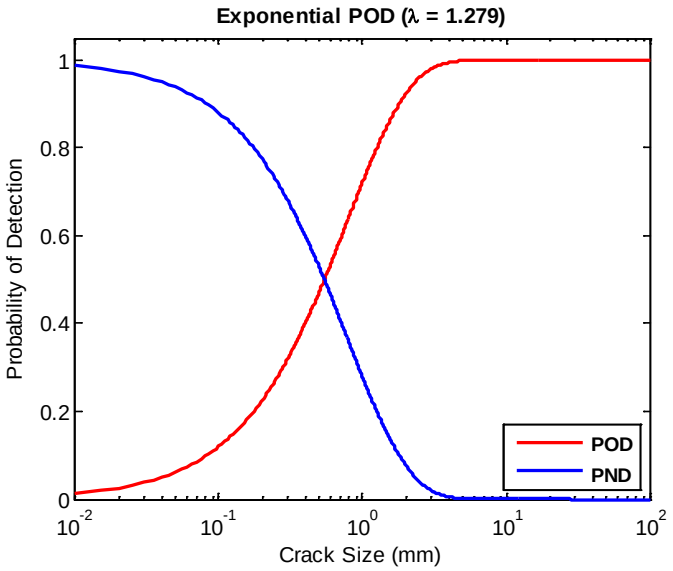

Figure 11. POD and PND Curves

MODELING OF θ

In general, the Bayesian updating methodology is capable of handling multiple θ variables. For this study, only one variable will be selected in order to focus on the main research issue. The selected θ variable is the mean value of the initial flaw size (IFS). The true IFS size is assumed to have an exponential distribution with a mean value of 0.11 mm. The prior PDF of θ is

modeled as: (1) a uniform distribution between 0 and 0.25 mm, or (2) a normal distribution, with a mean value of 0.13 mm and a coefficient of variation of 20%, i.e., $f(\theta) \sim \text{Normal}(0.13, 20\%)$. To illustrate the range of IFS, Figure 2 plots the PDF curves for three $\theta's$ and 100 random samples of crack sizes based on $\theta = 0.11$ mm.

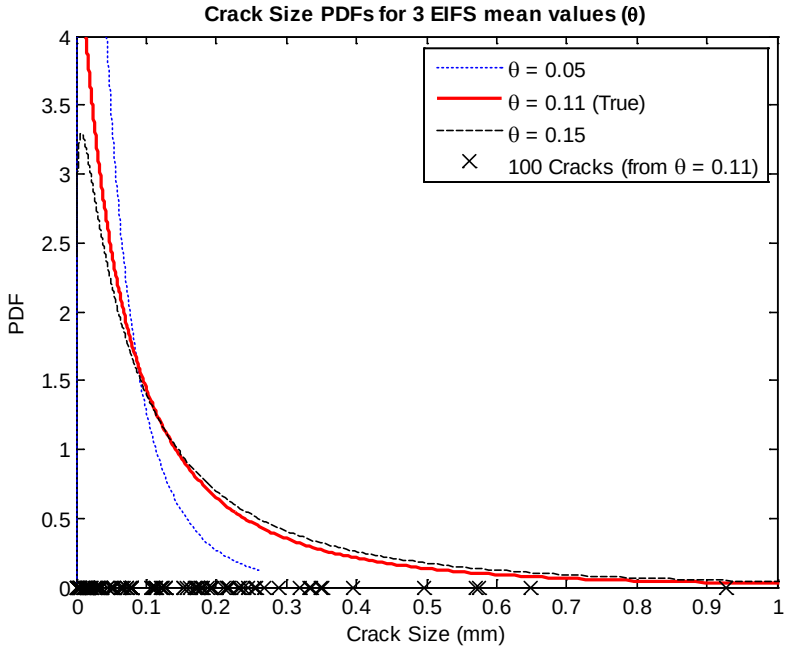

Figure 12. Crack Size PDFs and Random Crack Sizes

SIMULATION OF DETECTION DATA

The crack sizes at the time of inspection are simulated using the true initial flaw size PDF as illustrated in Figure 2. To simplify the analysis, only one inspection, at $t = 5$ years, is assumed. By applying equation 19, 500 defect sizes were randomly generated to simulate detected defect sizes. In one random simulation, 17.6% of the defects is detected for $\lambda = 1.279$ mm. Figure 3 shows the histograms of the detected and missed defects. The detection probability reached about 50% for $\lambda = 7.67$ mm, 90% for $\lambda = 102$ mm, and 100% for $\lambda = 10000$ mm. For the study, the value of λ was adjusted to simulate the effectiveness of detections. Three POD cases were chosen for comparison: Ideal (detection probability = 100%), Bad POD (detection probability = 0 %), and Fair POD (detection probability = 20 - 50%).

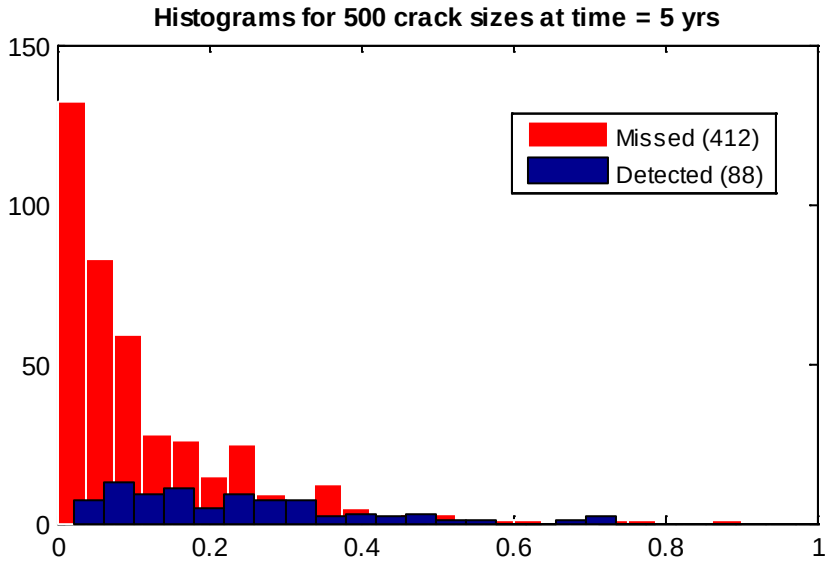

Figure 13. Histograms of the Detected and Missed Cracks

IDEAL POD WITH DEFECT-SIZE MEASUREMENTS

This case provides the best-possible Bayesian updating result and therefore can suggest the minimum number of detections needed. Since all the defects can be detected and measured, $L(\theta)$ can be computed using $L_D(\theta)$ as formulated in equation 4.

To compute the PDFs, Approach-3 described above was used to generate an empirical CDF given each of the θ values selected for analyzing $L(\theta)$. As an example, Figure 4 shows the original CDF, the fitted CDF, and the computed PDF using 1000 randomly generated crack sizes. To improve the fitting performance, the empirical CDF was scaled using standard normal variate, and the crack size was scaled by a log-transformation. For this problem, the scaled polynomial model appears to be adequate for investigating the $L_D(\theta)$ behavior. In general, if needed, the CDF-fit can be improved by using splines, kriging, or other interpolation models.

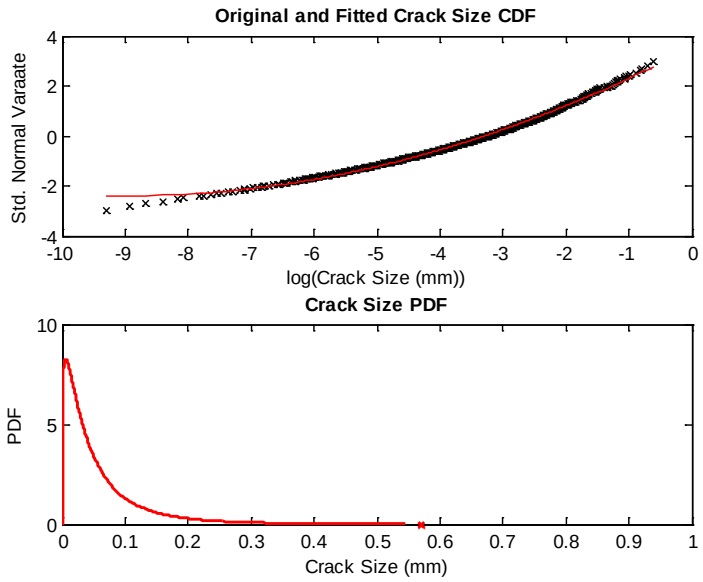

Figure 14. Original and Fitted Crack Size CDF and the Computed PDF

Figure 5 summarizes the result of the likelihood of detection, using equation 4, for 10, 20, 50 and 100 defects. The result shows that the maxima of the $L_D(\theta)$ curves converge toward the true mean value of 0.11 mm as the number of detected cracks becomes larger. The curvatures of the curves are clearly larger for more detections, implying that more detections will provide more discriminating evidence towards the true θ. Thus the shapes of the curves are consistent with the expectation that the optimal θ should converge towards the true mean value as more observables/evidences become available.

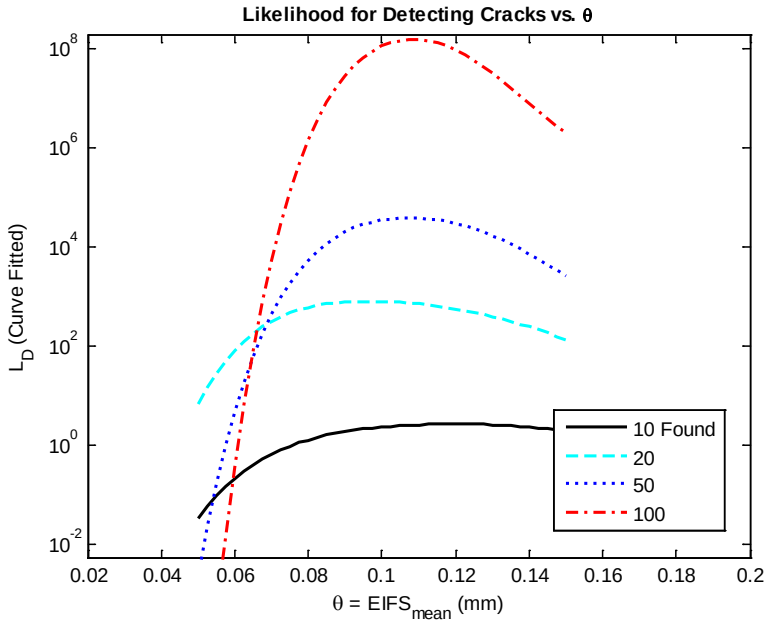

Figure 15. Likelihood of Detection

The $L_D(\theta)$ curves in Figure 5 show that the resulting θ identified at the peak of $L_D(\theta)$ is better with 10 defects than with 20 defects. This inconsistency can be traced to the sampling variability. To investigate the issue, a total of 5 sets of 100 random crack size samples were used to compute $L_D(\theta)$ for 1 to 100 detected cracks. For each number of cracks, the optimal θ was collected, and the optimal θ versus the number of detected defects were plotted as shown in Figure 6. From the resulting scatters, one can conclude that the sampling variability caused slow convergence – it appears that more than 50 detections are needed. This suggests, not surprisingly, that a good prior would be essential when the number of detections is small.

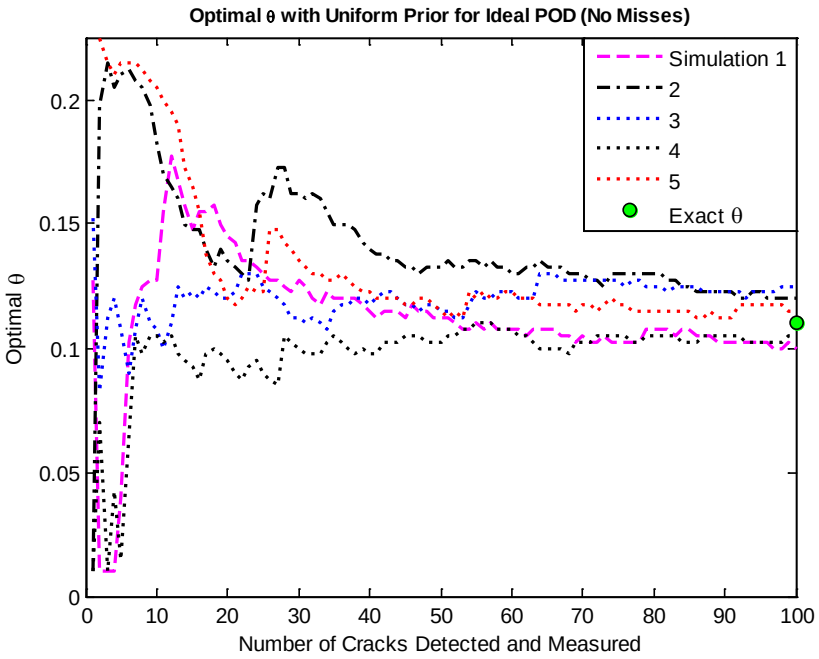

Figure 16. Optimal θ versus the Number of Defects for 5 Random Populations of Crack Sizes

BAD POD (NO DETECTIONS)

This case examines the worst-case scenario where the detection device is very poor, resulting in no detections. In general, the all-misses scenario can be caused by either ineffective detectors or extremely small defects. In our test case, however, since the defect size are significant (see Figure 2), it is clear that the cause of the all-misses is the bad POD.

$L(\theta)$ can be computed using $L_M(\theta)$ because all the defects are missed. Figure 7 shows $L_M(\theta)$ for 10, 20, 50 and 100 defects. All the curves show that the optimal $\theta's$ are the lower bound of θ.

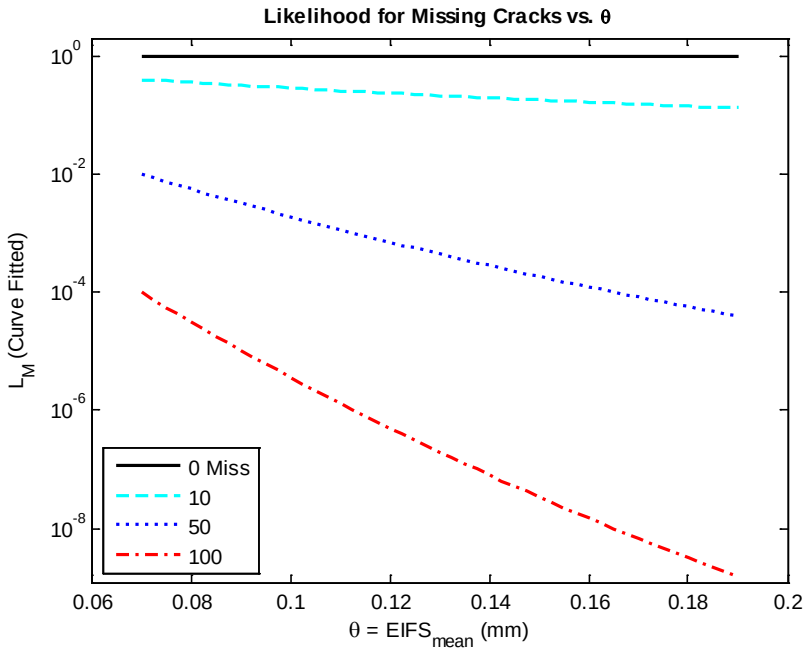

Figure 17. Likelihood of Missing Detections

By comparing Figure 7 with Figure 5, several interesting observations can be made: (1) For each curve, $L_M(\theta)$ is a monotonic function – with a negative slope, which implies that the updated mean value of IFS would favor the smallest possible θ associated with small initial defects that can explain why all the detects have been missed. (2) The absolute slopes of the curves are greater for larger numbers of misses, implying that more misses will provide more discriminating evidence that the true θ is small. (3) While the maxima of $L_D(\theta)$ are well within the bounds of θ (close to the true mean value), the maxima of $L_M(\theta)$ are at the left extreme and do not provide information toward the mean value.

The third observation is particularly important. It supports the expectation that a good POD will provide useful information for updating. More importantly, it implies that the results from a bad POD can provide misleading evidence and should not be used for Bayesian updating.

FAIR POD

From risk-reduction perspectives, an inspection has no benefit when the POD is near zero. It is more practical to conduct inspections when the defects can be found with a significant probability, before the probability-of-failure cannot be tolerated. In the case below, a population-POD of 0.5, i.e., half of the defect population is expected to be detected, is used to study the effect of including $L_M(\theta)$ in the likelihood function. To gain a better understanding of the significance of including the missed defects, two prior PDFs are assumed: a uniformly-distributed prior and a normally-distributed prior. In both cases, the posterior PDFs for Ideal POD, Bad POD, and Fair POD are compared.

Uniform Prior

The uniform-prior assumption is useful in that it is free of prior bias so that the effect of including $L_M(\theta)$ is easier to assess. Figure 8 presents the posterior PDFs (all curves have been normalized to have the same maximum height), which are identical to the $L_M(\theta)$ curves since the prior PDF is a constant. It can be observed that: (1) For Ideal POD, the size measurements lead to an excellent optimal θ. (2) For Bad POD, the optimal θ is the lower bound of θ, therefore, the counting of the misses does not produce an improved optimal θ. (3) For Fair POD (with 50% population POD) with the inclusion of the counting of the misses, the optimal θ is fair. (4) For Fair POD but without the inclusion of the counting of the misses, the optimal θ is clearly inferior to the case with the inclusion. One can conclude, therefore, that the inclusion of the counting of the misses has a significant effect for Fair POD.

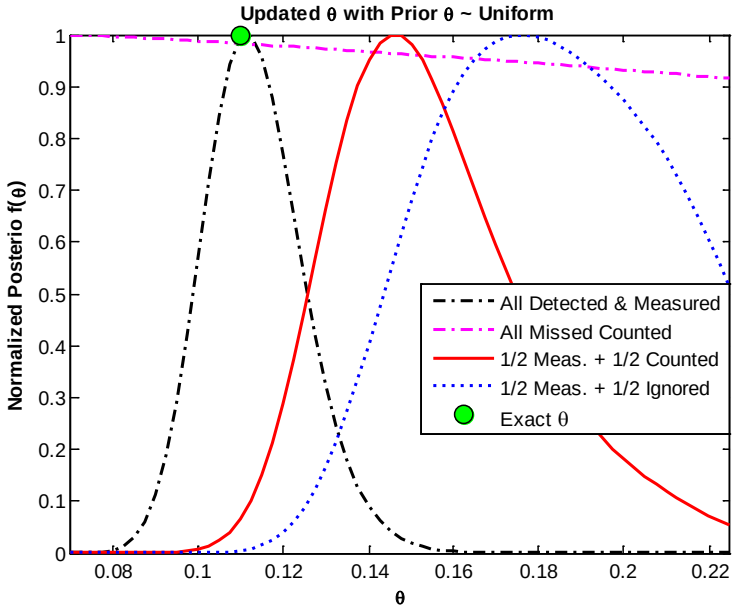

Figure 18. Updated PDFs with Uniform Prior for Ideal, Bad, and Fair PODs

Normal Prior

The prior PDF is $f(\theta) \sim \text{Normal}(0.13\text{mm}, 20\%)$, which has an optimal θ larger than the exact value (0.11 mm). Figure 9 shows that the normalized posterior PDFs**.** It can be observed that: (1) For Ideal POD, the optimal θ is slightly inferior when compared with the Uniform Prior case, which can be explained by the shape of the prior PDF. (2) For Bad POD, the optimal θ is essentially the same as that from the prior PDF, which implies that the prior PDF dominates the effect from the inclusion of the counting of the misses. (3) For Fair POD, and with the inclusion of the counting of the misses, the optimal θ is closer to the true value than that from the Uniform Prior case (Figure 8), which can also be explained by the bias in the prior PDF. (4) For Fair POD but without the inclusion of the counting of the misses, the optimal θ is again inferior to the one that include the misses. One can conclude that, while the prior PDF has a strong

influence to the updated optimal θ, the inclusion of the counting of the misses still has a significant effect for Fair POD.

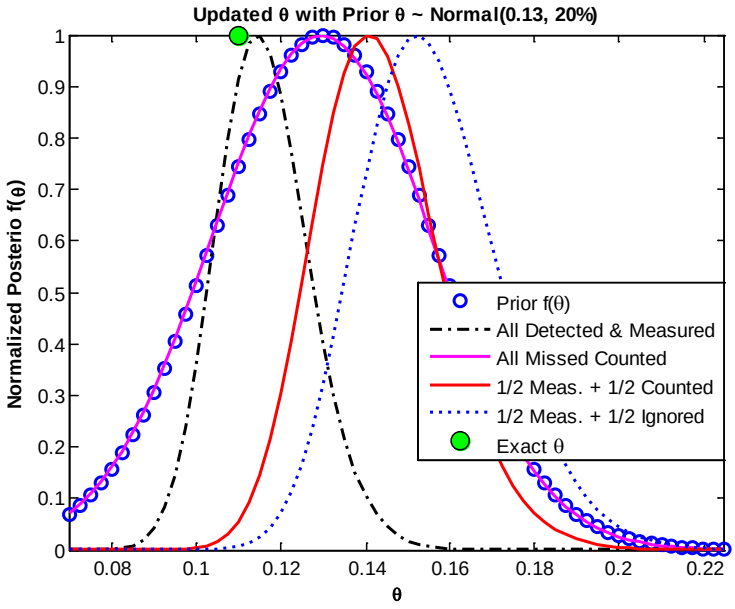

Figure 19. Updated PDFs with Normal Prior for Ideal, Bad, and Fair PODs

5.0 SUMMARY AND DISCUSSIONS

This report presents a DT-based Bayesian updating framework which includes both the detected and the missed detections. To demonstrate the methodology, a tailored sampling-based approach has been developed to compute likelihood functions for all the inspection results.

Using a DT example, the result suggests that (1) a good POD with sizing information have a useful dominating effect for updating, (2) the non-detection results from a bad POD can provide misleading evidence and should not be used for Bayesian updating, (3) when the inspection POD is reasonably effective, the inclusion of the count of non-detections can provide useful information for Bayesian updating.

In summary, this study suggests that recording and utilizing complete inspection results, i.e., including non-detections, can be important and beneficial for aircraft reliability and risk management, including RBMO applications.

The effect of uncertainty in POD model should be investigated in the future, because of the important role POD played in DT and also the fact that POD can be highly uncertain.

6.0 REFERENCES

1. Wu, Y-T. , Zhao, J., Shiao, M., Millwater H.R. "Efficient Methods for Probabilistic Damage Tolerance Inspection Optimization," Proceedings of the 51st AIAA/ASME/ASCE/AHS Structures, Structural Dynamics and Materials Conference, April 2010.

2. Wu, Y.T., Shiao, M., and Millwater, H.R., "A Bayesian-Updating Computational Method for Probabilistic Damage Tolerance Analysis," by., *Proceedings of the 51st AIAA/ASME/ASCE/AHS Structures, Structural Dynamics and Materials Conference*, April 2010.
3. Shiao, M., "Risk-Based Maintenance Optimization," *Proceedings of the International Conf. on Structural Safety and Reliability,* 2006.
4. Wu, Y-T., Shiao, M., Shin, Y., and Stroud, W.J., "Reliability-Based Damage Tolerance Methodology for Rotorcraft Structures," *Transactions Journal of Materials and Manufacturing*, paper 2004-01-0681, July 2005.
5. Harris, D.O., 1987. "Probabilistic Crack Growth," in *Probabilistic Fracture Mechanics and Reliability*, Provan, J. Edt. Martinus Nijhoff Publishers.
6. Shiao, M., "Risk Forecasting and Updating for Damage Accumulation Processes with Inspections and Maintenance," 5th International Workshop on Structural Health Monitoring, Stanford, California, September, 2005.
7. Hovey, P.W., Berens, A.P., and Knopp, J. "Estimating the Distribution of the Size of Flaws Remaining after an Inspection", AFRL-ML-WP-TP-2006-496
8. Gamerman, D., *Markov Chain Monte Carlo*, Chapman & Hall, 1997.
9. Robert, C.P., and Casella, G., *Monte Carlo Statistical Methods*, Springer, 2004.
10. Ku, A., Serratella, C., Spong, R., Basu, R., Wang, G., and Angevine, D., "Structural Reliability Applications in Developing Risk-Based Inspection Plans for a Floating Production Installation", OMAE 2004-51119, 2004.

APPENDIX E—STRENGTH-CONDITIONED IMPORTANCE SAMPLING METHOD FOR AIRCRAFT DAMAGE-TOLERANCE RELIABILITY ANALYSIS

Strength-Conditioned Importance Sampling Method for Aircraft Damage-Tolerance Reliability Analysis

By

Justin Y-T. Wu

CompRel, Inc., Raleigh, NC

Feb. 2014

1.0 ABSTRACT

Aircraft damage-tolerance reliability models, in general, involve time-independent strength-related random variables and time-dependent stress random processes. The single-flight reliabilities between the flights are correlated due to strength-related random variables. These correlations often make computing the interval reliability difficult, and is inevitably very time consuming. In conventional methods, either the correlations are ignored or the approximate reliability bounds are used to address the issues. This report summarizes a new Strength-Conditioned Importance Sampling (SCIS) methodology which integrates the Strength-Conditioned Expectation Method (SCEM) with a special Importance Sampling (IS) methodology. The SCEM makes the flight-to-flight reliabilities independent which allows the interval reliability for each strength realization to be computed accurately and easily. More importantly, the efficiency issue is dealt with by using a tailored IS approach to reduce drastically the number of random samples which is required to achieve a desired level of accuracy. In theory, the SCIS method is versatile and can handle either gradual or sudden strength-changing events. Furthermore, for risk-optimization purpose, the IS samples can be re-used to compute reliabilities for various maintenance plans. This report documents the SCIS method and presents a demonstration example using a fracture mechanics model.

2.0 INTRODUCTION

It is well known that metal fatigue could cause major aircraft structural failures. To help prevent failures, significant efforts and progress have been made in the last few decades to develop safer design methodologies including probabilistic design methodology and tools, with the emphasis on fatigue and fracture (e.g., Refs. 1-4). Other sources of structural failures which have received relatively less attention are environmental effects (due to, e.g., moisture and temperature variations) and impact damage that can significantly reduce the strengths over time. With the increasing use of new materials for aircraft structures, the ability to model and assess the risk of strength degradations has become more important, especially for dealing with events which may cause significant gradual or sudden changes in the remaining strength and life. If the damages or degradations are not detected and fixed in time, they can potentially cause unexpected structural failures.

This report presents a probabilistic damage-tolerance analysis (PDTA) methodology designed for time-dependent reliability models which involve various strength random variables and stochastic loading processes. Figure 1 illustrates a time-dependent reliability model where the reliability is governed by the degree of overlapping of the applied load distribution and the remaining strength distribution which deteriorates due to the growth of defects or other damages. In general, the rate of strength reduction, and therefore the rate of failure, could be enhanced due to aging and environmental factors and the impacts can occur multiple times.

Aircrafts are routinely inspected including walk-around inspections for apparent damages and scheduled inspections for detecting smaller or hidden damages using specialized NDE devices. When a defect or damage is detected and fixed, the strength is altered, possibly drastically. Therefore, in building a reliability model, the quality of the repaired/replaced parts should be incorporated in modeling the altered strength. With a proper reliability model, the inspection schedules can be optimized by controlling the risk subject to reliability, operational and other constraints. For example, the timing of the inspections should be selected such that the dangerous defects/damages can be detected with a high probability of detection but before the probability-of-failure becomes unacceptable. Several risk-based maintenance optimization (RBMO) approaches have been proposed in recent years (Refs. 5-8). These approaches, however, were designed for metal fatigue models and cannot be easily applied to more general time-dependent reliability models.

In PDTA, the sources of uncertainty include systematic and random errors of the failure models, applied loads, material properties, geometries, environmental factors, defect and damage occurrence rates, and detection capability. As illustrated in Figure 1, aircraft structural reliability models, in general, can involve time-independent strength-related random variables (RVs) and time-dependent stress random processes. While vary among different aircraft in a fleet, the strength-related RVs, such as the fracture toughness and the initial flaw size, at a certain location, are essentially time independent for individual aircraft. Therefore, the single-flight reliabilities between the flights are correlated due to strength-related random variables. These correlations often make computing the interval reliability

difficult and inevitably very time consuming. As a result, either the correlations are ignored or the approximate reliability bounds have to be used to address the issues.

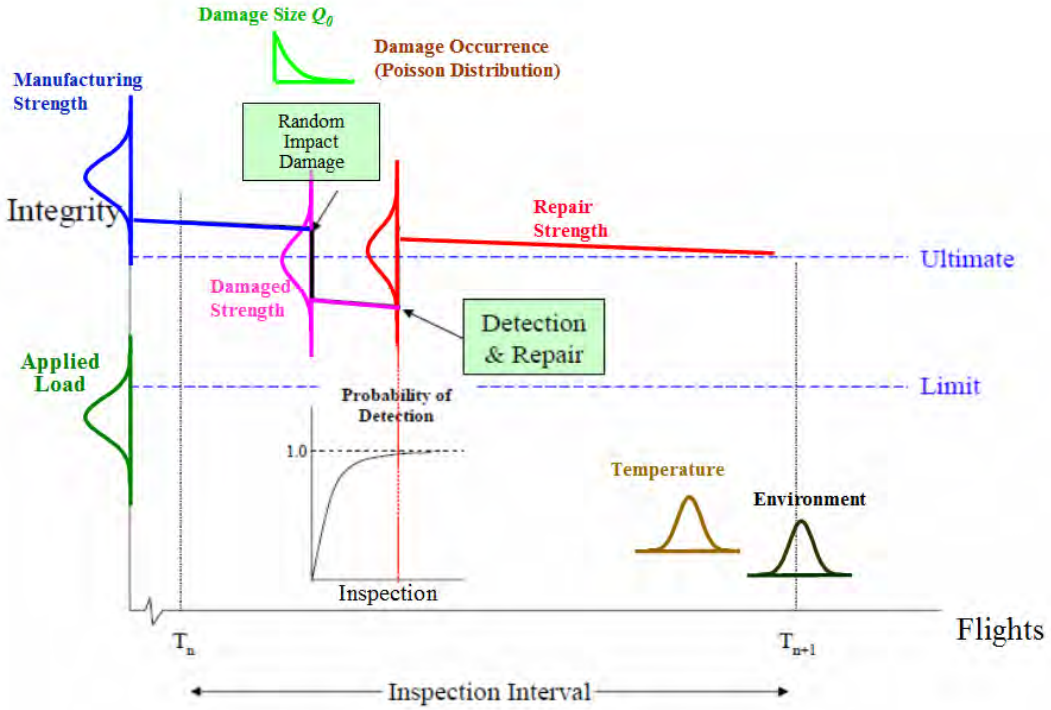

Figure 1. Description of Time-Dependent Reliability Problem

To accurately and efficiently compute time-dependent reliability and conduct RBMO, this report presents a new Strength-Conditioned Importance Sampling (SCIS) methodology which integrates the Strength-Conditioned Expectation Method (SCEM) with a special Importance Sampling (IS) methodology. The SCEM makes the flight-to-flight reliabilities independent which allows the interval reliability for each strength realization to be computed accurately and easily. More importantly, the efficiency issue is dealt with by using a tailored IS approach to drastically reduce the number of random samples which is required to achieve a desired level of accuracy. Furthermore, for risk-optimization purpose, the IS samples can be re-used to compute reliabilities for various maintenance plans.

This report documents the SCIS method and presents a demonstration example using a fracture mechanics model. The SCIS approach has been implemented in a Matlab program, FlyRisk, for the demonstration. The SCIS reliabilities for both the "with" and "without" inspection cases are computed and validated using standard Monte Carlo with large sample sizes.

3.0 STRENGTH-CONDITIONED METHODOLOGY

Overview of Time Dependent Reliability Model

The basic assumption for the proposed methodology is that the initial structural strength, R, is a function of time-independent random variables, $\boldsymbol{X}$, and the residual strength may change over time, t, due to loading (random and impact) and environmental (temperature, moisture, etc.) effects, until the structure has survived the service life, repaired/replaced, or failed. Because the duration of each flight is relatively short, R is assumed to be constant during each single flight. However, the applied load is a stochastic process which can vary significantly during each flight. For this study, the probability distribution of the loads is assumed to be independent between the flights.

Based on the above assumptions, a structural failure will occur if, during any flight, *i*, the strength is exceeded by the maximum stress, denoted as $S_i(t_i)$. Therefore, the single-flight probability of survival, or reliability, for the *i*-th flight is:

$$P_{Survival}(t_i) = P[R_i(\boldsymbol{X}, t_i) > S_i] \qquad (1)$$

The cumulative or interval reliability for the duration of $t = t_1$ to t_N is the probability of survival for N flights and can be formulated as:

$$P_{Survival}(t_N) = P\{[R_1 > S_1] \cap [R_2 > S_2] ... \cap [R_N > S_N]\} \quad (2)$$

Denoting $E_i = R_i > S_i$, Equation 2 is abbreviated as:

$$P_{Survival}(t_1 : t_N) = P\{[E_1 \cap E_2 ... \cap E_N\} \qquad (3)$$

Due to the correlations between $R_i's$ or $E_i's$, an analytical solution for the cumulative reliability is generally unavailable. There are several solutions to compute $P_{Survival}(t_1 : t_N)$, including the bounding approach, which provides approximate answers, and the Monte Carlo approach, which is usually time-consuming. In the following, we will discuss the limitation of the bounding approach and propose an alternative random sampling approach that is highly efficient relative to the MC approach.

Reliability Bounds

The statistical correlation between any two events $E_i = R_i - S_i$ and $E_j = R_j - S_j$ is:

$$\rho_{E_i E_j} = \frac{E\left[E_i E_j\right] - E\left[E_i\right] E\left[E_j\right]}{\sigma_{E_i} \sigma_{E_i}} \qquad (4)$$

Assuming S_i are independent and identically distributed, it can be shown that

$$\rho_{E_i E_j} = \frac{\rho_{R_i R_j} \sigma_{E_i} \sigma_{E_j} + \sigma_S^2}{\sigma_{E_i} \sigma_{E_j}} \qquad (5)$$

Physically, since a realization of $\boldsymbol{X}$ that results in a relatively higher/lower $R_i(X, t_i)$ at t_i will likely results in a higher/lower $R_j(X, t_j)$ at t_j, the correlation $\rho_{R_i R_j}$ is expected to be positive and $\rho_{E_i E_j} \geq 0$. The positive correlation leads to the following uni-modal bounds (e.g., Ref. 9):

$$\prod_{i=1}^{N} P_{S_i} \leq P_S \leq \min_i P_{S_i} \qquad (6)$$

Without maintenance, reliability is either constant or monotonically decreasing due to strength deterioration. Therefore, the last single-flight reliability is the reliability upper bound, i.e., $\min_i P_{S_i} = P_{S_N}$. For a conservative aircraft risk assessment, the lower bound of the reliability, or the upper of the probability-of-failure, is used.

Expressed in terms of probabilities of failure, Equation 6 can be converted to:

$$\max_i P_{f_i} \leq P_f \leq 1 - \prod_{i=1}^{N} (1 - P_{f_i}) \qquad (7)$$

For small P_{f_i}, the case for aircraft applications, the above equation can be approximated as:

$$\max_i P_{f_i} \le P_f \le \sum_{i=1}^{N} P_{f_i} \qquad (8)$$

Thus, the upper bound of the interval probability-of-failure, which is conservative, is approximately the sum of the single-flight probability-of-failures, $\sum P_{f_i}$.

Example: Consider a special case where there is no strength deduction and the single-flight probability remains constant, $P_{f_i} = \lambda$. The corresponding bounds are:

$$P_{f_i} \le P_f \le NP_{f_i} \qquad (9)$$

For a constant failure rate λ, the time to failure has an exponential distribution and the exact probability-of-failure is:

$$P_{f_{Exact}} = 1 - e^{-\lambda t_N} \qquad (10)$$

For example, let N = 20000 flights with a small single-flight failure rate of $\lambda = 1.0e-8$. The exact probability-of-failure is $P_{f_{Exact}} = 1.9998e-4$, and the bounds are:

$$1.e-8 \le P_f \le 2.\text{e-4} \qquad (11)$$

which shows that the upper bound, more important for aircraft risk assessment, is excellent while the lower bound has a large error.

Even if the single-flight probability-of-failure is 2 orders of magnitude higher than the above example, the exact interval probability-of-failure is $P_{f_{Exact}} = 1.98e-2$ and the bounds are:

$$1.e-6 \le P_f \le 2.\text{e-2} \qquad (12)$$

which shows that the upper bound is approximately 1% higher than the exact. For aircraft applications, the above cases suggest that the upper bound solution $\sum P_{f_i}$ can be a good approximation provided that there is no significant strength deterioration during the flight- interval of interest.
However, for the case with a decreasing strength, as in fatigue crack growth, aging, or after impacts, the single-flight probability-of-failure should be increasing:

$$P_{f_1} < P_{f_2} \ldots < P_{f_N} \qquad (13)$$

Therefore Equation 8 becomes

$$P_{f_N} < P_f < NP_{f_N} \qquad (14)$$

When the service life approaches the wear out stage, the P_{f_i} may increase sharply. As a result, the value of $\sum P_{f_i}$ may be dominated by the later flights, and the bounds can be expressed as:

$$P_{f_N} < \sum_{i=1}^{N} P_{f_i} << NP_{f_N} \qquad (15)$$

In other words, the upper bound NP_{f_N} is too conservative. In summary, for aircraft risk assessment, the upper bound can provide a quick estimate but the bound is too conservative in general for decreasing strengths. The method described below can remove the conservatism and is computationally efficient.

Strength-Conditioned Expectation Method (SCEM)

The foundation of the SCIS approach is the strength-conditioned expectation method (SCEM) which separates the strength random variables $\boldsymbol{X}$ and the random stress S to create independencies between the conditional $E_i's$ for accurate reliability calculations. By conditioning on the $\boldsymbol{X}$ random variables, $P_{Survival}(t_1 : t_N)$ can be computed by generating a set of $\boldsymbol{X}$ realizations and taking the sampling average. Figure 2 illustrates the concept of SCEM using 20 realizations of $\boldsymbol{X}$ variables.

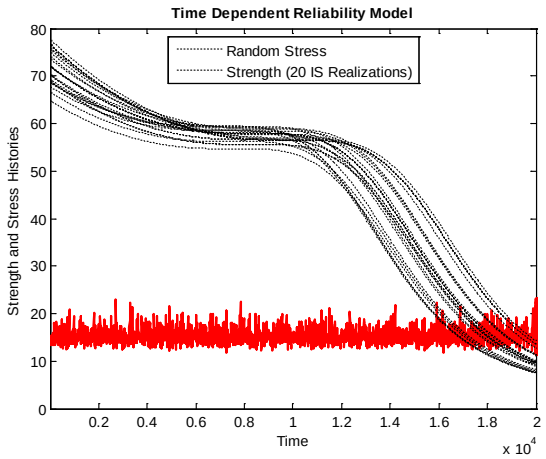

Figure 2. Concept of Strength-Conditioned Expectation Method (SCEM)

For each j-th realization of $\boldsymbol{X}$, the $S_i's$ are independent, therefore, the conditional failure events are independent, which leads to:

$$\begin{aligned} & P^c_{Survival_j}(t_1 : t_n) \\ & = P[(R_1(\boldsymbol{X}_j, t_1) > S_1) \cap \ldots \cap (R_n(\boldsymbol{X}_j, t_n) > S_n)] \\ & = \prod_{i=1}^{n} P[(R_i(\boldsymbol{X}_j, t_i) > S_i)] \\ & = \prod_{i=1}^{n} P^c_{Survival_j}(t_i) \end{aligned} \tag{16}$$

where $P^c_{Survival_j}(t_i)$ is the conditional single-flight reliability which is relatively easier to compute than the unconditional single-flight reliability $P_{Survival}(t_i)$.

The unconditional cumulative survival probability is the integral of the unconditional survival probability weighted by the PDF of $\boldsymbol{X}$:

$$P_f(t_1 : t_n) = \int P^c_f(t_1 : t_n \mid \mathbf{x}) f_{\boldsymbol{X}}(\mathbf{x}) d\mathbf{x} \tag{17}$$

which can be expressed in terms of the expectation function and estimated using a sampling average:

$$\begin{aligned} P_{Survival}(t_1 : t_n) &= E[P^c_{Survival_j}(t_n)]_{f_{\boldsymbol{X}}} \\ &= \frac{1}{J} \sum_{j=1}^{J} \left[\prod_{i=1}^{n} P^c_{Survival_j}(t_n) \right] \end{aligned} \tag{18}$$

where J is the number of random samples. The cumulative probability-of-failure is denoted as $P_f(t_1 : t_n) = 1 - P_{Survival}(t_1 : t_n)$.

Similar to Equation 18, the single-flight probability-of-failure is:

$$P_f(t_i) = E[P_{f_j}^c(t_i)]_{f_{\boldsymbol{X}}} = \frac{1}{J}\sum_{j=1}^{J} P_{f_j}^c(t_i) \qquad (19)$$

The drawback in using the above averaging approach is that a large J is typically needed for estimating a very small $P_S(t_N)$.

STRENGTH-CONDITIONED IMPORTANCE SAMPLING (SCIS)

The proposed SCIS approach, presented below, is mathematically rigorous for treating correlated random variables between flights, is versatile for treating gradual or sudden strength-changing events, and is computationally much more efficient than SCEM. In addition, since the SCIS approach is sampling based, the sampling structure for computer-based simulation lends itself to simulate highly complex random events.

The SCIS method requires only a small fraction of the random samples for reliability computations. The efficiency is achieved by generating the $\boldsymbol{X}$ samples in a smaller, focused sampling region Ω that covers the domain of the events where $P_{S_j}(t_n)$ is nonzero and Equation 19 is modified to:

$$\begin{aligned} P_S(t_n) &= P_\Omega \frac{1}{J_\Omega}\sum_{j=1}^{J_\Omega}\prod_{i=1}^{n} P_{S_j}(t_i) + (1 - P_\Omega)\cdot 0 \\ &= P_\Omega \cdot P_{S|\Omega}(t_n) \end{aligned} \qquad (20)$$

in which P_Ω is the probability in Ω and $P_{S|\Omega}(t_n)$ is the conditional reliability in Ω.

The focused sampling can be generated, in general, by a Markov Chain Monte Carlo method or other advanced sampling methods (see, e.g., Refs. 10-13). To maximize the efficiency, the SCIS-based MCMC method has been designed to minimize the sampling region while controlling the sampling error.

In the SCIS procedure, the samples of $\boldsymbol{X}$ are generated using only the last single-flight failure probability. Subsequently, the samples are used for all the flights starting from the first flight to compute cumulative reliability.

The unconditional single-flight failure probability is the integration of the unconditional single-flight failure probability weighted by the PDF of $\boldsymbol{X}$:

$$P_f(t_n) = \int_\Omega P_f^c(t_n)\cdot f_{\boldsymbol{X}}(\boldsymbol{x})d\boldsymbol{x} \qquad (21)$$

To minimize the sampling region, the domain of $\boldsymbol{X}$, Ω, is divided into 2 domains, Ω_1 and Ω_2, such that $\Omega = \Omega_1 + \Omega_2$, where the probabilities in the two domains are:

$$p_{\Omega_i} = \int_{\Omega_i} f_{\boldsymbol{X}}(\boldsymbol{x})d\boldsymbol{x} \quad (i = 1:2) \qquad (22)$$

with $p_{\Omega_1} + p_{\Omega_2} = 1$. Using Equation 22, Equation 21 can be rewritten as

$$\begin{aligned} P_f(t_n) &= p_{\Omega_1}\int_{\Omega_1} P_f^c(t_n)\frac{f_{\boldsymbol{X}}(\boldsymbol{x})}{p_{\Omega_1}}d\boldsymbol{x} + p_{\Omega_2}\int_{\Omega_2} P_f^c(t_n)\frac{f_{\boldsymbol{X}}(\boldsymbol{x})}{p_{\Omega_2}}d\boldsymbol{x} \\ &= p_{\Omega_1}E[P_f^c(t_n)]_{\Omega_1} + p_{\Omega_2}E[P_f^c(t_n)]_{\Omega_2} \\ &= p_{\Omega_1}E[P_f^c(t_n)]_{\Omega_1}\left[1 + \frac{p_{\Omega_2}}{p_{\Omega_1}}\frac{E[P_f^c(t_n)]_{\Omega_2}}{E[P_f^c(t_n)]_{\Omega_1}}\right] \end{aligned} \qquad (23)$$

The division of Ω is defined by selecting a truncation limit of $P_f^c \cdot f(\boldsymbol{X})$, P_{Limit}, such that

$$X \subset \Omega_1 \text{ if } P_f^c \cdot f(\boldsymbol{x}) \geq P_{Limit}$$
$$X \subset \Omega_2 \text{ if } P_f^c \cdot f(\boldsymbol{x}) < P_{Limit} \tag{24}$$

The purpose of the above truncation is to minimize the number of SCSI samples by ignoring the samples in the Ω_2 domain with a small, controlled error in $P_f(t_n)$. The truncation limit can be found by generating a set of pilot samples of $P_f^c(t_n)$ using the Markov Chain Monte Carlo method with a prescribed target PDF of $P_f^c(t_n)f(\boldsymbol{x})$. Assuming K samples have been generated, the corresponding samples in the two domains, denoted as K_1, K_2, are approximately proportional to p_{Ω_1} and p_{Ω_2}. Therefore, Equation 23 becomes:

$$\begin{aligned} P_f(t_n) &\approx p_{\Omega_1} E[P_f^c(t_n)]_{\Omega_1} \left[1 + \frac{K_2}{K_1} \frac{E[P_f^c(t_n)]_{\Omega_2}}{E[P_f^c(t_n)]_{\Omega_1}} \right] \\ &= p_{\Omega_1} E[P_f^c(t_n)]_{\Omega_1} \left[1 + \frac{\sum_{i=1}^{K_2} (P_{f_i}^c(t_n))_{\Omega_2}}{\sum_{i=1}^{K_1} (P_{f_i}^c(t_n))_{\Omega_1}} \right] \end{aligned} \tag{25}$$

in which the relative error in P_f due to truncation is:

$$\varepsilon = \frac{\sum_{i=1}^{K_2} (P_{f_i}^c)_{\Omega_2}}{\sum_{i=1}^{K_1} (P_{f_i}^c)_{\Omega_1}} \tag{26}$$

After selecting an error, a search procedure can be devised to find the truncation limit P_{Limit} and accept the corresponding K_1 samples for SCIS. Alternatively, a new set of SCIS samples can be regenerated using the selected P_{Limit}.

By applying the samples within the truncation envelope, Equation 23 is approximated by:

$$P_f(t_n) \approx p_{\Omega_1} \sum_{i=1}^{K_1} (P_{f_i}^c)_{\Omega_1} \tag{27}$$

Based on Equation 25, p_{Ω_1} is

$$p_{\Omega_1} = \frac{P_f(t_n)}{\sum_{i=1}^{K_1} (P_{f_i}^c)_{\Omega_1}} \tag{28}$$

in which $P_f(t_n) = 1 - P[(R_n(\boldsymbol{X}, t_n) > S_n)]$ can be computed by a limit-state reliability method. It should be noted that $P_f(t_n)$ needs to be computed only once. The associated IS samples are then used for computing both the single-flight failure probability $P_f(t_i)$ and the cumulative failure probability $P_f(t_1 : t_i)$ for all the flights, i.e., $t_i = t_1 : t_n$.

It should be noted that the SCIS framework is intended to address different materials including composites. In fact, from the theoretical perspective, a major advantage of the SCIS method is in its capability to handle a broad range of strength-changing models, either gradual or sudden, including degradation, impact damage, and maintenance. For various types of strength-changing events, the main difference in applying the SCIS approach is in the use of respective strength-changing models, while the creation of the IS samples are based on their weighted conditional probabilities-of-failure, $P_f^c(t_n)f(\boldsymbol{x})$. For highly complex strength-changing events, the successful implementations of SCIS may require improved sampling algorithms in order to generate high quality SCIS samples efficiently.

In the following section, the SCIS approach will be demonstrated using a metal fatigue damage-tolerance example because such a model is well accepted and is easy to calculate and therefore suitable for researching various approaches.

4.0 DEMONSTRATION EXAMPLE

The selected example analyzes the risk of crack growth at a fastener hole. The random variables were duplicated from a paper by Shiao et al. (Ref. 14). The random variables include EIFS, fracture toughness, and maximum stresses.

The equivalent initial flaw size (EIFS), a_i, has the following Weibull distribution with $\eta = 0.0061$ in. and $\beta = 0.996$.

$$F_{a_i}(a) = 1 - \exp[-(a_i/\eta)^{\beta}] \qquad (29)$$

The fracture toughness, K_C, is normally distributed with a mean = 35 and a standard deviation of 3.1 $ksi \cdot \sqrt{in}$. The maximum stress, *S*, has a Gumbel distribution defined in Equation 30 with A = 1.31 *ksi* and B = 14.6 *ksi*.

$$F_S(s) = \exp\{-\exp[-(s-B)/A]\} \qquad (30)$$

The CDFs and the PDF of the random variables are plotted in Figures 3 to 5.

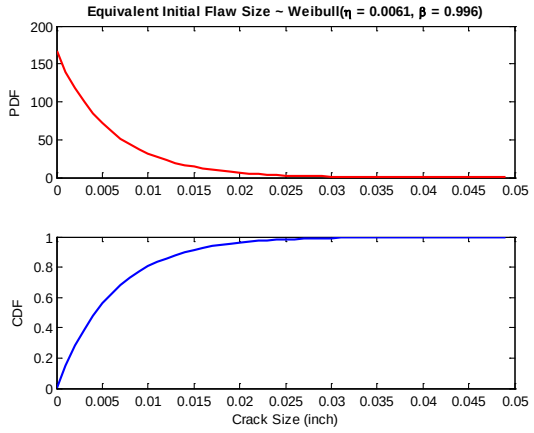

Figure 3. PDF and CDF of EIFS

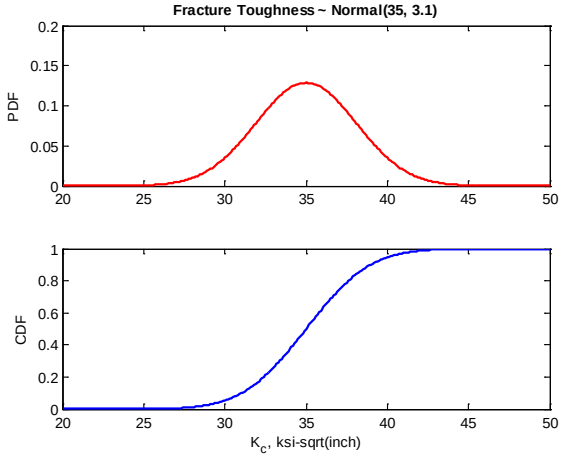

Figure 4. PDF and CDF of Fracture Toughness

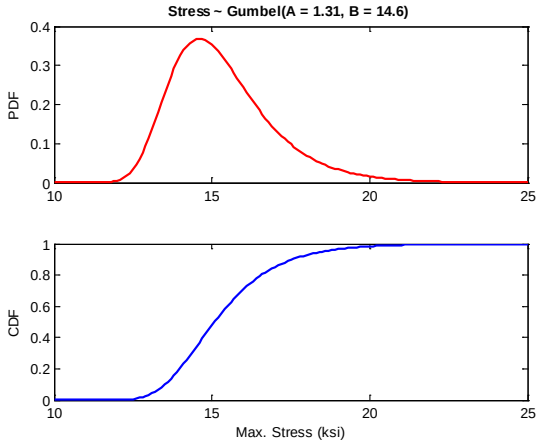

Figure 5. PDF and CDF of Maximum Stress

The crack size a versus time t for damage-tolerance analysis is shown in Figure 6 as the "master" curve. For any realization of EIFS, the curve is shifted to match the crack size at time $t = 0$. For this study, the curve is fitted using Equation 31:

$$a(t) = a_o \exp(bt) = 0.0003 \cdot \exp(0.0001015t) \qquad (31)$$

For a given EIFS, the shifted curve is:

$$a(t) = a_o \exp(bt + t_{shift}) \qquad (32)$$

in which the time shift is:

$$t_{shift} = \frac{1}{b} \ln \frac{a_i}{a_o} \qquad (33)$$

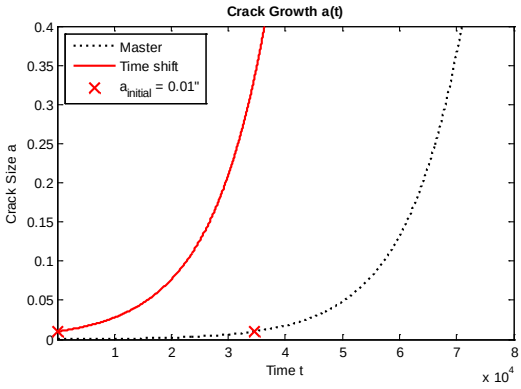

Figure 6. Crack Size Versus Time Model

The relationship between the stress intensity factor ($R(a) = K_C / \sigma$) and the crack size is shown in Figure 7.

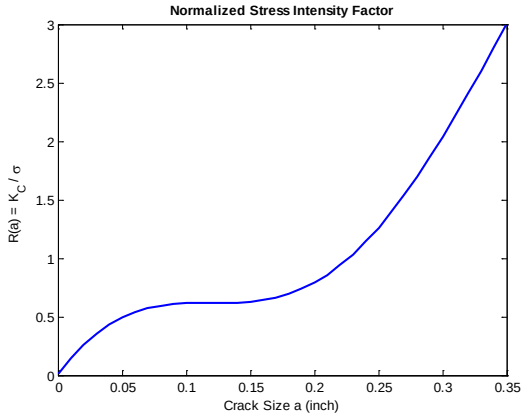

Figure 7. Normalized Stress Intensity Factor

Four POD curves were selected which were modeled using the following equation:

$$POD(a) = \frac{1}{1+\exp\left[-\frac{\pi}{\sqrt{3}}\frac{\ln(a-a_{\min})-\ln(a_{50}-a_{\min})}{q}\right]} \tag{34}$$

where a_{50} is the crack size which can be detected 50% of the time, q is a scale parameter, and $a_{\min}$ is the minimum crack size that can be detected. The parameters for the POD curves are listed in Table 1 and the curves are plotted in Figure 8.

Table 1. Parameters for Four POD Curves

	POD 1	POD 2	POD 3	POD 4
a_{50}	0.05	0.05	0.10	0.10
q	0.50	0.75	0.50	0.75
a_{min}	0.00	0.00	0.00	0.00

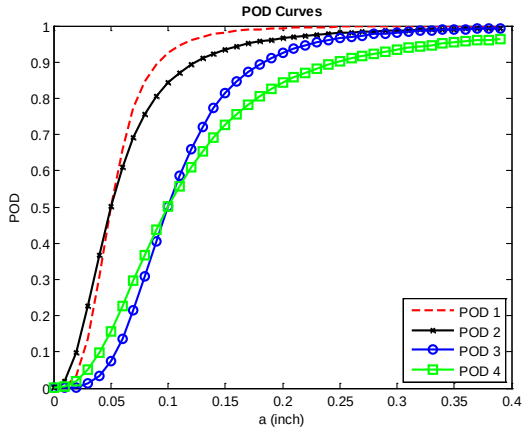

Figure 8. Probability of Detection Curves

The failure limit-state function is:

$$g(t) = Strength - Stress = R - S = \frac{K_C}{Y(a(t))} - S \tag{35}$$

The strength-conditioned probability-of-failure is:

$$P_f^c(t_i) = \Pr.\left[\frac{K_C}{Y(a(t_i))} < S\right] = 1 - F_S\left(\frac{K_C}{Y(a(t_i))}\right) \qquad (36)$$

Reliability Without Maintenance

Using SCEM with Monte Carlo random samples, the single-flight probability-of-failure $P_f(t_i)$ for t_i = 1 to 20,000 flights is repeated 10 times for 100,000, 1 million, and 10 million $\boldsymbol{X}$ samples. The results are summarized in Figures 9 to 11. The results suggest that, for sufficient accuracy, more than 10 million samples is needed for $P_f(t_i)$ < 1.e-06, more than 1 million samples is needed for $P_f(t_i)$ < 1.e-05, and at least 100,000 is needed for $P_f(t_i)$ < 1.e-04. For demonstration purposes, a minimum of 100,000 samples was used for various test cases. By comparison, the SCIS approach only required 1,000 IS samples.

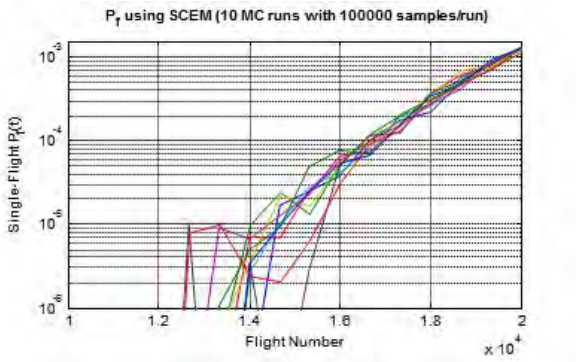

Figure 9. Single-Flight Probability-of-failure using SCEM with 100,000 MC Samples

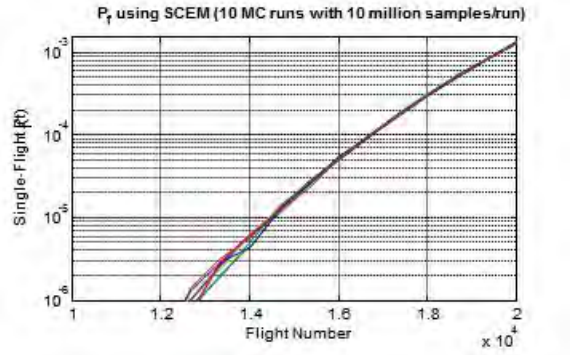

Figure 10. Single-Flight Probability-of-failure using SCEM with 1 Million MC Samples

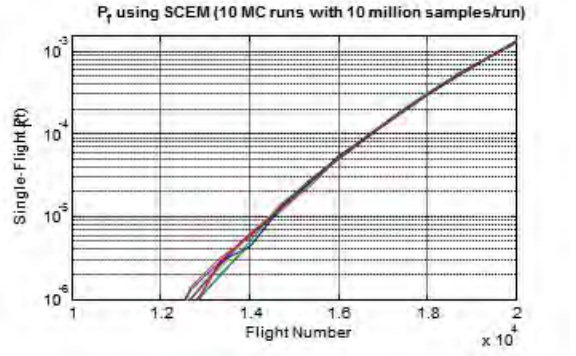

Figure 11. Single-Flight Probability-of-failure using SCEM with 10 Million MC Samples

To examine the accuracy of the SCIS solutions, the MC approach with 10 million samples was applied to compute the single-flight probability-of-failure $P_f(t_i)$ for t_i = 1 to 20,000 flights. The simulation produced a near-exact solution of $P_f(20000) = 1.30e-3$. Applying the MCMC approach, 10,000 IS samples were generated to find the truncation limit. Figure 12 shows that, for 1% error, $P_{Limit} = 2.08e-05$. The probability of the sampling domain p_{Ω_1} is 2.412e-03, computed using Equation 28.

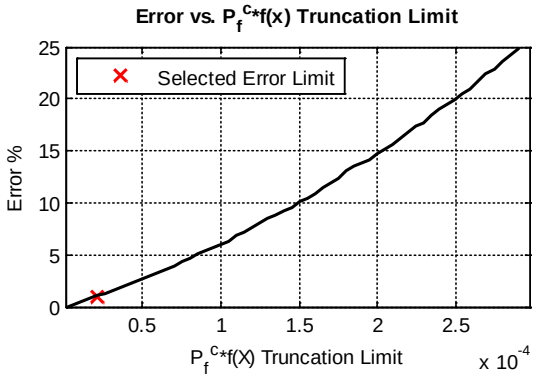

Figure 12. Probability Estimation Error versus Conditional Probability-of-Failure Truncation Limit

Subsequently, 1,000 IS samples in Ω_1 were regenerated by another MCMC procedure. Figure 13 displays the $P_f^c(20000) \cdot f(\boldsymbol{X})$ function versus the SCIS samples for the two strength random variables (EIFS and K_c) in the standardized normal (u) space.

Figure 14 compares the SCIS results (with 1,000 IS samples) with the SCEM results (with 100,000 MC samples) for both single-flight $P_f(t_i)$ and cumulative probability $P_f(t_1 : t_i)$ for $t_i = t_1 : t_n$. The results from the two methods match closely, which demonstrate the accuracy and efficiency of the SCIS method.

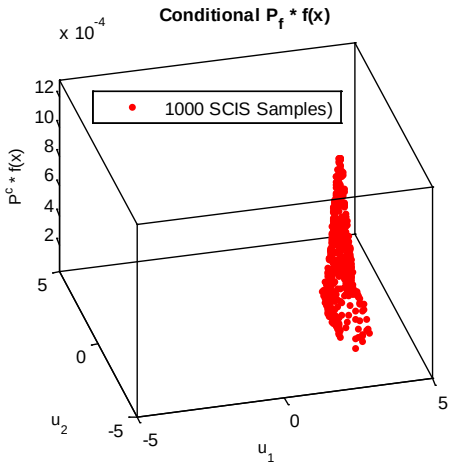

Figure 13. $P_f^c(20000) \cdot f(\boldsymbol{x})$ ***for the SCIS Samples with*** $P_{Limit} = 2.08e-05$

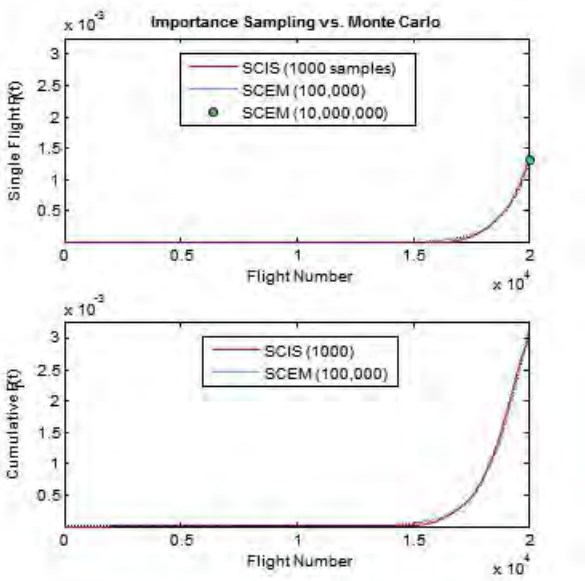

Figure 14. Comparison of Probability-of-Failure Results using SCEM-IS and SCEM_MC Methods

Figure 15 compares the SCEM result with the bounding solution. The bounding solution, which is equivalent to ignoring the correlations between flights, is clearly too conservative for practical use.

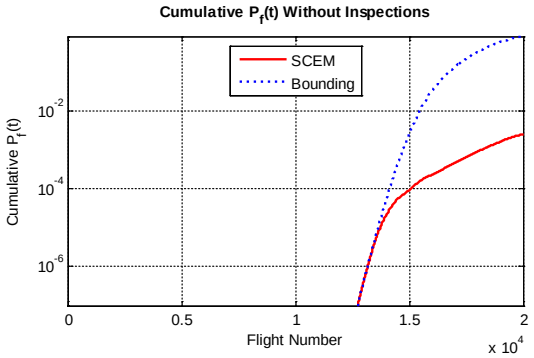

Figure 15. Comparison of Cumulative Probability-of-Failure Results using SCEM and Bounding Methods

5.0 SUMMARY

As demonstrated, the SCIS approach accurately treated correlated random variables between flights and was computationally highly efficient as compared with the Monte Carlo or the SCEM approach. Moreover, after the SCIS samples are created, they can be re-used to compute the reliabilities with inspections (Ref. 15). Because the sampling is strength conditioned, the SCIS approach is potentially very well suited for dealing with various strength degradation effects.

6.0 REFERENCES

1 McClung, R.C., Leverant, G.R., Wu, Y.-T., Millwater, H.R., Chell, G.G., Kulhman, C.J., Lee, Y.-D., Riha, D.S., Johns, S.R., & McKeighan, P.C., "Development of a Probabilistic Design System for Gas Turbine Rotor Integrity," FATIGUE '99, The Seventh International Fatigue Conference, Beijing, China, June 1999.

2 Wu, Y-T., Enright, M.P., and Millwater, H.R., "Probabilistic Methods for Design Assessment of Reliability With

Inspection," *AIAA Journal*, Vol. 40, No. 5, pp. 937-946, 2002.

3 Millwater, H.R., Wu, Y.-T., Fitch, S., Riha, D.S., Enright, M.P., Leverant, G.R., McClung, R.C., Kuhlman, C.J., Chell, G.G., & Lee, Y.-D., "A Probabilistically-Based Damage Tolerance Analysis Computer Program for Hard Alpha Anomalies In Titanium Rotors," Proceedings, 45th ASME International Gas Turbine & Aeroengine Technical Congress, Munich, Germany, May 8-11, 2000.

4 Berens, A.P., Hovey, P.W., and Skinn, D.A., "Risk Analysis for Aging Aircraft Fleets," U.S. Air Force Wright Laboratory Report, WL-TR-91-3066, Vol. 1, October 1991.

5 Wu, Y-T., Shiao, M., Shin, Y., and Stroud, W.J., "Reliability-Based Damage Tolerance Methodology for Rotorcraft Structures," Transactions Journal of Materials and Manufacturing, paper 2004-01-0681, July 2005.

6 Wu, Y-T. and Shin, Y, "Probabilistic Damage Tolerance Methodology For Reliability Design And Inspection Optimization," Proceedings of the 45th AIAA/ASME/ASCE/AHS Structures, Structural Dynamics and Materials Conference, April 2004.

7 Shiao, M., "Risk-Based Maintenance Optimization," *Proceedings of the International Conference on Structural Safety and Reliability,* 2006.

8 Wu, Y.-T., Zhao, J., Shiao, M., & Millwater, H.R., "Efficient Methods for Probabilistic Damage Tolerance Inspection Optimization," Proceedings of the 51st AIAA/ASME/ASCE/AHS Structures, Structural Dynamics and Materials Conference, April 2010.

9 Ang, A. H.-S and Tang, W.H., *Probability Concepts in Engineering Planning and Design*, Volume II; Decision, Risk, and Reliability, New York, John Wiley & Sons, 1984.

10 Gamerman, D., *Markov Chain Monte Carlo*, Chapman & Hall, 1997.

11 Robert, C.P., and Casella, G., *Monte Carlo Statistical Methods*, Springer, 2004.

12 Ang, G.L., Ang, A.H-S., and Tang, W.H., "Optimal Importance Sampling Density Estimator," *Journal of Engineering Mechanics*, Vol. 118, No. 6, June 1992, pp. 1146-1163.

13 Au, S.K. and Beck, J.L., "Estimation of Small Failure Probabilities in High Dimensions by Subset Simulation," *Probabilistic Engineering Mechanics*, Vol. 16, No. 4, pp. 263-277, 2001.

14 Shiao, M., Boyd, K., and Fawaz, S., "A Risk Assessment Methodology and Tool for Probabilistic Damage Tolerance-Based Maintenance Planning," 8th FAA/NASA/DoD Aging Aircraft Conference, January 31-February 3, 2005.

15 Wu, Y.-T., Shiao,M., & Seneviratne, W., "Strength-Conditioned Expectation Method for Aircraft Structural Reliability Analysis," Proceedings of the 52nd AIAA/ASME/ASCE/AHS Structures, Structural Dynamics and Materials Conference, April 2011.